ABUNDANCES AND DISTRIBUTIONS OF SELECTED WATERBIRD SPECIES AROUND THE PROPOSED OMØ SYD OFFSHORE WIND FARM AREA

Scientific Report from DCE – Danish Centre for Environment and Energy No. 551 2023

AARHUS
UNIVERSITY
DCE – DANISH CENTRE FOR ENVIRONMENT AND ENERGY

ABUNDANCES AND DISTRIBUTIONS OF SELECTED WATERBIRD SPECIES AROUND THE PROPOSED OMØ SYD OFFSHORE WIND FARM AREA

Scientific Report from DCE – Danish Centre for Environment and Energy No. 551 2023

Ib Krag Petersen[1]
Lindesay Scott-Hayward[2]
Monique MacKenzie[2]

[1] Aarhus University, Institute of Ecoscience
[2]CREEM, St. Andrews University, Scotland

AARHUS
UNIVERSITY
DCE – DANISH CENTRE FOR ENVIRONMENT AND ENERGY

Data sheet

Series title and no.:	Scientific Report from DCE – Danish Centre for Environment and Energy No. 551
Category:	Scientific advisory report
Title:	Abundances and distributions of selected waterbird species around the proposed Omø Syd offshore wind farm area.
Author(s):	Ib Krag Petersen, Lindesay Scott-Hayward and Monique MacKenzie
Institution(s):	1: Institute of Ecoscience, AU 2: CREEM, St. Andrews University, Scotland.
Publisher:	Aarhus University, DCE – Danish Centre for Environment and Energy ©
URL:	http://dce.au.dk/en
Year of publication:	February 2026
Editing completed:	April 2023
Referee(s):	Ole Roland Therkildsen
Quality assurance, DCE:	Jesper Fredshavn
Linguistic QA:	
External comments:	The comments can be found here: http://dce2.au.dk/pub/komm/SR551_komm.pdf
Financial support:	NIRAS A/S
Please cite as:	Petersen, I.K., Scott-Hayward, L. & Mackenzie, M. 2022. Abundances and distributions of selected waterbird species around the proposed Omø Syd offshore wind farm area. Aarhus University, DCE – Danish Centre for Environment and Energy, 100 pp. Scientific Report No. 551 http://dce2.au.dk/pub/SR551.pdf

Reproduction permitted provided the source is explicitly acknowledged

Abstract: This report presents estimation of abundances and distributions of six waterbird species from the Smålandsfarvand study area in southern Denmark. The analyses also include estimation of the number of displaced individuals of each of the six waterbird species from the proposed Omø Syd Offshore Wind Farm, given a set of described displacement scenarios. The analyses will serve as background data for a NATURA2000 environmental assessment related to the wind farm. That assessment was beyond the scope of this report.

Keywords:	Offhore wind farm, avian displacement, spatial model, impact assessment
Layout:	Tinna Christensen
Front page photo:	Common 'eider in its natural habitat in Denmark. ' Photo: Dennis Jacobsen/Colourbox.com
ISBN:	978-87-7156-772-4
ISSN (electronic):	2244-9981
Number of pages:	100
Internet version:	The report is available in electronic format (pdf) at http://dce2.au.dk/pub/SR551.pdf

Contents

Preface

This report presents results from analyses of 37 aerial surveys of birds in the Smålandsfarvand area. The report was commissioned by NIRAS A/S and will serve as background data for a NATURA2000 environmental assessment related to the proposed Omø Syd Offshore Wind Farm. The report has been compiled by AU/DCE and University of St. Andrews, Scotland. AU has compiled and prepared data for analyses. University of St. Andrews has been in charge of the modelling of abundances and distributions of the bird species involved in this analysis.

Six bird species or species groups were selected for the analyses. These were Red-throated Diver/Black-throated Diver, Red-necked Grebe, Common Eider, Long-tailed Duck, Common Scoter and Red-breasted Merganser.

For each species or species group and for each survey the total abundance and distribution was modelled. Based on those data species persistency estimation could be achieved for each species and across grouped data.

Furthermore, the total number of displaced birds from the proposed wind farm could be estimated. These estimations were based on displacement scenarios and from the available surveys, from which estimation of abundances and distributions could be achieved. These conditions are described in detail in the report.

Sammenfatning

I denne rapport præsenteres analyser af data fra 37 optællinger af fugle i Smålandsfarvandet. Optællingerne blev gennemført fra fly, og udført som linjetransektoptællinger, under anvendelse af Distance Sampling metoden. Data blev kombineret fra en række projekter, med variationer imellem optællingernes dækningsgrad og optællingsprotokol.

Analyserne blev foretaget for seks udvalgte arter/artsgrupper, nemlig rødstrubet lom/sortstrubet lom, gråstrubet lappedykker, ederfugl, havlit, sortand og toppet skallesluger. Arterne blev udvalgt på grund af deres relevans i relation til planer om opførelse af Omø Syd havvindmøllepark. På baggrund af disse data kunne antallet af fortrængte rastefugle i området i og omkring den planlagte havvindmøllepark beregnes, bygget på fortrængningsscenarier.

Analyserne blev gennemført under en kontrakt med NIRAS A/S, der vil anvende data til en NATURA2000 konsekvensrapport til Omø Syd Kystnær Havvindmøllepark. Analyserne i denne rapport er gennemført i samarbejde med St. Andrews Universitet, Skotland. En vurdering af de biologiske implikationer af de estimerede fortrængninger ligger udenfor rammerne af denne opgave. Der er i denne rapport udelukkende analyseret antal og fordelinger af rastende og overvintrende fugle, og rapporten rummer ingen analyser af kollisionsrisici i relation til den planlagte havvindmøllepark.

Rødstrubet lom/sortstrubet lom blev registreret i varierende antal i undersøgelsesområdet over de 37 optællinger. Der blev maksimalt estimeret mere end 1.300 lommer i området ved en optælling i oktober 2014. Over disse optællinger blev det maksimale antal af fortrængte lommer estimeret til at være imellem 297 og 1.246 individer.

Gråstrubet lappedykker blev registreret i betydelige antal i undersøgelsesområdet. Af de 37 optællinger havde 14 optællinger nok observationer til at totale antal og fordelinger kunne estimeres. Det højeste estimat for en optælling var 2.209 individer. Der er anvendt to fortrængningsscenarier for gråstrubet lappedykker, med forskellige effektafstande væk fra mølleparken. Scenariet med den største effektafstand (10 km) blev der beregnet et maksimalt antal fortrængte fugle på 254 til 833 individer, mens de beregnede værdier var 47 til 153 individer for det alternative scenarie (5 km).

Ederfugle er til stede i undersøgelsesområdet hele året. De total antal pr. optælling varierede fra 1.216 i maj 2000 til 107.986 i marts 2014. Baseret på to fortrængningsscenarier blev der beregnet maksimale antal fortrængte ederfugle på imellem 2.113 og 11.981 individer for scenariet med en 2 km effektzone omkring parken, og imellem 1.489 og 8.742 ederfugle for det alternative scenarie med en effekt zone på 1 km.

Havlit forekommer udelukkende i undersøgelsesområdet efterår, vinter og forår. Det maksimale antal forekommende havlitter i undersøgelsesområdet blev beregnet til 1.449 individer. Det maksimale antal fortrængte havlitter for en enkelt optælling var imellem 72 og 595 fugle, baseret på en optælling fra marts 2015.

Sortand forekommer i undersøgelsesområdet hele året. Det maksimale antal sortænder estimeret for undersøgelsesområdet var 39.732 fugle, baseret på en optælling i april 2014. Beregning af antallet af fortrængte sortænder fra den planlagte Omø Syd havvindmøllepark var maksimalt imellem 4.408 og 7.427 individer, baseret på optælling fra april 2014.

Toppet skallesluger forekommer i undersøgelsesområdet hele året, omend i varierende antal. Det maksimale estimerede antal toppede skalleslugere i området var 5.287 individer, baseret på data fra en optælling i februar 2021. Det maksimale estimerede antal fortrængte toppede skalleslugere fra den foreslåede havvindmøllepark var imellem 10 og 65 individer, beregnet på grundlag af data fra optællinger ved midvinter 2016.

Summary

This report presents analysis of abundances and distributions from 37 surveys of birds in the Smålandsfarvand area, southern Denmark. The surveys were performed as aerial line transect surveys, following the Distance Sampling method. The surveys were combined from various projects, conducted between 1999 and 2021, and with a slightly varying survey coverage and sampling protocol.

The analysis was carried out with the aim to derive bird abundances and distributions for six selected bird species or species groups, namely Red-throated Diver/Black-throated Diver, Red-necked Grebe, Common Eider, Long-tailed Duck, Common Scoter and Red-breasted Merganser. These species were selected because of their relevance in relation to a proposed Omø Syd Offshore Wind Farm in the area. On the background of those results the number of displaced birds per survey could be estimated, using defined displacement scenarios.

The analyses were commissioned by NIRAS A/S, who will perform a NATURA2000 Environmental Impact Assessment for Omø Syd Nearshore A/S. This analyses in this report have been conducted in a collaboration with University of St. Andrews, Scotland. An assessment of the biological importance of the described displacements was beyond the scope of this report. Likewise, this report makes no attempt to assess the effect of potential collision effect from the proposed wind farm.

Red-throated Divers/Black-throated Divers were recorded in the study area in varying numbers across the 37 aerial surveys, estimating up to more than 1,300 individuals within the area in October 2014. From this survey 297 to 1,246 individuals were estimated to be displaced by an Omø Syd Offshore Wind Farm.

Red-necked Grebes were recorded in significant numbers in the study area. Altogether, 14 of the 37 aerial surveys had enough data to estimate total abundances and distributions of Red-necked Grebes. The maximum estimated numbers were 2,209 individuals within the survey area. Two displacement scenarios were used. For the scenario using the most precautionary displacement degrees, the maximum number of estimated displaced grebes was between 254 and 833 individuals. Using the alternative displacement, the number of displaced Red-necked Grebes was estimated to be between 47 and 156 individuals.

Common Eiders are present in the study area all year. The estimated number ranged from 1,216 in May 2000 to 107,986 in March 2014. Based on two displacement scenarios the highest displacement number was between 2,113 and 11,981 displaced Common Eiders, estimated for a survey performed in October 2014 under the first displacement scenario, while minimum numbers of between 2 and 10 individuals was estimated for a survey in April 2021. For the alternative displacement scenario, the corresponding numbers were between 1,489 and 8,742 individuals in the maximum displacement survey and between 1 and 6 individuals for the minimum displacement survey.

Long-tailed Duck is primarily a wintering and passage species in the study area. Maximum numbers were found for the winter 2013 survey, when 1,449 individuals were estimated. The maximum displaced number of Long-tailed Duck was between 72 and 595 individuals, based on a survey from March 2015.

Estimation of Common Scoter could be achieved from 32 and the 37 aerial surveys in the study area. The highest estimated number was 39,732 individuals, based on a survey from April 2014. Estimation of the number of displaced Common Scoters revealed a maximal displacement of Common Scoters of between 4,408 and 7,427 individuals, based on data from a survey from April 2014.

Estimation of Red-breasted Merganser was achieved from 20 of the 37 aerial surveys. The highest estimated number was 5,287 individuals, based on survey data from February 2021. Estimation of number of displaced Red-breasted Merganser was maximally between 10 and 65 individuals, estimated on the background of data from the midwinter survey of 2016.

1 Introduction

The Smålandsfarvandet study site consist of a 2,141 km^2 marine area between Langeland, Lolland and Sjælland. In the central, western parts of the area European Energy A/S is planning for an offshore wind farm, Omø Syd Offshore Wind Farm, covering 24.53 km^2. The survey area contains or partly contains six EU Special Protection Areas (SPA), one of which was designated in December 2021 (Smålandsfarvandet). The proposed offshore wind farm lies within this latter SPA.

Aarhus University, DCE – Danish Centre for Environment and Energy was commissioned by NIRAS A/S to collate and analyse aerial survey data of birds present in the area to derive abundance estimates and fine scale distribution maps for selected bird species. Such data enable estimation of potential displacement effects for the selected species. It is beyond the scope of this task to assess biological importance of the found bird distributions and displacements.

This report does not consider the potential level of collision risk from the proposed Omø Syd Offshore Wind Farm.

Visual aerial surveys were conducted in the Smålandsfarvandet region from 1999 to 2021. These 37 surveys comprise data from several projects. During these, two broad transect definitions, i.e. the definition of the width of the transect bands that observations were designated to, were used. For that reason, two different distance sampling analyses (Buckland et al. 2001) were applied, one for each transect definition type, and a spatial analysis using a count model (Hedley & Buckland 2004) for each of the 37 individual surveys.

The following sections describe in turn the survey types (with two differing sets of transect band definitions) and the distance sampling methods applied to them, the spatial analysis framework including model selection, diagnostics, inference, and outputs and lastly the results of the analysis for each species. The appendices consist of an executive summary of methods and a description of the associated data files.

This report was compiled in a collaboration between Aarhus University /DCE and CREEM (Centre for Research into Ecological & Environmental Modelling) at St. Andrews University, Scotland. The analyses from the CREEM group are described in Scott-Hayward &Mackenzie (2022).

2 Material and Methods

2.1 Species selection

Six bird species or species groups have been selected for analysis in this report, namely Red-throated Diver/Black-throated Diver, Red-necked Grebe, Common Eider, Common Scoter, Long-tailed Duck and Red-breasted Merganser. The selection criterion was based on the fact that the proposed Omø Syd Offshore Wind Farm is situated within an SPA, "Smålandsfarvandet". The area has been designated for Common Eider and Red-necked Grebe, which have consequently been included in this analysis. The divers, Red-throated Diver/Black-throated Diver are both on the EU Birds Directive Appendix 1 and present in significant numbers in the study area and have therefore also been included in this analysis. The remaining species of diving ducks, Common Scoter, Long-tailed Duck and Red-breasted Merganser are present in the study area in substantial numbers, and they are therefore included in this analysis.

2.2 Survey Methods

This analysis was based on data from a total of 37 aerial line transect surveys of birds in the Smaalandsfarvand area (Figure 2.1) conducted between September 1999 and August 2021.

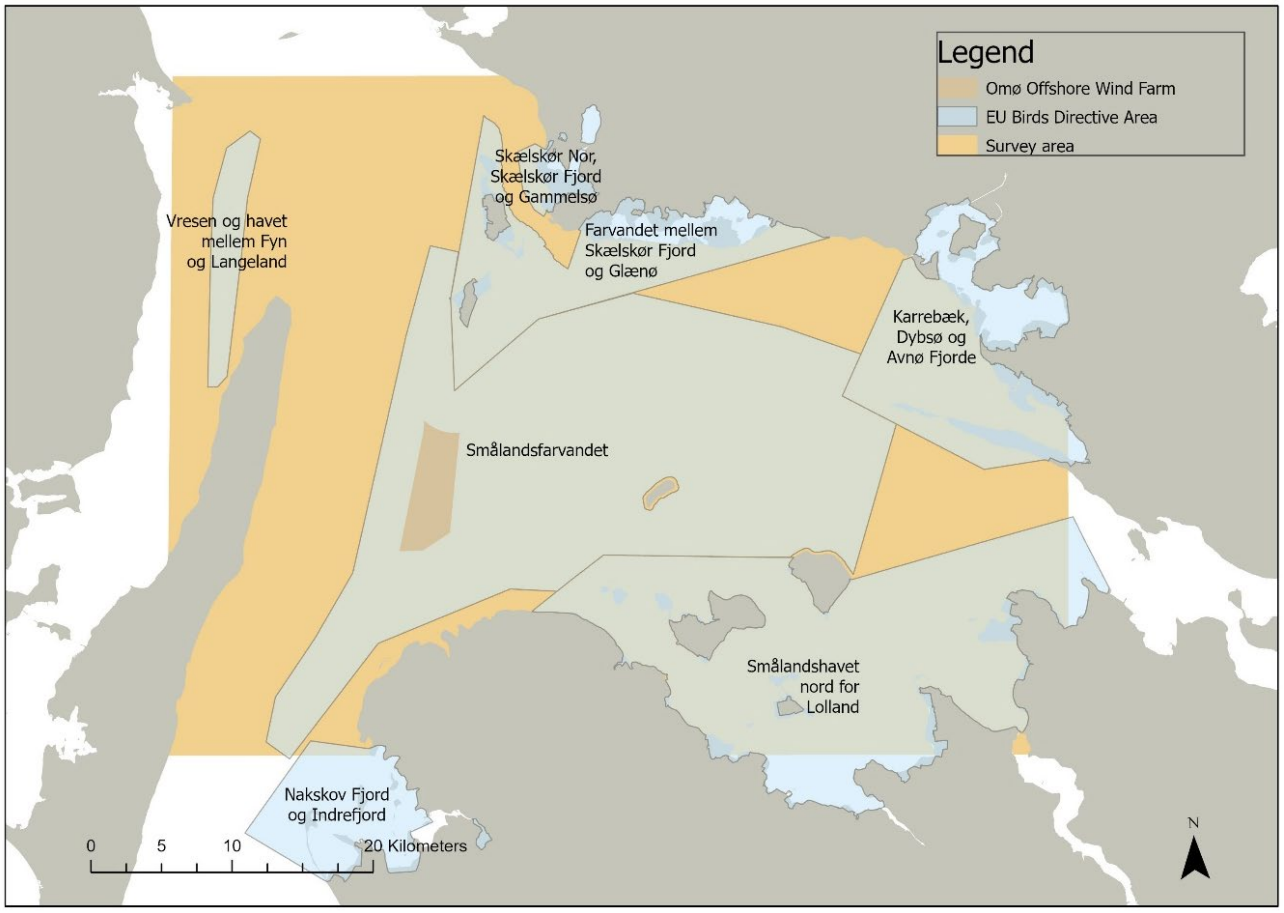

Figure 2.1. The study area in Smaalandsfarvandet. The position of the proposed Omø Syd offshore wind farm and EU Birds Directive areas in the area are indicated.

Visual aerial surveys were used to collect data on seabirds using line transect distance sampling methods (Buckland et al. 2001). During these surveys, trained observers searched for birds, recording birds sitting on the water, flushing and flying into distance bands. These bands were defined in different ways for the data provided by European Energy A/S and are described in detail below.

Transect lines with survey coverage were segmented into approximately 500m long and up to 1000m wide line segments. The bird detections were recorded in three bins (A-C) with cut offs at 44 -163, 163-432 and 432-1000 m and were predominantly observed from both sides of the plane. No band under the plane was recorded.

All latitude/longitude locations were converted to UTMs using UTM Zone 32N. The transects for the surveys are shown in Figure 2.

The number of sightings and segments per survey is presented in Table 2.1.

2.2.1 Data provided with four perpendicular transect bands

The data consists of 9 line transect surveys from October 2013 to April 2015 (Figure 3, DHI 2015, ORBICON 2016). Each transect line was segmented into approximately 500m long segments. In 2013/14 the detections were recorded in four bins (D and A-C) with cut offs at 44, 163, 432, and 1000m and were predominantly observed from both sides of the plane. Transect band D was the inner band under the plane. In 2014/15 the five surveys used a different transect band definition (a, a1, a2, b, c and d). The confusing record of a1 and a2 led to all of the "a" bands being combined to give the same transect band definition as specified above (D, A-C).

All latitude/longitude locations were converted to UTMs using UTM Zone 32N. The transects for the surveys are shown in Figure 2.1 and Figure 2.2.

The number of segments per survey is presented in Table 2.1.

2.2.2 Data provided with three transect bands

This data consists of 7 surveys collected by The National Environmental research Institute, Denmark (NERI, now Aarhus University/DCE) as part of an environmental assessment in the period September 1999 to May 2000 in relation to a proposed Omø Stålgrunde offshore wind farm (Petersen & Clausager 2000), 6 wider scale surveys in 2008, 2012, 2013, 2016, 2018 and 2019 collected by NERI and DCE/Aarhus University as part of the national monitoring programme for birds (NOVANA) (Petersen et al. 2010, Holm et al. 2021, https://novana.au.dk/fugle) and 15 surveys in consecutive months from September 2020 to August 2021, conducted by European Energy A/S (occasionally 2 surveys per month).

Transect lines with survey coverage were segmented into approximately 500m long and up to 1000m wide line segments. The bird detections were recorded in three bins (A-C) with cut offs at 44 -163, 163-432, and 432-1000 m and were predominantly observed from both sides of the plane. No band under the plane was recorded. All data provided by the national monitoring programme used an additional transect band, further away from the survey track

line than the outer "C" band, mentioned above. Data from this transect band outside of the "C"-band was omitted from these analyses.

All latitude/longitude locations were converted to UTMs using UTM Zone 32N. The transects for each of the surveys are shown in Figure 2.2 and Figure 2.3

The number of sightings and segments per survey is presented in Table 2.1.

Table 2.1. Survey dates or periods for each of 37 aerial survey coverages of the Omø Stålgrunde survey area between 1999 and 2021. The data provider is indicated, and the length of the covered survey transect lines ("Coverage") and the number of derived transect segments ("Number of segments") are given.

Period/Date	Data provider	Coverage (Km Transect)	Number of segments
19990902	AU/DCE OWF	285	585
19991111	AU/DCE OWF	281	580
19991216	AU/DCE OWF	297	613
20000214	AU/DCE OWF	284	582
20000312	AU/DCE OWF	285	581
20000418	AU/DCE OWF	284	579
20000523	AU/DCE OWF	283	581
Winter 2008	AU/DCE NOVANA	450	912
Winter 2012	AU/DCE NOVANA	456	920
Summer 2013	AU/DCE NOVANA	435	886
20131010	European Energy A/S	496	1011
20131120	European Energy A/S	491	998
20140308	European Energy A/S	479	977
20140411	European Energy A/S	492	1001
20141030	European Energy A/S	255	525
20141121	European Energy A/S	274	566
20141228	European Energy A/S	274	563
20150309	European Energy A/S	270	552
20150409	European Energy A/S	265	542
Winter 2016	AU/DCE NOVANA	456	922
Summer 2018	AU/DCE NOVANA	455	922
Winter 2019	AU/DCE NOVANA	450	908
20200915	European Energy A/S	276	562
20201012	European Energy A/S	522	1055
20201114	European Energy A/S	446	902
20201127	European Energy A/S	525	1507
20201213	European Energy A/S	525	1055
20210109	European Energy A/S	524	1057
20210201	European Energy A/S	527	1060
20210214	European Energy A/S	526	1058
20210322	European Energy A/S	526	1059
20210414	European Energy A/S	525	1057
20210427	European Energy A/S	524	1055
20210515	European Energy A/S	524	1053
20210616	European Energy A/S	526	1061
20210709	European Energy A/S	526	1056
20210812	European Energy A/S	525	1059

-

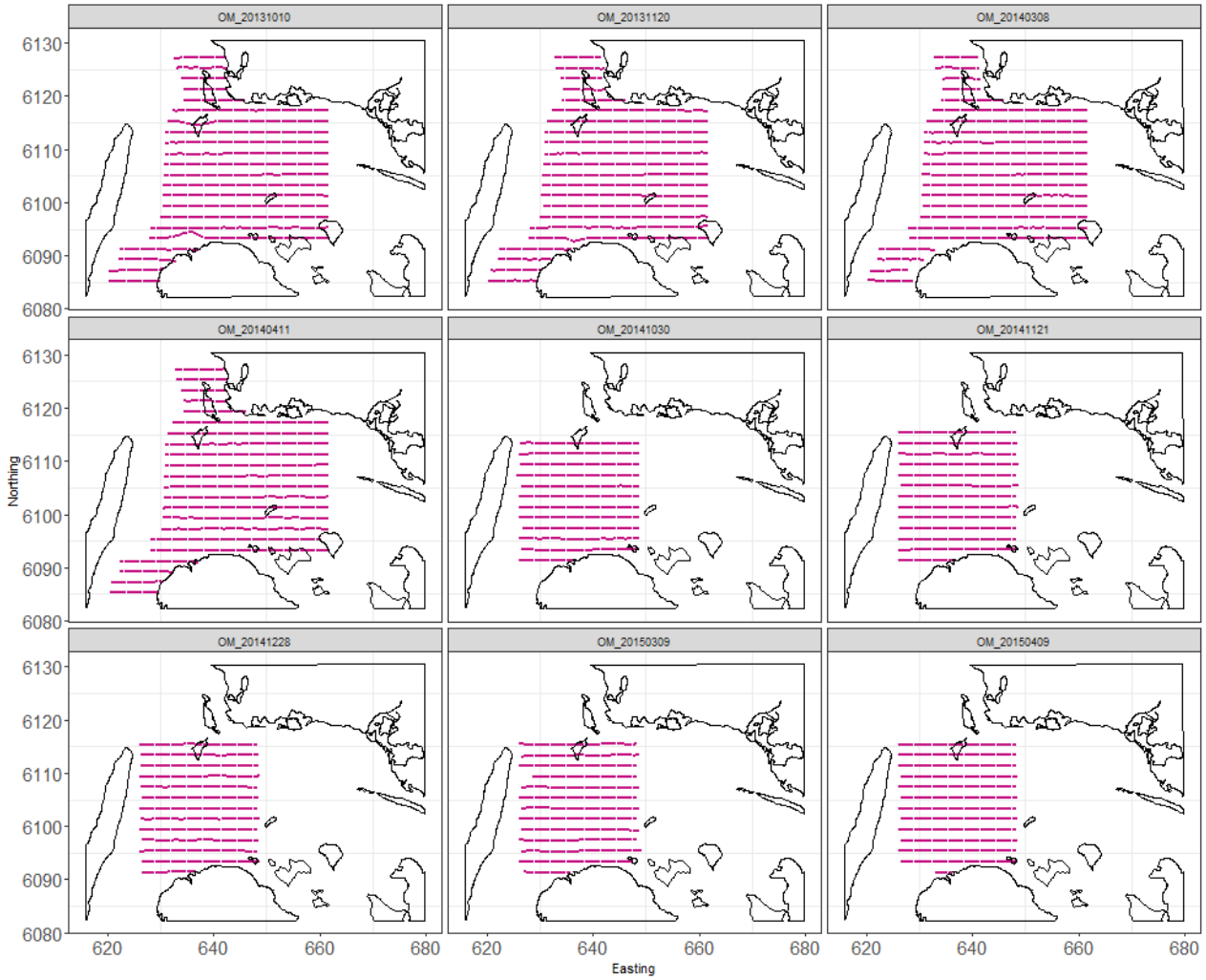

Figure 2.2. Survey effort of the European Energy surveys between 2013 and 2015. The purple dots represent each segment of effort.

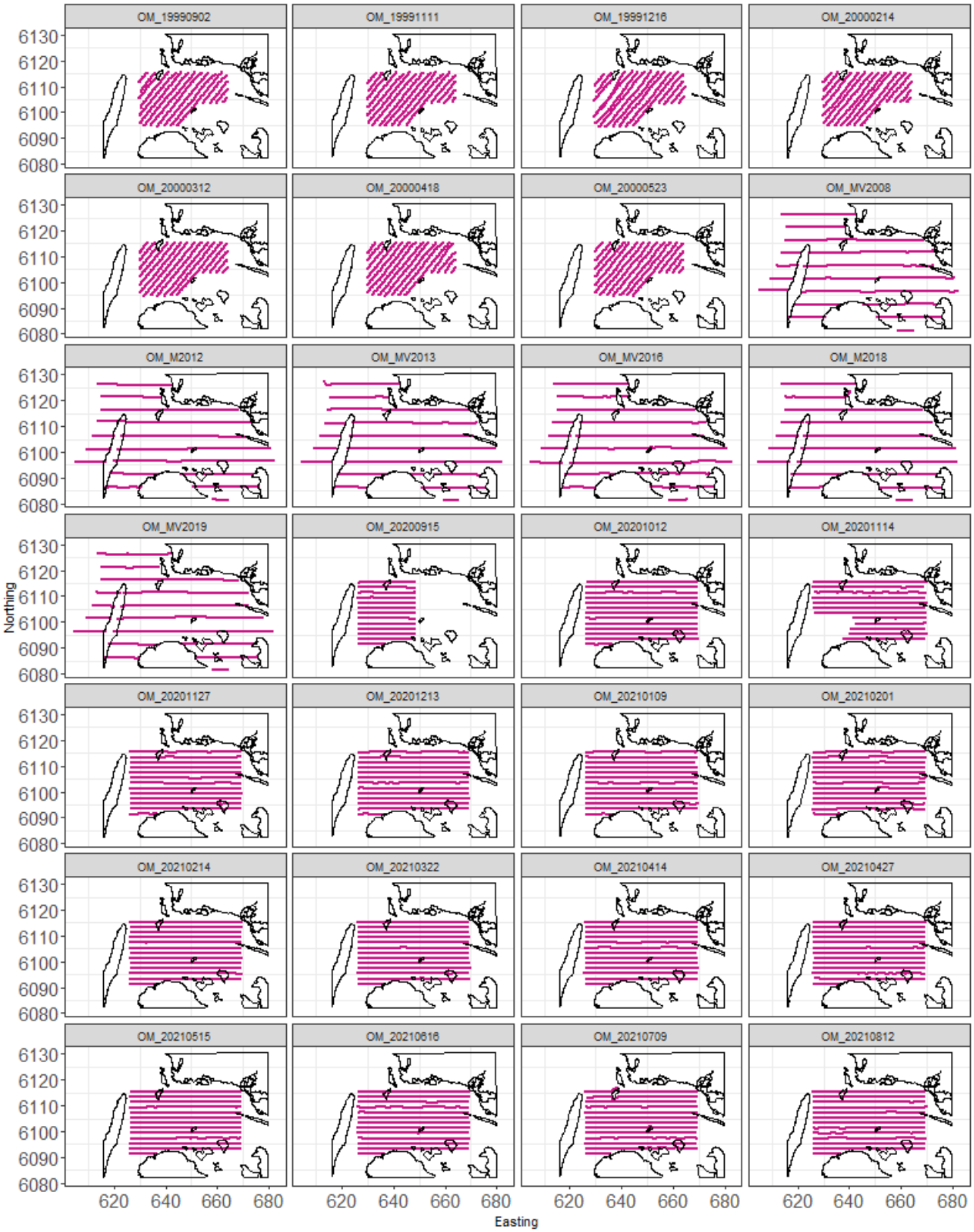

Figure 2.3. Survey effort of the Aarhus University surveys. The purple dots represent each segment of effort.

2.3 Distance Sampling Analysis

Distance sampling analyses were conducted for each of the species/species groups by pooling the information from each survey in the two categories, "Aarhus" or "European Energy A/S".

When fitting detection functions, the effects of covariates, other than perpendicular distance, are incorporated into the detection function model (Multiple Covariate Distance Sampling, MCDS). In these cases, the probability of detection becomes a multivariate function, $g(y; v)$, which represents the probability of detection at perpendicular distance y and covariates,v ($v = v_1 \ldots v_Q$, where Q is the number of covariates). In this study, using a half-normal detection function ($e^{(-y^2/\sigma^2)}$) the covariates were incorporated via the scale term, σ, where for sighting j, σ has the form:

$$\sigma_j = \exp\left(\beta_0 + \sum_{q=1}^{Q}(\beta_q v_{jq})\right)$$

where β_0 and β_q (q = 1 … Q) are parameters to be estimated[1]. Both half-normal and hazard rate detection functions were fitted with AIC used to choose between the two models. The candidate variables trialled were bird group size, sea state, glare, behaviour and season (see Table 2.2). Observations with sea states greater than four were removed. The seasons are defined in Table 2.3.

Table 2.2. Table detailing the covariates used in the detection function fitting.

Covariates	European Energy Values	Aarhus University Values
Sea State	0, 1, 2, 2.5, 3 (calm to rough)	0, 0.5, 1, 1.5, 2, 2.5, 3 (calm to rough)
Glare	-	1 (full sun), 2, 3 (cloudy)
Behaviour	S (sitting or diving) and F (flying or flushing)	S (sitting or diving) and F (flying or flushing)
Season	Autumn, Wintering, Spring	Autumn, Wintering, Spring, Moulting

Table 2.3. Table specifying the date ranges of the seasons.

Season	Date Range
Moulting	15th June – 14th September
Autumn	15th September – 14th November
Wintering	15th November – 28th February
Spring	1st March – 14th June

2.4 Spatial Analysis Framework

The following sections describe the modelling methods employed for this analysis and a description of the outputs that follow. For a high-level executive summary of the methods please see Appendix A.

2.4.1 Model Framework

The response variable for the spatial models are bird counts in a small area (segment) that have been corrected for detectability. Thus, the response was modelled using a quasi-Poisson framework, with estimated (over)dispersion. A set of candidate explanatory variables were associated with each segment. In this study, each survey was analysed separately so there were no discrete temporal variables to trial. Two continuous (one-dimensional) covariates

were available; bathymetry (Figure 2.4) and distance to coast (Figure 2.5). To account for localised surface patterns (because of unmeasured covariates) a spatial surface was also fitted to each model. Specifically, a two-dimensional CReSS-based surface using a Gaussian radial basis function, was included in the model.

As an illustration, the following equation represents an example of a Poisson model fitted with year as a temporal variable and a one-dimensional smooth term (e.g., bathymetry) alongside a two-dimensional spatial smooth:

$$y_{ijt} = Poisson(\mu_{ijt})$$

$$\mu_{ijt} = e^{(\beta_0 + \beta_1 Year + s_1(Bathymetry_{ijt}) + s_2(XPos_{ijt}, YPos_{ijt}))}$$

where y_{ij} is the estimated count for transect *i* segment *j* and s_1 represents a quadratic *B*-spline smooth of bathymetry and s_2 is a two dimensional smooth of space (with coordinates $XPos$ and $YPos$ in UTMs). Implicit in this model are also coefficients for the intercept (β_0), year (β_1) and any quadratic *B*-spline based coefficients associated with the smooth terms. The effort associated with each observation varied depending on the associated segment area and so segment area was included as an offset term (on the log scale).

In addition to the temporal variables, both a globally applicable bathymetry term and a more nuanced spatial term were trialed for inclusion in each model, to indicate how best to model spatial patterns in each case. In particular, this helped signal if any spatial patterns were sufficiently described by a (one-dimensional) depth metric (which applies the same across the surface determined solely on the depth) or if a more considered approach to spatial patterns was required for each survey.

For example, if bathymetry was selected and a two-dimensional spatial element was *not* deemed necessary (as determined by the model selection procedure governed by objective fit criteria) then this signals that any spatial patterns are primarily a function of the depth, regardless of the geographical location of this depth in the survey area.

If the two-dimensional spatial term was selected for inclusion in a model, then the spatial density patterns (over and above any depth-related terms) were accommodated using a spatially adaptive term which permits different amounts of flexibility across the surface in a parsimonious way (hence, relatively complex spatial patterns can be accommodated with very few parameters).

Selection between competing models was undertaken using a 10-fold cross validation metric, whilst preserving any within-transect correlation via the appropriate blocking structures.

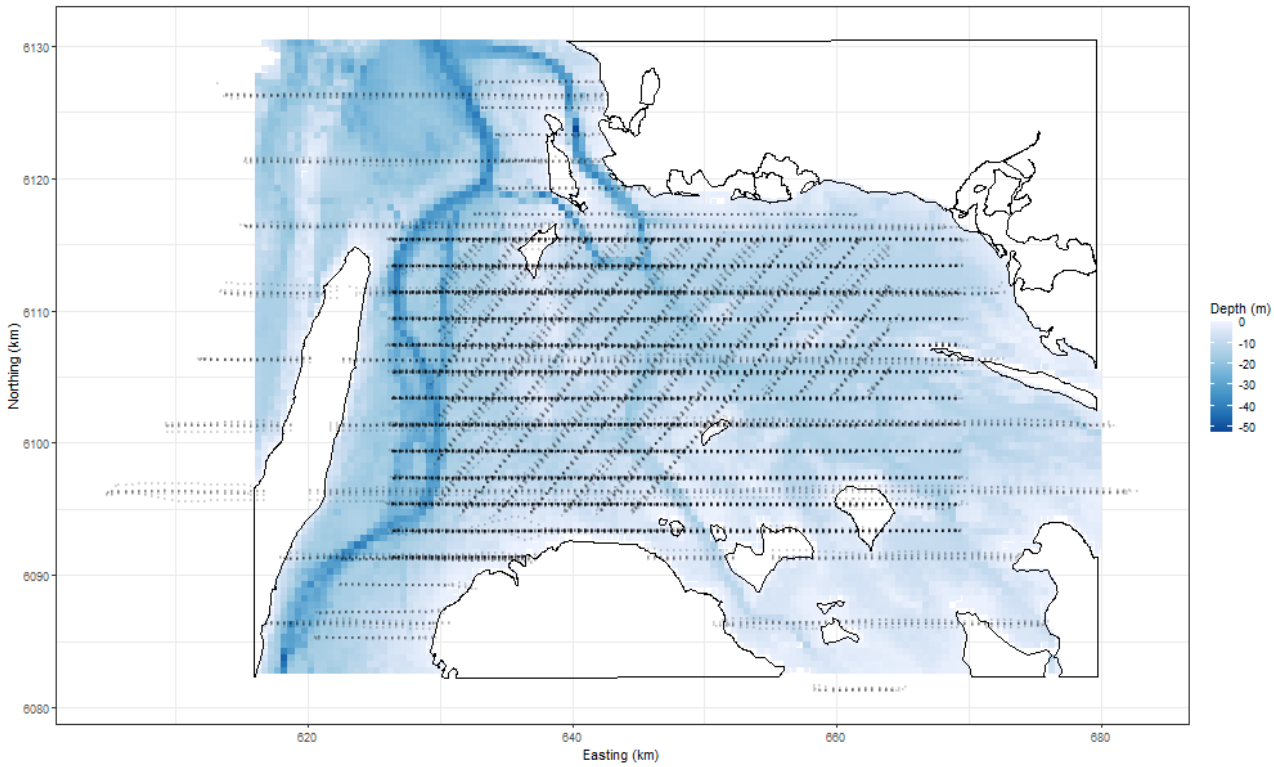

Figure 2.4. Visual representation of bathymetry. The black and grey dots represent survey effort from all of the survey effort.

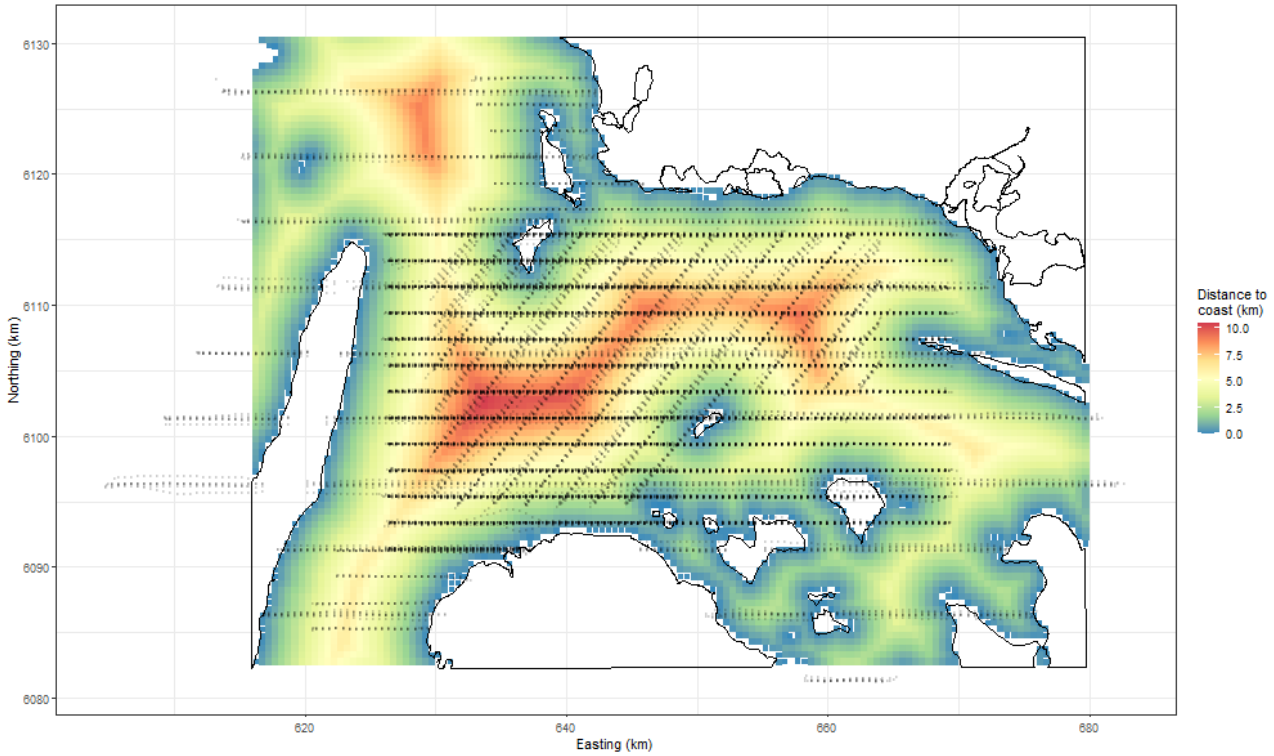

Figure 2.5. Visual representation of distance to coast. The black and grey dots represent survey effort from all of the surveys.

2.4.2 Model specification, selection and fitting

CReSS-SALSA based spatially adaptive generalized additive models, with targeted flexibility, were fitted to data from each survey to allow for non-linear relationships between the one-dimensional and two-dimensional covariates and the response (Scott-Hayward 2013, Scott-Hayward et al. 2014, Walker et al. 2010).

Depth and distance to coast were permitted to have a linear or nonlinear relationship with the response in each case, and when a smooth term was included in a model it was specified to be a quadratic (degree 2) *B*-spline and permitted to exhibit flexibility (dictated by the degrees of freedom and bounded by 3 and 5; df=[3,5]) underpinned by objective fit criteria. The degrees of freedom for these terms determine the flexibility of these smooth (and nonlinear) relationships - the more degrees of freedom, the more flexible the relationship can be. The location of this flexibility (along the x-axis) in these terms (e.g., bathymetry) was also determined as part of the model selection process. This permitted the relationship in some areas of the covariate range to be relatively complex (e.g., in shallow waters) and the relationship in other areas (e.g., in deep waters) to be relatively simple.

The spatial patterns in each analysis were based on a two-dimensional spatial term (of variable complexity). The flexibility of the spatial element constituted part of the model selection procedure and for each survey was determined using a Spatially Adaptive Local Smoothing Algorithm (SALSA[3,4]). While this model selection element technically occurred between limits (df=[2,100]), the flexibility chosen in each case was not bounded in practice by those values since the selection procedure occurred well within the bounds of the specified range.

The MRSea R package, designed to fit both CReSS (Scott-Hayward et al, 2019a, 2019b) and SALSA type models, was used for model fitting and a 10-fold cross-validation (CV) procedure was used to govern all model selection elements. The CV procedure attempts to balance the fit to data unseen by the model while minimising the number of parameters (parsimony) and was used to determine which terms to include in each model and the extent of the flexibility exhibited by each term for those selected. Note, this cross validation was predicated on preserving correlated blocks of survey data (transect lines) so that any residual autocorrelation present was not disrupted when choosing folds. This was considered necessary to ensure independent sampling units under the scheme.

Parameter inference

The response data were collected along survey lines in sequence, and so consecutive observations are likely to be correlated in space and time (i.e., points close together in space and/or time are likely to be more similar that points distance in time and/or space). Further, the covariates included in the model are unlikely to explain these patterns in full and so some elements of these patterns are likely to remain in model residuals. These patterns are a violation of residual independence (which underpin traditional model approaches such as Generalized Additive Models) and thus robust standard errors were routinely used as part of the MRSea modelling framework to account for residual autocorrelation.

Uncertainty about model parameter estimates proceeded via robust standard errors due to the nature of the survey procedure. These essentially work by inflating the standard errors (which would normally be obtained under traditional approaches) in relation to the positive correlation observed within prespecified blocks of residuals. In cases, where this residual correlation is minimal, the adjustments are small, and when the correlation is more extreme, the inflation is larger.

A transect-based blocking structure was used to reflect potential correlation within blocks while independence (i.e., no correlation) between blocks was assumed. To ensure this assumption was realistic, the decay of any residual correlation to zero (i.e., independence) with the distance between points (within blocks along transects) was assessed visually. Specifically, transects in each survey were used as the blocking structure and an Auto Correlation Function (ACF) plot on this basis was used to check the suitability of this blocking structure, via a 'decay to zero' trend within blocks.

2.4.3 Modelling diagnostics

To assess the adequacy of model fit in each case, a range of diagnostic measures were used.

The assumed mean-variance relationship under the model was assessed visually using plots of the fitted values from the model against the variance of the residuals. In this example, quasi-Poisson models were employed which assume a proportional mean-variance relationship; $V(Y) = \varphi V(\mu) = \varphi\mu$, where φ is known as the dispersion parameter. The dispersion parameter was estimated for each model and this estimate was used in the visual assessment of this mean-variance relationship assumed to hold under the model.

Pearson residuals for each model were also visualised spatially to ensure there were no areas of consistent bias across the survey area, which would be indicated by clusters of negative or positive residuals in spatially similar locations.

Residual independence was not assumed to hold under the model and instead model inference proceeded under robust standard errors. As described, Auto Correlation Function (ACF) plots were instead used to check the suitability of this blocking structure, via a 'decay to zero' trend within blocks and are available for inspection, on request.

2.4.4 Model Predictions and estimates of uncertainty

Predictions of counts based on each selected model were made to a grid of points (each point representing a 500m^2 grid cell) across the study region. As the survey transects all covered slightly differing areas and to prevent wild extrapolation, predictions were made only to a convex hull around each set of individual survey data. Abundance within the survey-based prediction region was obtained by summing the grid cell counts.

The uncertainty in these predictions was comprehensively quantified using a parametric bootstrap on the spatially adaptive model. The parametric bootstrap process samples the parameter estimates using the robust variance-covariance matrix from the spatial model to generate 500 sets of bootstrapped predictions. From these 95 percentile-based intervals for abundance estimates and a coefficient of variation were obtained for each grid cell. For surveys with visual aerial counts, these percentile-based intervals also include the uncertainty associated with detection function estimation, also generated via a bootstrap method.

A calculation of 'persistence' was also undertaken across the two data types using the geo-referenced estimates of density (abundance/associated area) across the survey area. The persistence estimation describes the importance of a grid cell in relation to a given species over multiple data sets. Persistence

scores were calculated for every grid cell in the following way: Each bootstrap replicate was allocated a binary value based on whether, or not, the estimate in each location was above the mean estimated density (1) throughout the survey area or below this mean estimated density (0). This was performed for all 500 sets of plausible predictions in each grid cell (based on the bootstrap replicates) and the proportion of these bootstrap predictions in excess of the mean (indicated by the value of 1) was calculated for each grid cell to give a persistence score for that location. A persistence score of 1 indicates that the density in that grid cell was estimated to be above average in every bootstrap replicate in every survey (so uniformly above the mean; high persistence) while a value of 0.1 indicates that just 10% of the estimates were above the estimated mean, and thus indicates low persistence in that location. Where possible, persistence maps were made for (1) the portion of the study region covered by ALL surveys, (2) the portion of the study region covered by all the large-scale surveys and (3) the portion of the study region covered by the 2020-2021 consecutive surveys.

2.5 Windfarm Area Assessment

2.5.1 Impact Scenarios

Impact scenarios for each of the selected bird species and relating to the proposed windfarm footprint were evaluated for each of the surveys from 2012 onwards. The scenarios for each species are given in Table 2.4 and were imposed on the predictions for each survey. The percentage change in abundance was applied to the footprint region with a linear trend returning to the existing abundances from the footprint edge to some buffer distance. There was no re-distribution to the surrounding areas of the birds "lost" under the impact scenario. The scenario was imposed on every set of bootstrap predictions (500 sets) to calculate the density of birds in the footprint plus buffer area before and after the change along with percentile-based 95% confidence intervals. Additionally, the change in density was calculated.

Table 2.4. Table detailing the impact scenarios for each species. A negative percentage indicates a decline in abundance and a positive one indicates an increase in abundance.

Species	Scenario 1		Scenario 2	
	Percentage Change	Buffer (km)	Percentage Change	Buffer (km)
Diver	-80	16		
Red-necked Grebe	-80	10	-50	5
Common Eider	-25	2	-25	1
Common Scoter	-50	5		
Long-tailed Duck	-50	2		
Red-breasted Merganser	-30	2		

The selection of displacement scenarios is based on data from literature. For the divers we used a scenario where the density within the footprint of the wind farm was reduced by 80 % and with a gradually reduced effect out to a distance of 16 km from the periphery of the wind farm. This was based on Petersen et al. (2014), Mendel et al. (2019) and Heinäien (2020). For Common

Scoter we used a 50 % reduction within the footprint of the wind farm and a gradually reduced effect out to 5 km distance from the periphery of the wind farm. This was based on Petersen et al. (2014). For Long-tailed Duck we used a scenario where density was reduced by 50 % within the footprint of the wind farm, and a gradually reduced effect out to 2 km from the periphery of the wind farm. This was based on Petersen et al. (2011). To our knowledge, there is no available empirical data on the displacement effect of Red-necked Grebe, Common Eider and Red-breasted Merganser from offshore wind farms greater than a single line of turbines. The displacement scenarios for those species are therefore based on estimations. For Red-necked Grebe and Common Eider two scenarios were used, a scenario assumed to be worst case and one assuming les displacement. For Common Eider the scenario with 25 % reduced density of birds within the footprint of the wind farm and a gradually reduced effect out to 2 km distance from the periphery was also used in ornithological assessments of proposed wind farms in Lillebælt Syd, Aflandshage and Nordre Flint Offshore Wind Farms.

3 Results

3.1 Red-throated Diver/Black-throated Diver *Gavia stellata/ Gavia arctica*

3.1.1 Analysis

Detection function from data with four transect bands

The average probability of sighting diver sp. was estimated to be 0.17 (CV=0.07). This probability was estimated using a hazard-rate detection function and no covariates (Figure 3.1).

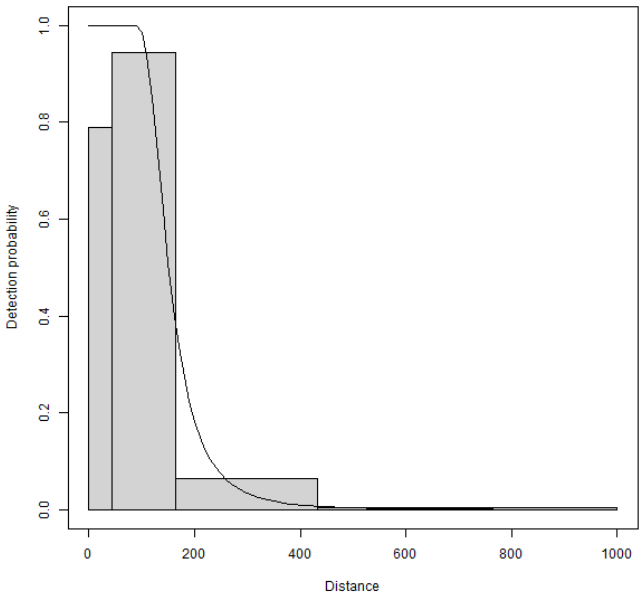

Figure 3.1. Figure showing the estimated detection function for Red-throated/Black-throated Diver. The histograms are the distances of the observed sightings.

3.2 Detection function from data with three transect bands

The average probability of sighting diver sp. was estimated to be 0.37 (CV=0.08). This probability was estimated using a half normal detection function and no covariates (Figure 3.2). There were no sightings in transect band C.

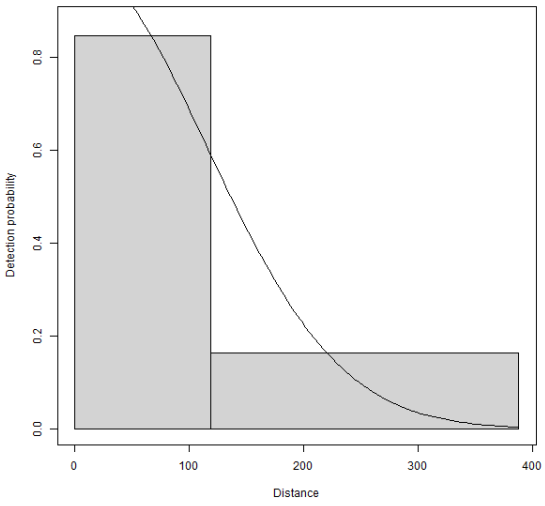

Figure 3.2. Figure showing the estimated detection function for Red-throated/Black-throated Diver. The histograms are the distances of the observed sightings.

3.2.1 Spatial analysis

The two datasets were combined for the spatial analysis and contained 31,512 segments, 1.5% of which were segments containing Red-throated/Black-throated Diver sightings. Figure 3.3 shows the distribution of the distance corrected counts for all 37 surveys. Seven of the 37 surveys had zero observations and a further 20 had too few observations for a spatial analysis to be conducted (less than 12 observations).

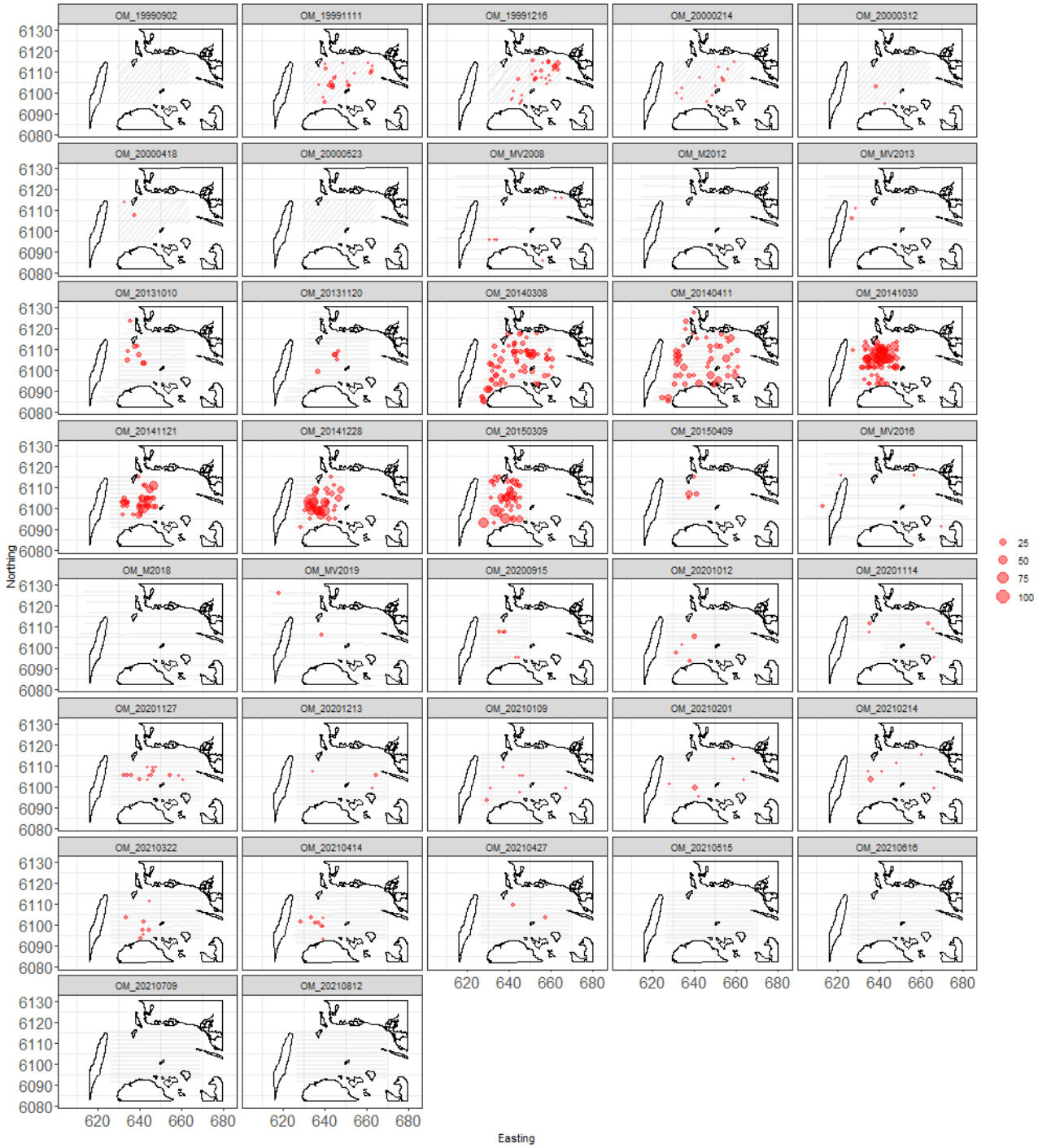

Figure 3.3. Counts for the Red-throated/Black-throated Divers across the 37 surveys. The red circles indicate the distance-corrected counts along the transect lines while the polygons represent land. Grey dots are segments with a count of zero.

3.2.2 Model Selection results

Only 10 surveys had sufficient observations to enable a fitted model (e.g., n>10) and while each model selected included a spatial term of typically low complexity (2-5 parameters), the depth and distance to coast covariates (either as a linear or smooth term) were not selected for any of the survey-based models. This shows that while there was compelling evidence for non-uniform spatial patterns in each survey, there was no evidence for a depth or distance to coast based over and above these terms (Table 3.1).

The estimated abundances and associated 95 percentile confidence intervals for each survey with sufficient data for a spatial modelling analysis are given in Table 3.2 while the equivalent values for density and a visual representation of these estimates (with associated uncertainties) are shown in Figure 3.4.

Table 3.1. Model selection results for Red-throated/Black-throated Divers for each survey. The Variables column represents the terms in the model while the 'degrees of freedom' column indicates the number of parameters allocated to each smooth term. The extra-Poisson dispersion parameter estimates are listed in the far-right column. Empty cells indicate too few observations for the spatial analysis, e.g. n=12.

Year	Month	Survey	Variables	Degrees of freedom	Dispersion parameter estimate
1999	09	OM_19990902	-		
	11	OM_19991111	s(x.pos, y.pos)	4	4.28
	12	OM_19991216	s(x.pos, y.pos)	2	6.08
2000	02	OM_20000214	s(x.pos, y.pos)	2	2.68
	03	OM_20000312	-		
	04	OM_20000418	-		
	05	OM_20000523	-		
2008	01/02	OM_MV2008	-		
2012	08/09	OM_MV2012	-		
2013	01	OM_MV2013	-		
2013	10	OM_20131010	-		
	11	OM_20131120	-		
2014	03	OM_20140308	s(x.pos, y.pos)	8	13.81
	04	OM_20140411	s(x.pos, y.pos)	4	14.80
	10	OM_20141030	s(x.pos, y.pos)	4	20.33
	11	OM_20141121	s(x.pos, y.pos)	6	11.26
	12	OM_20141228	s(x.pos, y.pos)	2	32.89
2015	03	OM_20150309	s(x.pos, y.pos)	2	24.08
	04	OM_20150409	-		
2016	01	OM_MV2016	-		
2018	07	OM_M2018	-		
2019	12	OM_MV2019	-		
2020	09	OM_20200915	-		
	10	OM_20201012	-		

	11	OM_20201114	-		
	11	OM_20201127	s(x.pos, y.pos)	5	1.38
	12	OM_20201213	-		
2021	01	OM_20210109	-		
	02	OM_20210201	-		
	02	OM_20210214	-		
	03	OM_20210322	-		
	04	OM_20210414	-		
	04	OM_20210427	-		
	05	OM_20210515	-		
	06	OM_20210616	-		
	07	OM_20210709	-		
	08	OM_20210812	-		

Table 3.2. Estimated density of Red-throated/Black-throated Divers for each survey. The 95% CI are percentile-based confidence intervals. The area is the area of the prediction region (convex hull around the data).

Year	Month	Survey	Area (km^2)	Estimated Count	95% CI Count	Estimated Density	95% CI Density
1999	11	OM_19991111	585	247	(142,454)	0.4	(0.2,0.8)
	12	OM_19991216	617	391	(168,5688)	0.6	(0.3,9.2)
2000	02	OM_20000214	591	98	(46,239)	0.2	(0.1,0.4)
2014	03	OM_20140308	1071	1005	(436,1952)	0.9	(0.4,1.8)
	04	OM_20140411	1071	906	(415,1373)	0.8	(0.4,1.3)
	10	OM_20141030	474	1321	(487,2636)	2.8	(1,5.6)
	11	OM_20141121	507	504	(213,950)	1	(0.4,1.9)
	12	OM_20141228	507	758	(279,1920)	1.5	(0.6,3.8)
2015	03	OM_20150309	515	633	(270,1147)	1.2	(0.5,2.2)
2020	11	OM_20201127	968	146	(77,349)	0.2	(0.1,0.4)

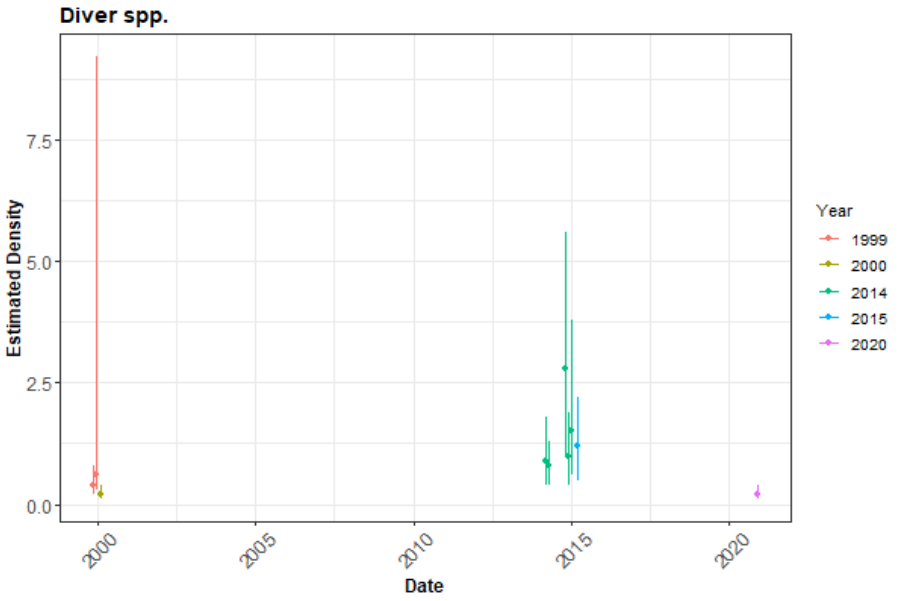

Figure 3.4. The estimated density of Red-throated/Black-throated Divers for each survey. The 95% CI are percentile-based confidence intervals are from a parametric bootstrap with 500 replicates. Densities are presented rather than counts as the study area for each survey is different.

3.2.3 Spatial Results

Figure 3.5 shows the estimated counts of Diver species in each 500x500 m grid cell for each survey. Generally, the estimated abundances fit well to the raw data and there are no concerning departures. The common scale applied to all surveys makes it difficult to see the underlying structure of the fitted surfaces in detail however, output CSV files are provided for all predictions and individual survey-based estimated surface plots are available in the file "extraplots-divers.docx".

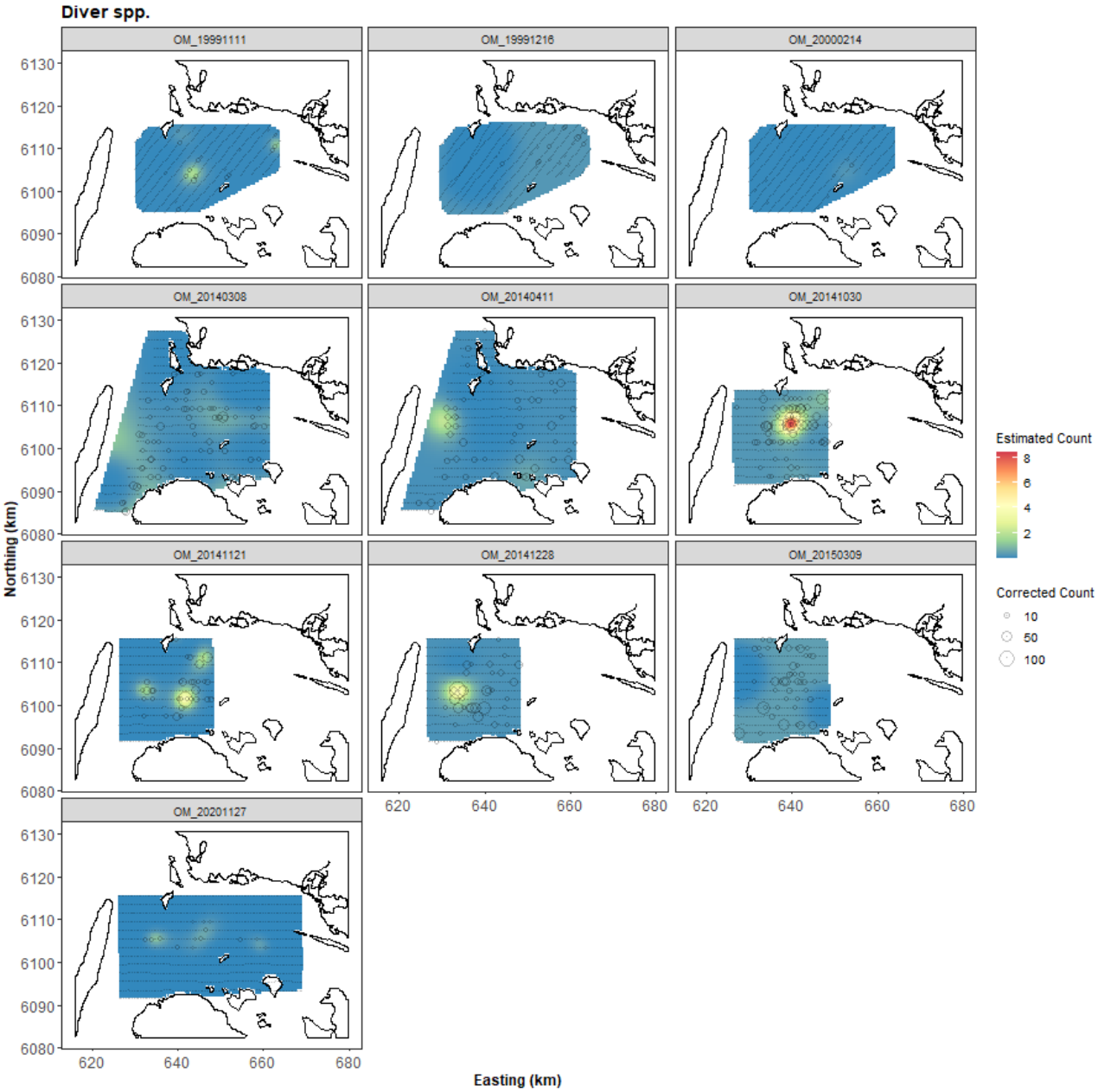

Figure 3.5. Figure showing the estimated Red-throated/Black-throated Diver abundance across the study site for each of the surveys. The title of each subfigure after the underscore ("OM_") details the survey year (4 digits), survey month (2 digits) and day (2 digits). The estimated counts are per 500x500m grid cell. The open circles show the observed corrected count. The coloured graphics represent the predicted values in each location.

3.2.4 Uncertainty in the spatial predictions

The highest coefficient of variation (CoV) scores was associated with the very smallest predictions, however it is known that the CoV metric is highly sensitive to any uncertainty for very small predictions. There was no material overlap between high values of the CoV metric and the transect lines/locations with non-zero counts and therefore results in no concerns in this case (Figure 3.6 and Figure 3.7).

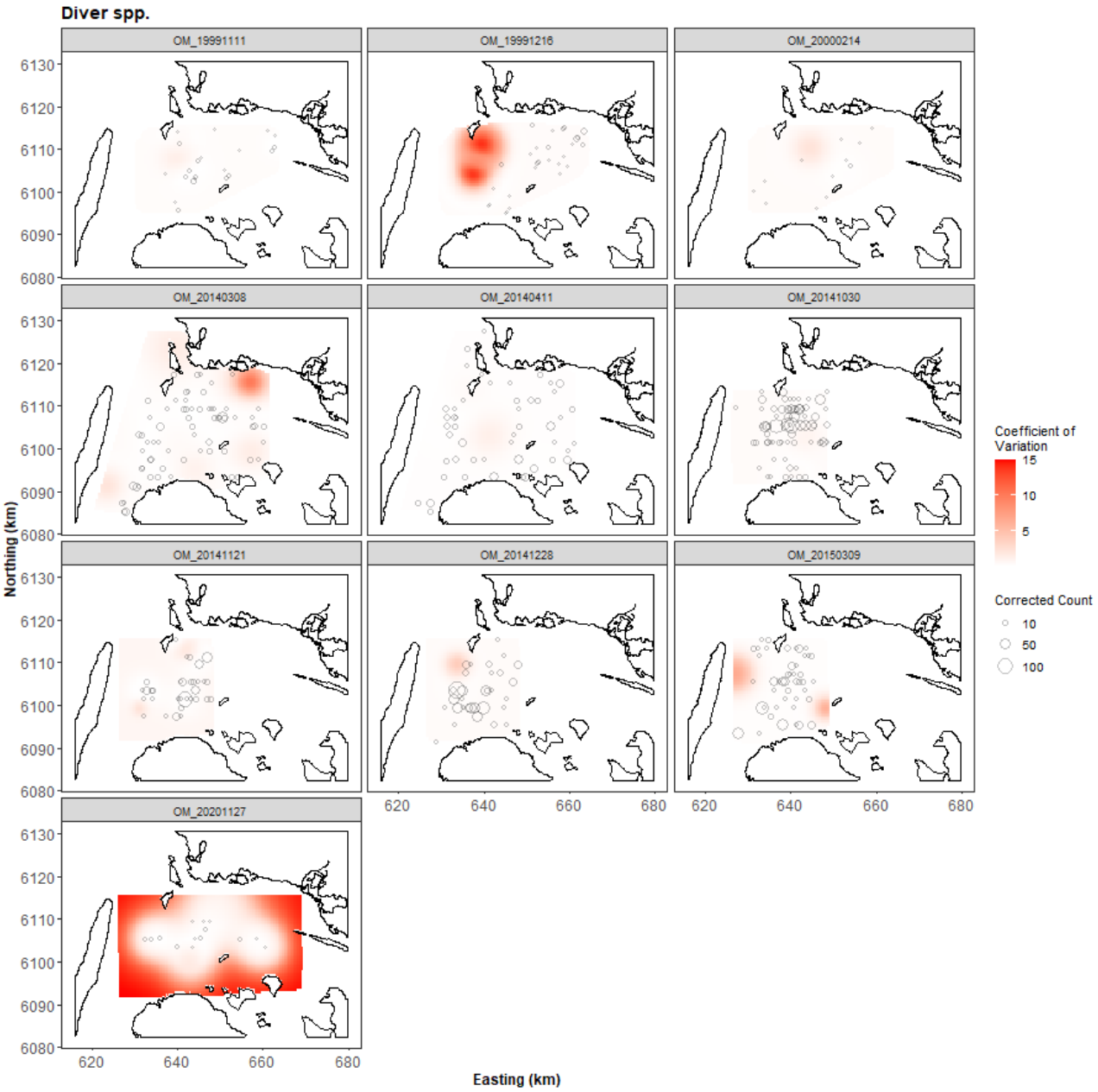

Figure 3.6. Figure showing the coefficient of variation across the study region for each of the surveys. The open circles show the distance corrected counts, where applicable. The presence of dark red CV scores in areas with virtually zero predictions are an artifact of the very small prediction rather than of any notable concern.

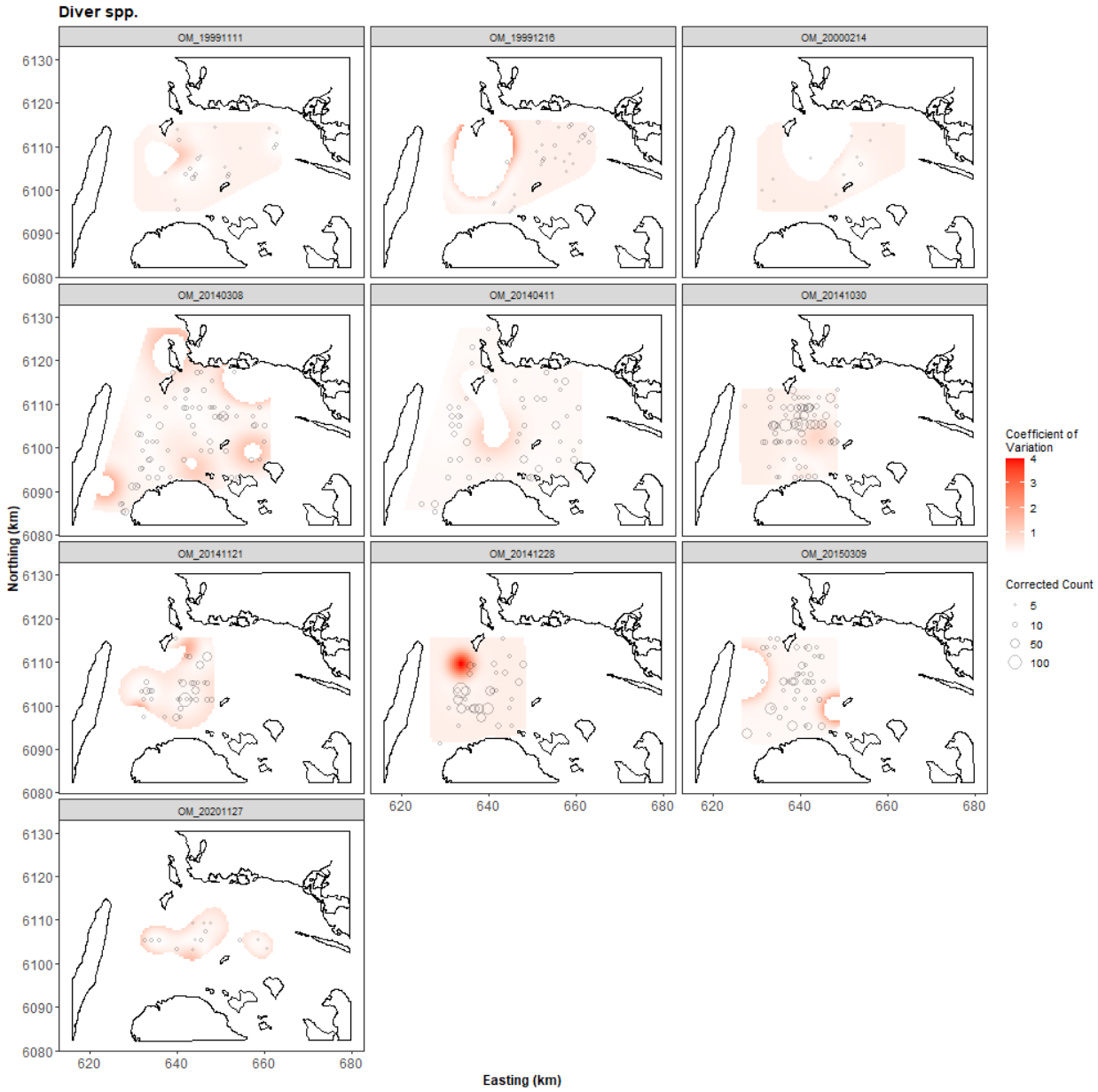

Figure 3.7. Figure showing the coefficient of variation across the study region for each of the surveys with a threshold applied to account for the very small predicted values. The open circles show the distance corrected counts, where applicable. The presence of dark red CV scores in areas with virtually zero predictions are an artifact of the very small prediction rather than of any notable concern.

3.2.5 Model Diagnostics

A blocking structure was used to account for potential residual non-independence for each model and a robust standard error approach was based on unique transects. In each case, we saw a reassuring decay to zero implying that an appropriate blocking structure was used.

The assumed mean-variance relationship was examined and generally showed agreement between the assumed (red) lines and the observed values. However, in some cases the residuals for the largest fitted values were in practice more variable than that assumed (above the line) suggesting that the variance is underestimated for these. There were no systematic clusters of negative or positive residuals for the 10 surveys and thus represent good agreement between the data and the model. The individual diagnostic plots are available on request.

3.2.6 Areas of Persistence

Across all surveys, there is evidence of moderate persistence in the central and north-eastern part of the reduced survey area (the area indicated in Figure 3.8), and very low persistence towards the north-west and south-eastern edge of the survey area (Figure 3.8). This moderate persistence (~0.6) also appears in the northern part of the proposed wind farm footprint, with slightly decreased persistence (~0.45) in the southern area of the proposed footprint. High persistence values indicate area that is consistently important to the species across multiple surveys.

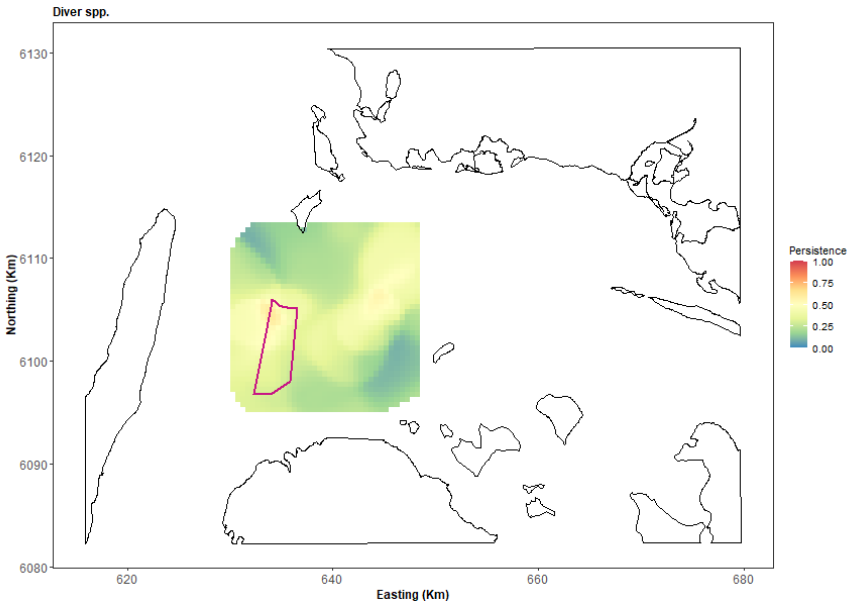

Figure 3.8. Persistence scores for Red-throated/Black-throated Diver across the persistence for survey data for all surveys. Due to insufficient data, there was insufficient models to further partition the persistence maps into smaller subsets. The area of the proposed offshore wind farm is indicated (polygon with red outline).

3.2.7 Impact Scenarios

The impact scenario for divers was an 80% decline in the footprint of the proposed wind farm with a linear return to no change in a 16 km buffer. This led to an estimated reduction in bird abundances which amounted to a maximally between 297-1246 birds in line with the densities predicted under each survey-specific model (Table 3.3). Figure 3.9 shows an example scenario based on one of the bootstrap replicates and a large-scale survey (OM_20140411).

Table 3.3. Table showing the effect of scenario 1 implementation on Red-throated/Black-throated Diver numbers in the proposed wind farm footprint and buffer regions. "Area" is the area in km^2 of the available prediction cells in the footprint + buffer area for each survey (2012 onwards). "95% CI Expected Impacted Birds" is the after abundance minus the before abundance. "95% CI" figures represent the 95 percentile-based confidence intervals for each estimate.

Survey	Area (km^2)	Density Before	95% CI Before	Density After	95% CI After	95% CI Expected Impacted Birds
OM_20140308	747.9	1.18	(0.56, 1.63)	0.66	(0.31, 0.92)	(-539, -187)
OM_20140411	746.4	0.89	(0.45, 1.17)	0.48	(0.24, 0.64)	(-400, -158)
OM_20141030	473.8	2.83	(1.13, 4.68)	1.26	(0.5, 2.11)	(-1246, -297)
OM_20141121	507.3	1.01	(0.45, 1.56)	0.51	(0.23, 0.8)	(-388, -114)
OM_20141228	506.8	1.53	(0.66, 2.99)	0.57	(0.23, 1.17)	(-916, -213)
OM_20150309	514.6	1.21	(0.55, 2.15)	0.59	(0.27, 1.01)	(-579, -146)
OM_20201127	590.2	0.23	(0.15, 0.39)	0.11	(0.07, 0.19)	(-116, -45)

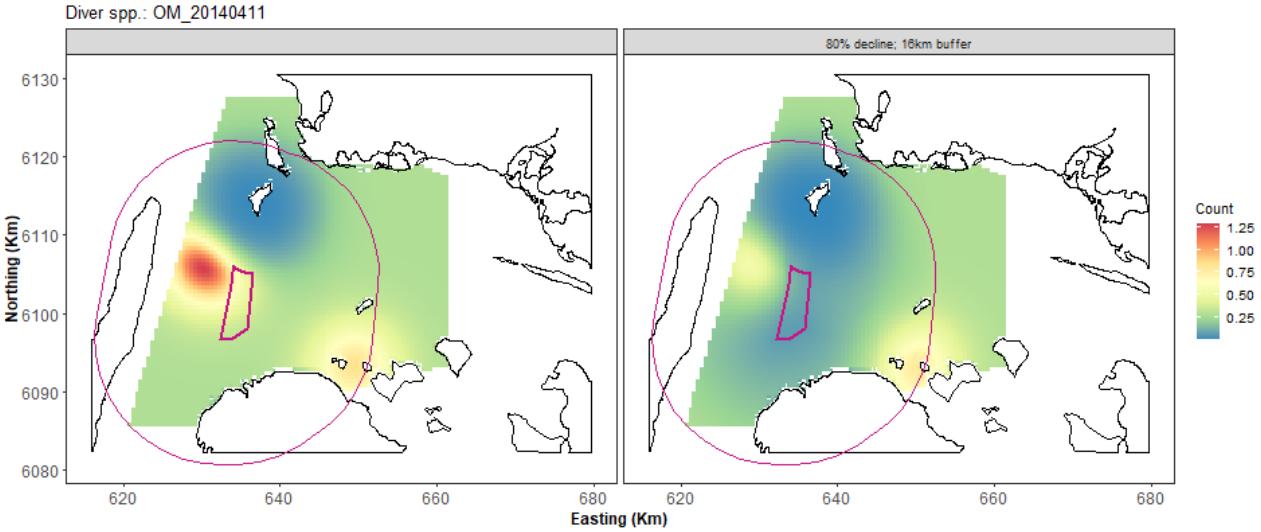

Figure 3.9. Example of scenario for Red-throated/Black-throated Diver. On the left is one of the estimated bootstrap predictions from the OM_20140411 model. On the right is the same set of predictions but with the scenario imposed. The footprint is shown by the thick purple line and the buffer the thinner purple line.

4 Red-necked Grebe *Podicept griseigna*

4.1 Distance Analysis

For both survey types there were too few observations in the band under the plane (D) and the outer bands (B/C) to allow for a distance analysis. For this reason, we assumed band A to be a strip transect with perfect detection.

4.2 Spatial analysis

The two datasets were combined for the spatial analysis and contained 31512 segments, 1.6% of which were segments containing red-necked grebe sightings. Figure 4.1 shows the distribution of the distance corrected counts for all 37 surveys. Eight of the 37 surveys had zero observations and a further 15 had too few observations for a spatial analysis to be conducted (less than 12 observations).

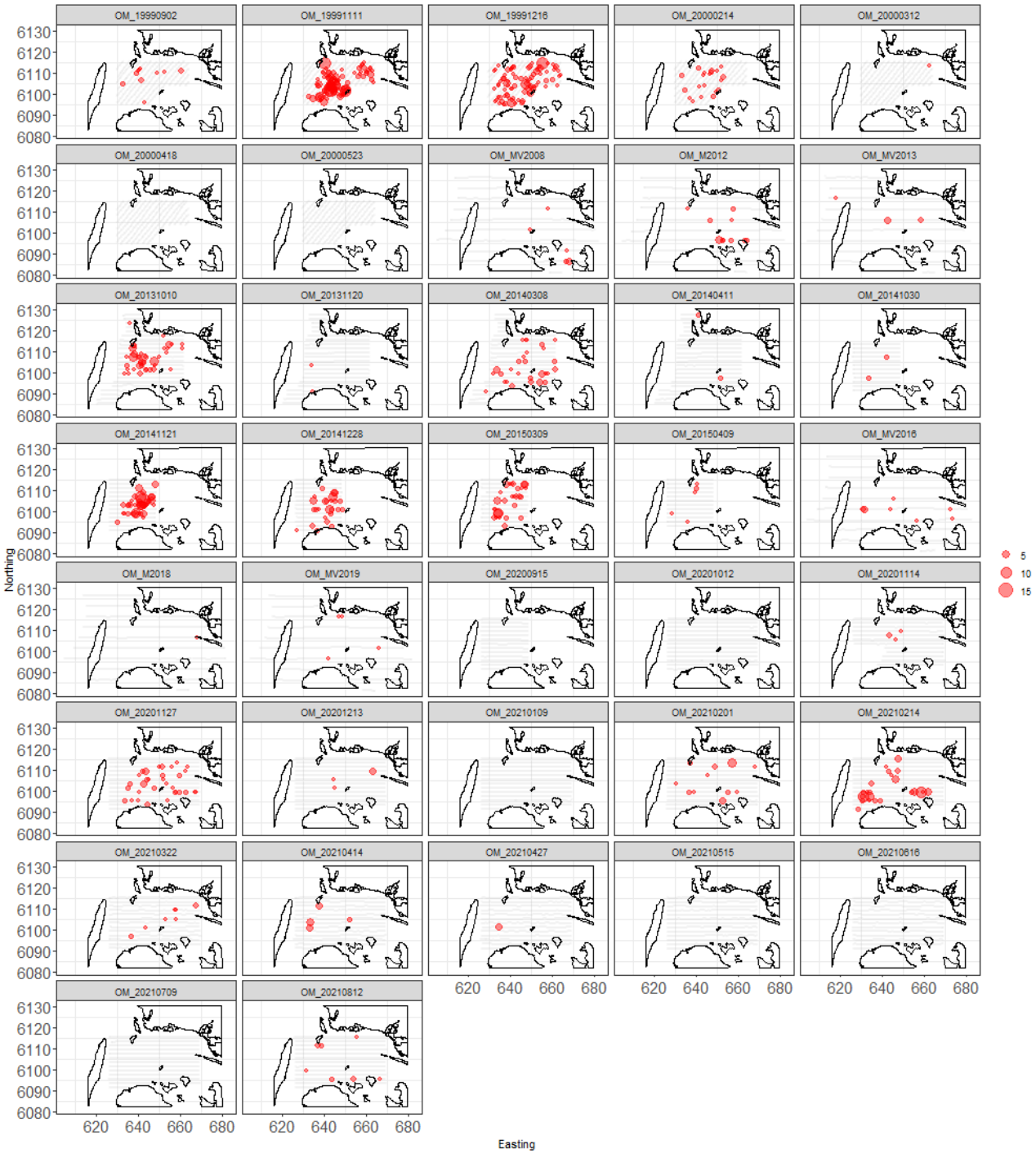

Figure 4.1. Counts for the Red-necked Grebe across the 37 surveys. The red circles indicate the distance-corrected counts along the transect lines while the polygons represent land. Grey dots are segments with a count of zero.

4.2.1 Model Selection results

For all surveys with sufficient observations to enable a fitted model (e.g. n>12), the model selected included a spatial term (of varying complexity) while the depth and distance to coast covariates (either as a linear or smooth term) were not selected for any surveys. This shows there was compelling evidence for non-uniform spatial patterns in each survey, but given these spatial patterns, there was no evidence for a depth or distance to coast based term. The spatial surfaces selected were relatively low dimensional but ranged from 2 to 7 parameters for the spatial term (Table 4.1).

The estimated abundances and associated 95 percentile confidence intervals for each survey are given in Table 4.1, while the equivalent values for density and a visual representation of these estimates (with associated uncertainties) are shown in Table 4.2 and Figure 4.2.

Table 4.1. Model selection results for Red-necked Grebe for each survey. The Variables column represents the terms in the model while the 'degrees of freedom' column indicates the number of parameters allocated to each smooth term. The extra-Poisson dispersion parameter estimates are listed in the far-right column. Empty cells indicate too few observations for the spatial analysis, e.g. n=12.

Year	Month	Survey	Variables	Degrees of freedom	Dispersion parameter estimate
1999	09	OM_19990902	s(x.pos, y.pos)	2	1.44
	11	OM_19991111	s(x.pos, y.pos)	5	3.68
	12	OM_19991216	s(x.pos, y.pos)	2	2.78
2000	02	OM_20000214	s(x.pos, y.pos)	2	1.67
	03	OM_20000312	-		
	04	OM_20000418	-		
	05	OM_20000523	-		
2008	01/02	OM_MV2008	-		
2012	08/09	OM_M2012	s(x.pos, y.pos)	5	1.08
2013	01	OM_MV2013	-		
2013	10	OM_20131010	s(x.pos, y.pos)	6	1.46
	11	OM_20131120	-		
2014	03	OM_20140308	s(x.pos, y.pos)	5	1.56
	04	OM_20140411	-		
	10	OM_20141030	-		
	11	OM_20141121	s(x.pos, y.pos)	4	2.59
	12	OM_20141228	s(x.pos, y.pos)	7	2.06
2015	03	OM_20150309	s(x.pos, y.pos)	4	3.39
	04	OM_20150409	-		
2016	01	OM_MV2016	s(x.pos, y.pos)	4	1.83
2018	07	OM_M2018	-		
2019	12	OM_MV2019	-		
2020	09	OM_20200915	-		
	10	OM_20201012	-		
	11	OM_20201114	-		
	11	OM_20201127	s(x.pos, y.pos)	3	1.73
	12	OM_20201213	-		
2021	01	OM_20210109	-		
	02	OM_20210201	s(x.pos, y.pos)	4	2.03
	02	OM_20210214	s(x.pos, y.pos)	3	4.99
	03	OM_20210322	-		

	04	OM_20210414	-		
	04	OM_20210427	-		
	05	OM_20210515	-		
	06	OM_20210616	-		
	07	OM_20210709	-		
	08	OM_20210812	-		

Table 4.2. Estimated density of Red-necked Grebe for each survey. The 95% CI are percentile-based confidence intervals. The area is the area of the prediction region (convex hull around the data).

Year	Month	Survey	Area (km^2)	Estimated Count	95% CI Count	Estimated Density	95% CI Density
1999	09	OM_19990902	591	138	(58, 350)	0.2	(0.1, 0.6)
	11	OM_19991111	585	2209	(1382, 4036)	3.8	(2.4, 6.9)
	12	OM_19991216	617	1447	(911, 2403)	2.3	(1.5, 3.9)
2000	02	OM_20000214	591	258	(134, 518)	0.4	(0.2, 0.9)
2012		OM_M2012	1926	393	(170, 1407)	0.2	(0.1, 0.7)
2013	10	OM_20131010	1085	680	(393, 1304)	0.6	(0.4, 1.2)
2014	03	OM_20140308	1071	451	(231, 1473)	0.4	(0.2, 1.4)
	11	OM_20141121	507	1048	(590, 4062)	2.1	(1.2, 8)
	12	OM_20141228	507	522	(291, 1042)	1	(0.6, 2.1)
2015	03	OM_20150309	515	567	(305, 1252)	1.1	(0.6, 2.4)
2016		OM_MV2016	1937	207	(139, 387)	0.1	(0.1, 0.2)
2020	11	OM_20201127	968	420	(213, 865)	0.4	(0.2, 0.9)
2021	02	OM_20210201	982	193	(71, 614)	0.2	(0.1, 0.6)
	02	OM_20210214	969	598	(266, 1544)	0.6	(0.3, 1.6)

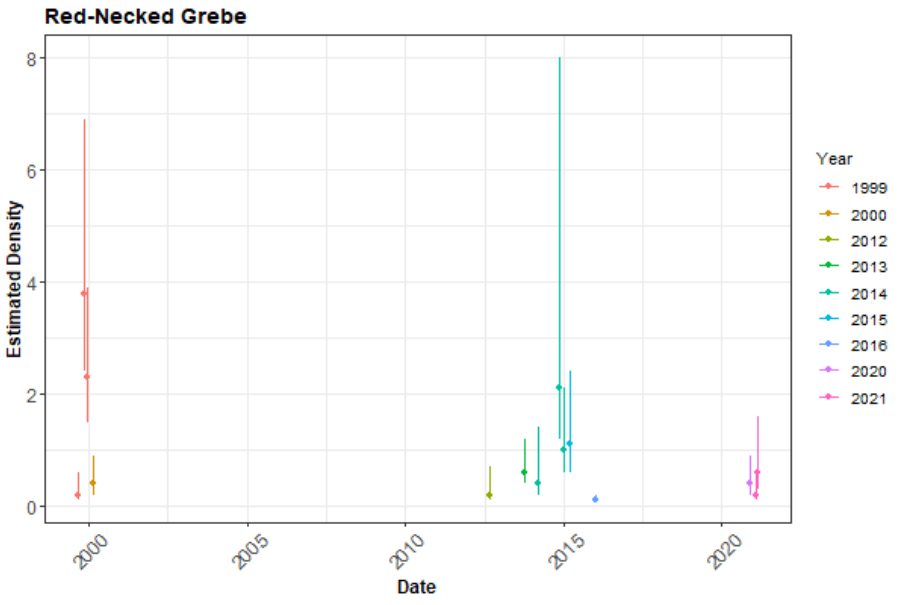

Figure 4.2. The estimated density of Red-necked Grebes for each survey. The 95% CI are percentile-based confidence intervals are from a parametric bootstrap with 500 replicates. Densities are presented rather than counts as the study area for each survey is different.

4.2.2 Spatial Results

Figure 4.3 shows the estimated counts of Red-necked Grebes species in each 500x500 m grid cell for each survey. Generally, the estimated abundances fit well to the raw data and there are no concerning departures. The common scale applied to all surveys makes it difficult to see the underlying structure of the fitted surfaces in detail however, output CSV files are provided for all predictions and individual survey-based estimated surface plots are available in the file "extraplots-grebe.docx".

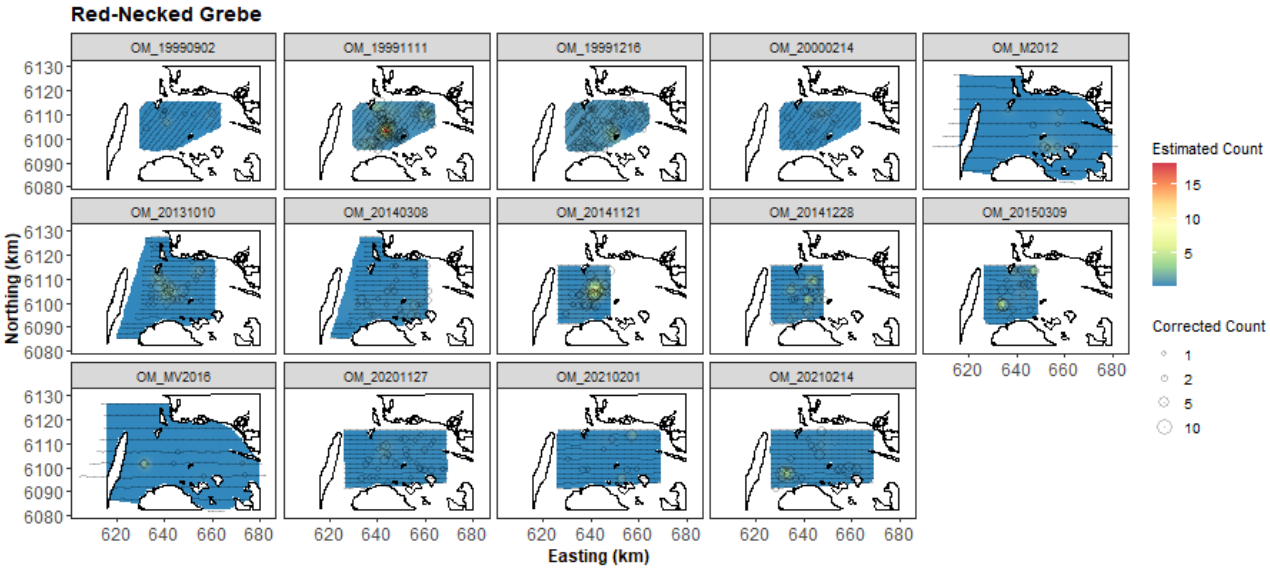

Figure 4.3. Figure showing the estimated Red-necked Grebe abundance across the study site for each of the surveys. The title of each subfigure after the underscore ("OM_") details the survey year (4 digits) and in years with multiple surveys, survey month (2 digits) and day (2 digits) follows the year. The estimated counts are per 500x500m grid cell. The open circles show the observed corrected count. The coloured graphics represent the predicted values in each location.

4.2.3 Uncertainty in the spatial predictions

The highest coefficient of variation (CoV) scores was associated with the very smallest predictions, however it is known that the CoV metric is highly sensitive to any uncertainty for very small predictions. There was no material overlap between high values of the CoV metric and the transect lines/locations with non-zero counts and therefore results in no concerns in this case (Figure 4.4 and Figure 4.5).

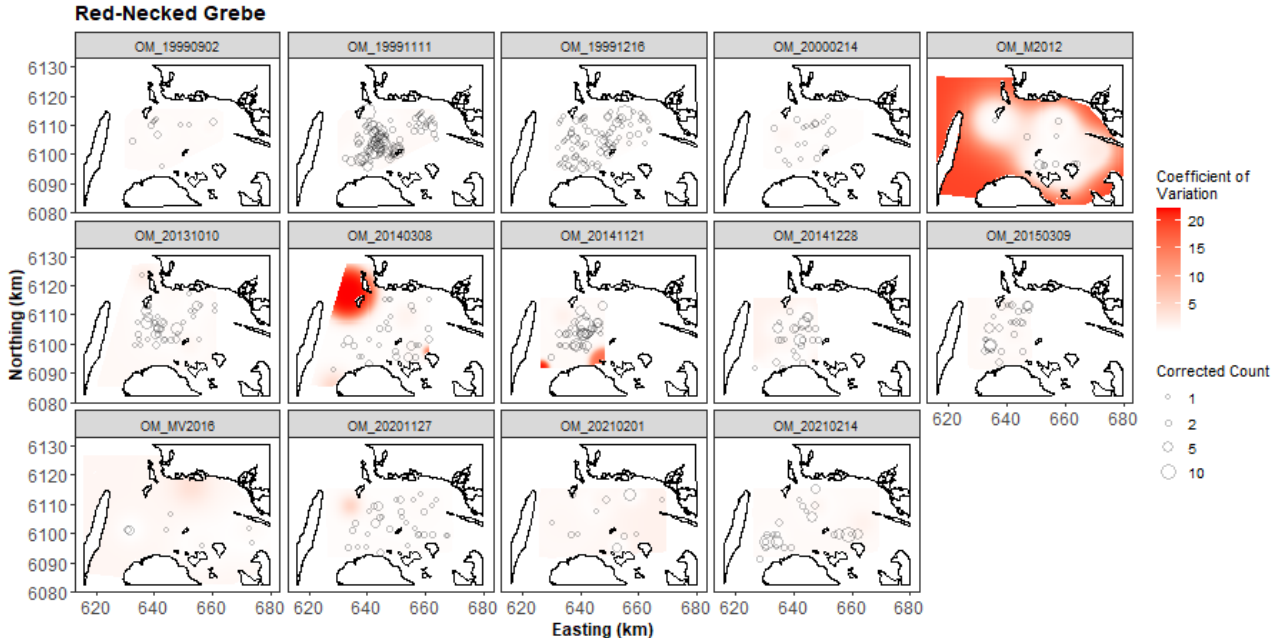

Figure 4.4. Figure showing the coefficient of variation across the study region for each of the surveys. The open circles show the distance corrected counts, where applicable. The presence of dark red CV scores in areas with virtually zero predictions are an artifact of the very small prediction rather than of any notable concern.

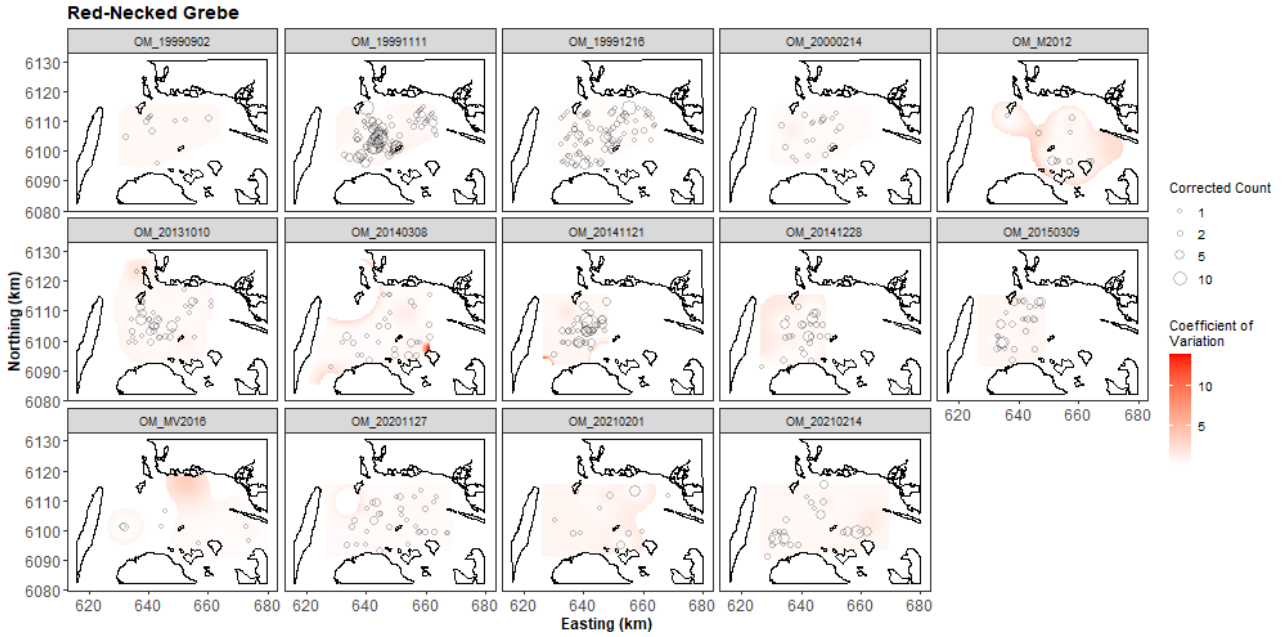

Figure 4.5. Figure showing the coefficient of variation across the study region for each of the surveys with a threshold applied to account for the very small predicted values. The open circles show the distance corrected counts, where applicable. The presence of dark red CV scores in areas with virtually zero predictions are an artifact of the very small prediction rather than of any notable concern.

4.2.4 Model Diagnostics

A blocking structure was used to account for potential residual non-independence for each model and a robust standard error approach was based on unique transects. In each case, we saw a reassuring decay to zero implying that an appropriate blocking structure was used.

The assumed mean-variance relationship was examined and generally showed agreement between the assumed (red) lines and the observed values. However, in some cases the residuals for the largest fitted values were in practice more variable than that assumed (above the line) suggesting that the variance is underestimated for these. There were no systematic clusters of negative or positive residuals for the 37 surveys and thus represent good agreement between the data and the model. The individual diagnostic plots are available on request.

4.2.5 Areas of Persistence

Across all surveys, there is evidence of moderate persistence in the central and eastern part of the reduced survey area, and very low persistence towards the northwest and south-eastern edge of the survey area (Figure 4.6). This moderate persistence (~0.5) also appears in a subset of the proposed wind farm footprint, with a decreased persistence (~0.25) in the northern area of the proposed footprint.

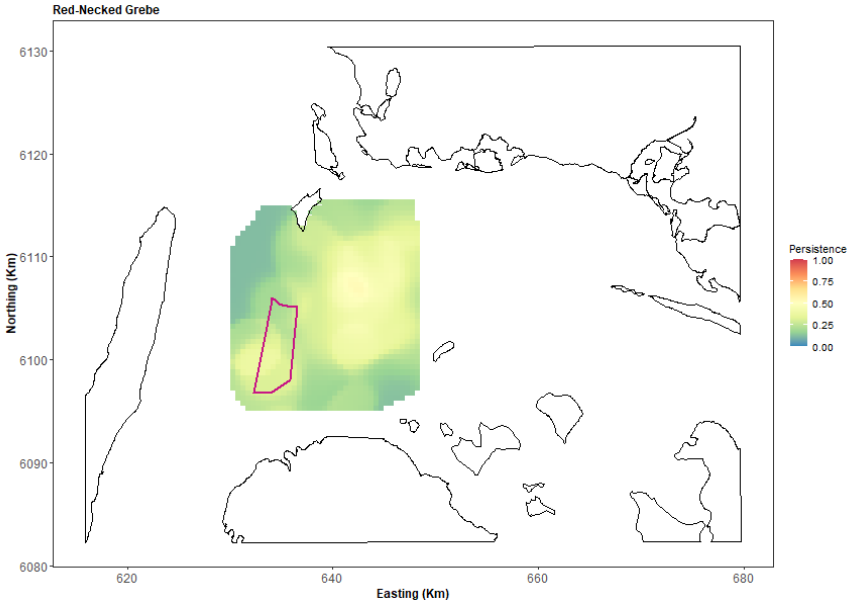

Figure 4.6. Persistence scores of Red-necked Grebe for survey data for all surveys. Due to insufficient data, there was insufficient models to further partition the persistence maps into smaller subsets. The area of the proposed offshore wind farm is indicated (polygon with red outline).

4.2.6 Impact Scenarios

The first scenario for Red-necked Grebes was an 80% decline in the footprint of the proposed wind farm with a linear return to no change in a 10km buffer. This led to a reduction in densities (<1 bird per km^2) across surveys, in line with the densities predicted under each survey-specific model (Table 4.3). These small differences resulted in no distinguishable differences in the before and after scenario proposed here. Figure 4.7 shows an example scenario based on one of the bootstrap replicates and the latest large-scale survey (OM_MV2016).

Table 4.3. Table showing the effect of scenario 1 implementation on Red-necked Grebe numbers in the proposed wind farm footprint and buffer regions. "Area" is the area in km^2 of the available prediction cells in the footprint + buffer area for each survey (2012 onwards). "Density Change" is the after density minus the before density. "95% CI" figures represent the 95 percentile-based confidence intervals for each estimate.

Survey	Area (km^2)	Density Before	95% CI Before	Density After	95% CI After	95% CI Expected Impacted Birds
OM_MV2012	522.2	0.07	(0.03, 0.4)	0.04	(0.02, 0.27)	(-65, -5)
OM_20131010	483.7	1.08	(0.84, 1.39)	0.67	(0.52, 0.88)	(-262, -146)
OM_20140308	477.5	0.39	(0.23, 0.79)	0.23	(0.13, 0.49)	(-158, -47)
OM_20141121	429.1	2.39	(1.62, 8.79)	1.5	(1.03, 6.32)	(-833, -254)
OM_20141228	428.6	1.1	(0.81, 1.7)	0.71	(0.52, 1.03)	(-289, -119)
OM_20150309	431.5	1.09	(0.72, 1.83)	0.53	(0.3, 1.03)	(-362, -175)
OM_MV2016	522.2	0.23	(0.2, 0.3)	0.07	(0.06, 0.1)	(-104, -73)
OM_20201127	434.1	0.45	(0.25, 0.78)	0.3	(0.17, 0.54)	(-109, -34)
OM_20210201	440.8	0.13	(0.05, 0.41)	0.08	(0.03, 0.23)	(-83, -7)
OM_20210214	430.6	0.88	(0.62, 1.36)	0.34	(0.22, 0.64)	(-323, -163)

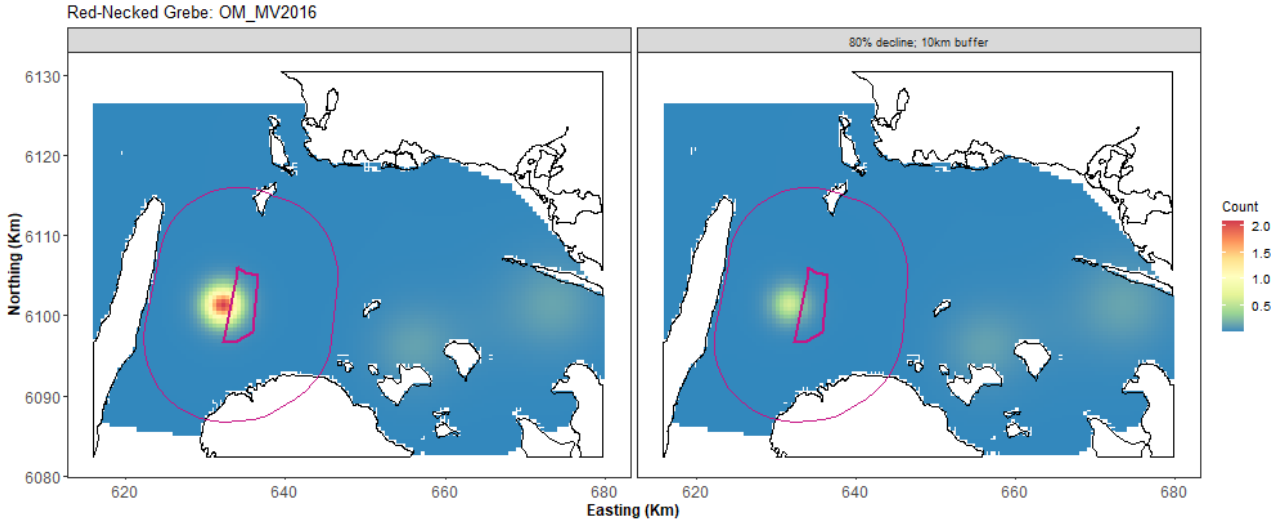

Figure 4.7. Example of displacement scenario1 for Red-necked Grebe. On the left is one of the estimated bootstrap predictions from the OM_MV2016 model. On the right is the same set of predictions but with the scenario imposed. The footprint is shown by the thick purple line and the buffer the thinner purple line.

The second scenario for Red-necked Grebes was a 50% decline in the footprint of the proposed wind farm with a linear return to no change in a 10km buffer. This also led to declines of less than one bird per km^2 (Table 4.4). These small differences resulted in no distinguishable differences in the before and after scenario proposed here. Figure 4.8 shows an example scenario based on one of the bootstrap replicates and the latest large-scale survey (MV2016).

Table 4.4. Table showing the effect of scenario 2 implementation on Red-necked Grebe numbers in the proposed wind farm footprint and buffer regions. "Area" is the area in km^2 of the available prediction cells in the footprint + buffer area for each survey (2012 onwards). "Density Change" is the after density minus the before density. "95% CI" figures represent the 95 percentile based confidence intervals for each estimate.

Survey	Area (km^2)	Density Before	95% CI Before	Density After	95% CI After	95% CI Expected Impacted Birds
OM_MV2012	218.5	0.05	(0.02, 0.31)	0.04	(0.02, 0.25)	(-14, 0)
OM_20131010	218.5	1.02	(0.73, 1.52)	0.84	(0.6, 1.24)	(-67, -25)
OM_20140308	218.5	0.44	(0.26, 0.87)	0.32	(0.19, 0.64)	(-49, -15)
OM_20141121	218.5	1.92	(1.27, 3.21)	1.56	(1.04, 2.5)	(-156, -47)
OM_20141228	218.5	0.8	(0.48, 1.53)	0.57	(0.34, 1.08)	(-99, -28)
OM_20150309	218.5	1.3	(0.94, 2.01)	0.79	(0.54, 1.31)	(-150, -88)
OM_MV2016	218.5	0.53	(0.47, 0.66)	0.33	(0.29, 0.42)	(-54, -40)
OM_20201127	218.5	0.29	(0.16, 0.5)	0.23	(0.12, 0.4)	(-24, -7)
OM_20210201	218.5	0.13	(0.03, 0.49)	0.1	(0.02, 0.36)	(-29, -2)
OM_20210214	218.5	1.39	(0.99, 1.96)	0.87	(0.62, 1.29)	(-152, -81)

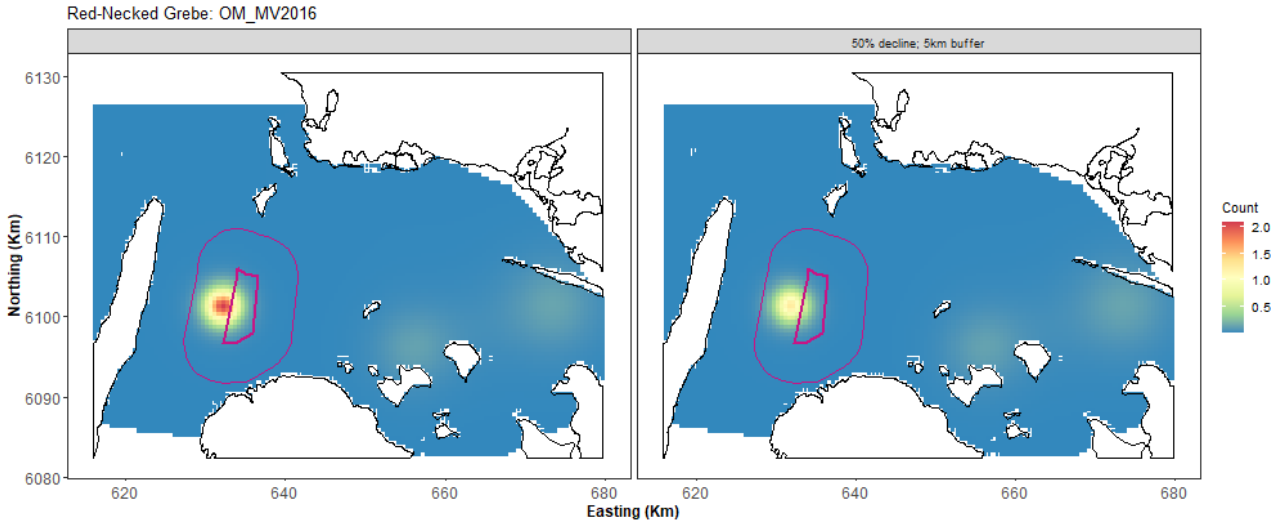

Figure 4.8. Example of displacement scenario 2 for Red-necked Grebe. On the left is one of the estimated bootstrap predictions from the MV2016 model. On the right is the same set of predictions but with the scenario imposed. The footprint is shown by the thick purple line and the buffer the thinner purple line.

5 Common Eider *Somateria mollissima*

5.1 Distance Analysis

5.1.1 Detection function from data with four transect bands

The average probability of sighting Common Eider was estimated to be 0.18 (CV=0.019). This probability was estimated using a hazard rate detection function that varied with cluster size (Figure 5.1) and season (Figure 5.2). No other covariates were selected. So, there is a seasonal effect to detection over and above the cluster size effect. The seasonal effect shows that detection is higher in spring compared with autumn and wintering.

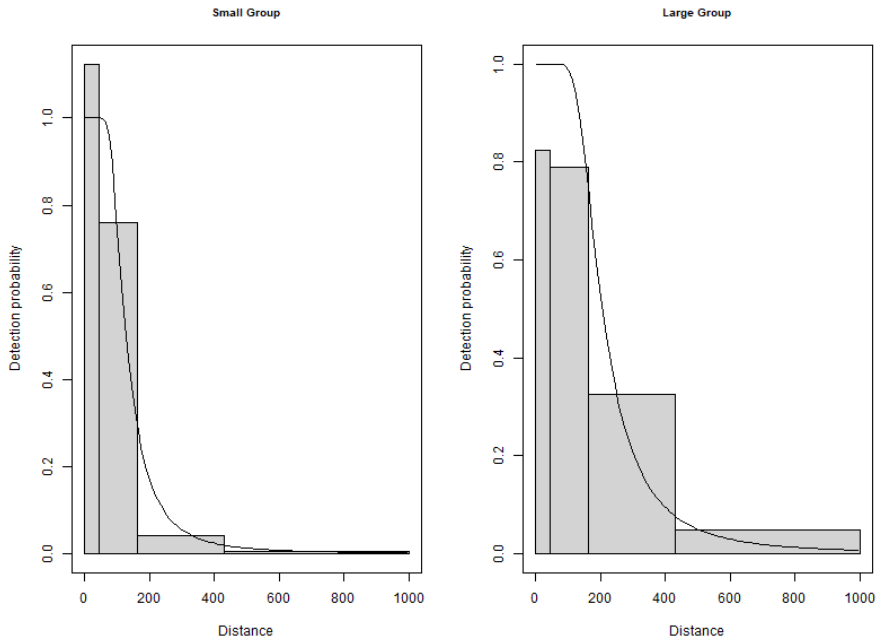

Figure 5.1. Figure showing the estimated detection function for examples of a large group and a small group of Common Eider. The histograms are the distances of the observed sightings.

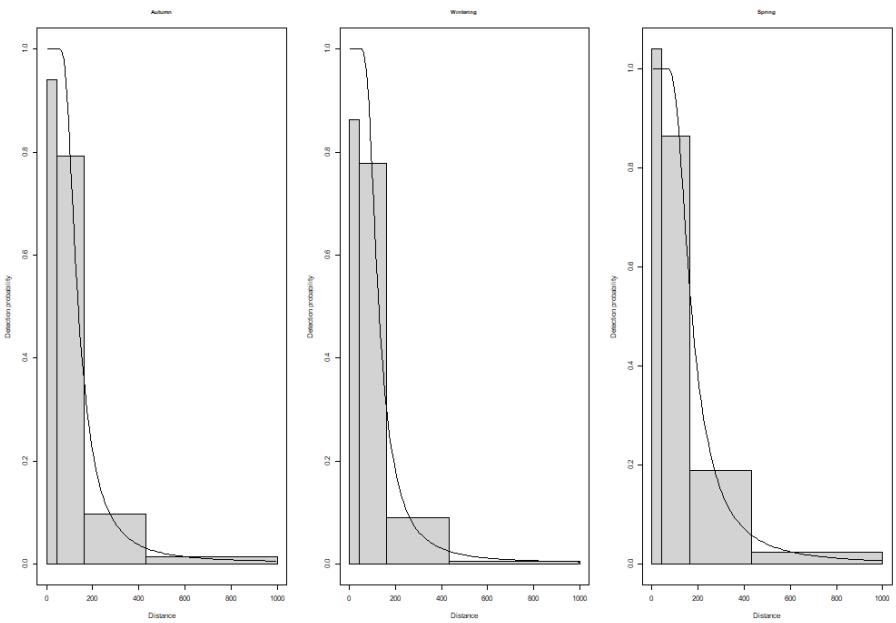

Figure 5.2. Figure showing the estimated detection function for Common Eider for each of the three seasons (Autumn, Wintering and Spring). The histograms are the distances of the observed sightings.

5.1.2 Detection function from data with three transect bands

The average probability of sighting Common Eiders was estimated to be 0.23 (CV=0.009). This probability was estimated using a hazard rate detection function that varied with cluster size (Figure 5.3). No other covariates were selected.

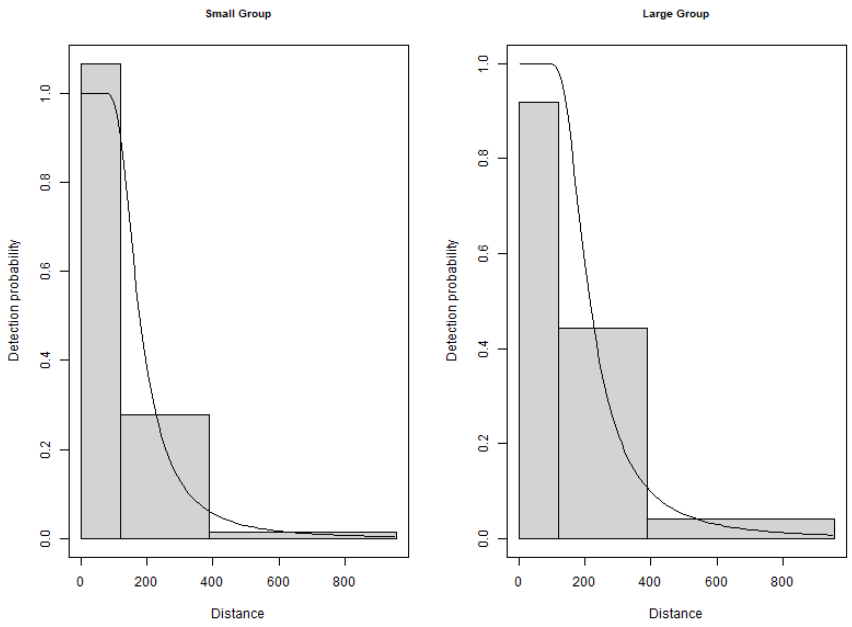

Figure 5.3. Figure showing the estimated detection function for examples of a large group and a small group of Common Eiders. The histograms are the distances of the observed sightings.

5.1.3 Spatial analysis

The two distance corrected datasets were combined for the spatial analysis and contained 31,512 segments, 27.6% of which were segments containing Eider sightings. Figure 5.4 shows the distribution of the distance corrected counts for all 37 surveys.

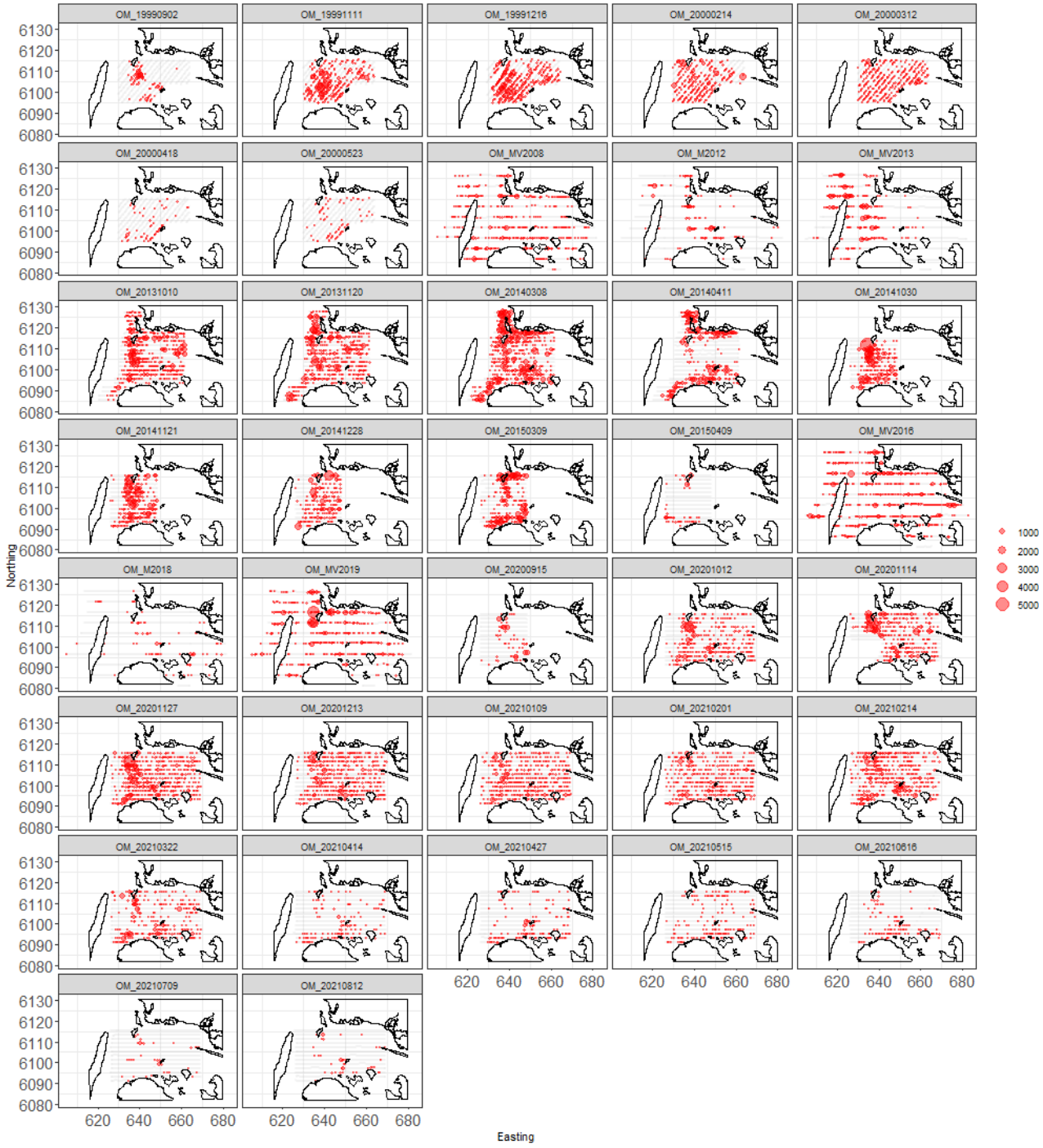

Figure 5.4. Distance-corrected counts for the Common Eider across the 37 surveys. The red circles indicate the distance-corrected counts along the transect lines while the polygons represent land. Grey dots are segments with a count of zero.

5.1.4 Model Selection results

For all surveys, the model selected included a spatial term (of varying complexity) while the depth and distance to coast covariates (either as a linear or smooth term) were not selected for any surveys. This shows there was compelling evidence for non-uniform spatial patterns in each survey, but given these spatial patterns, there was no evidence for a depth or distance to coast based term. The spatial surfaces selected were relatively low dimensional but ranged from 3 to 12 parameters for the spatial term (Table 5.1).

The estimated abundances and associated 95 percentile confidence intervals for each survey are given in Table 5.2 and Figure 5.5.

Table 5.1. Model selection results for Common Eiders for each survey. The Variables column represents the terms in the model while the 'df' column indicates the number of parameters allocated to each smooth term. The extra-Poisson dispersion parameter estimates are listed in the far right column.

Year	Month	Survey	Variables	Df	Dispersion parameter estimate
1999	09	OM_19990902	s(x.pos, y.pos)	8	151
	11	OM_19991111	s(x.pos, y.pos)	9	292
	12	OM_19991216	s(x.pos, y.pos)	10	180
2000	02	OM_20000214	s(x.pos, y.pos)	10	215
	03	OM_20000312	s(x.pos, y.pos)	10	72
	04	OM_20000418	s(x.pos, y.pos)	7	79
	05	OM_20000523	s(x.pos, y.pos)	8	58
2008	01/02	OM_MV2008	s(x.pos, y.pos)	8	129
2012	08/09	OM_M2012	s(x.pos, y.pos)	10	287
2013	01	OM_MV2013	s(x.pos, y.pos)	3	223
2013	10	OM_20131010	s(x.pos, y.pos)	6	358
	11	OM_20131120	s(x.pos, y.pos)	9	469
2014	03	OM_20140308	s(x.pos, y.pos)	10	426
	04	OM_20140411	s(x.pos, y.pos)	5	365
	10	OM_20141030	s(x.pos, y.pos)	5	490
	11	OM_20141121	s(x.pos, y.pos)	10	545
	12	OM_20141228	s(x.pos, y.pos)	8	313
2015	03	OM_20150309	s(x.pos, y.pos)	9	372
	04	OM_20150409	s(x.pos, y.pos)	6	177
2016	01	OM_MV2016	s(x.pos, y.pos)	7	229
2018	07	OM_M2018	s(x.pos, y.pos)	9	125
2019	12	OM_MV2019	s(x.pos, y.pos)	10	339
2020	09	OM_20200915	s(x.pos, y.pos)	9	241
	10	OM_20201012	s(x.pos, y.pos)	12	167
	11	OM_20201114	s(x.pos, y.pos)	9	317
	11	OM_20201127	s(x.pos, y.pos)	10	266
	12	OM_20201213	s(x.pos, y.pos)	9	129
2021	01	OM_20210109	s(x.pos, y.pos)	10	125
	02	OM_20210201	s(x.pos, y.pos)	8	129
	02	OM_20210214	s(x.pos, y.pos)	10	
	03	OM_20210322	s(x.pos, y.pos)	11	234
	04	OM_20210414	s(x.pos, y.pos)	9	46
	04	OM_20210427	s(x.pos, y.pos)	4	54
	05	OM_20210515	s(x.pos, y.pos)	8	27
	06	OM_20210616	s(x.pos, y.pos)	4	48
	07	OM_20210709	s(x.pos, y.pos)	5	60
	08	OM_20210812	s(x.pos, y.pos)	10	113

Table 5.2. Estimated density of Common Eiders for each survey. The 95% CI are percentile-based confidence intervals. The area is the area of the prediction region (convex hull around the data).

Year	Month	Survey	Area (km^2)	Estimated Count	95% CI Count	Estimated Density	95% CI Density
1999	09	OM 19990902	591	9124	(5846, 20064)	15.4	(9.9, 34.0)
	11	OM 19991111	585	32853	(18409, 64891)	56.1	(31.4, 110.9)
	12	OM 19991216	617	40364	(30537, 55144)	65.5	(49.5, 89.4)
2000	02	OM 20000214	591	17275	(9377, 35093)	29.2	(15.9,59.4)
	03	OM 20000312	590	18844	(12063, 31172)	31.9	(20.4, 52.8)
	04	OM 20000418	588	3055	(1435, 8957)	5.2	(2.4, 15.2)
	05	OM 20000523	596	1216	(685, 2478)	2.0	(1.2, 4.2)
2008	01/02	OM MV2008	1938	48780	(35247, 68943)	25.2	(18.2, 35.6)
2012	08/09	OM M2012	1926	22588	(8122, 73373)	11.7	(4.2, 38.1)
2013	01	OM MV2013	1940	60101	(41145, 91359)	31	(21.2, 47.1)
2013	10	OM 20131010	1085	50741	(31678, 87355)	46.7	(29.2, 80.5)
	11	OM 20131120	1070	60247	(29698, 146994)	56.3	(27.8, 137.4)
2014	03	OM 20140308	1071	107986	(77430, 213018)	100.8	(72.3,198.9)
	04	OM 20140411	1071	59236	(42327, 108059)	55.3	(39.5, 100.9)
	10	OM 20141030	474	44481	(28327, 126802)	93.9	(59.8, 267.6)
	11	OM 20141121	507	38487	(22177, 99372)	75.9	(43.7, 195.8)
	12	OM 20141228	507	20353	(11786, 42803)	40.2	(23.3, 84.5)
2015	03	OM 20150309	515	37031	(21200, 131007)	72	(41.2, 254.6)
	04	OM 20150409	491	2907	(1049, 9325)	5.9	(2.1, 18.9)
2016	01	OM MV2016	1937	90690	(64252, 135808)	46.8	(33.2, 70.1)
2018	07	OM M2018	1936	11800	(6037, 30721)	6.1	(3.1, 15.9)
2019	12	OM MV2019	1918	98435	(71713, 142790)	51.3	(37.4, 74.4)
2020	09	OM 20200915	508	6963	(2629, 27309)	13.7	(5.2, 53.8)
	10	OM 20201012	964	24858	(13510, 46702)	25.8	(14.0, 48.4)
	11	OM 20201114	879	37371	(21157, 73170)	42.5	(24.1, 83.2)
	11	OM 20201127	968	51993	(35575, 78206)	53.7	(36.8, 80.8)
	12	OM 20201213	966	30266	(22256, 42508)	31.3	(23.0, 44.0)
2021	01	OM 20210109	974	23507	(16498, 34790)	24.1	(16.9, 35.7)
	02	OM 20210201	982	18020	(12129, 27593)	18.4	(12.4, 28.1)
	02	OM 20210214	969	37166	(25261, 57591)	38.3	(26.1, 59.4)
	03	OM 20210322	980	20119	(11316, 39196)	20.5	(11.5, 40.0)
	04	OM 20210414	978	4331	(2763, 7471)	4.4	(2.8, 7.7)
	04	OM 20210427	970	5163	(3101, 8426)	5.3	(3.2, 8.7)
	05	OM 20210515	957	2521	(1497, 4847)	2.6	(1.6, 5.1)
	06	OM 20210616	977	2694	(1445, 4999)	2.8	(1.5, 5.1)
	07	OM 20210709	997	2502	(1370, 5078)	2.5	(1.4, 5.1)
	08	OM 20210812	976	3025	(1260, 10517)	3.1	(1.3, 10.8)

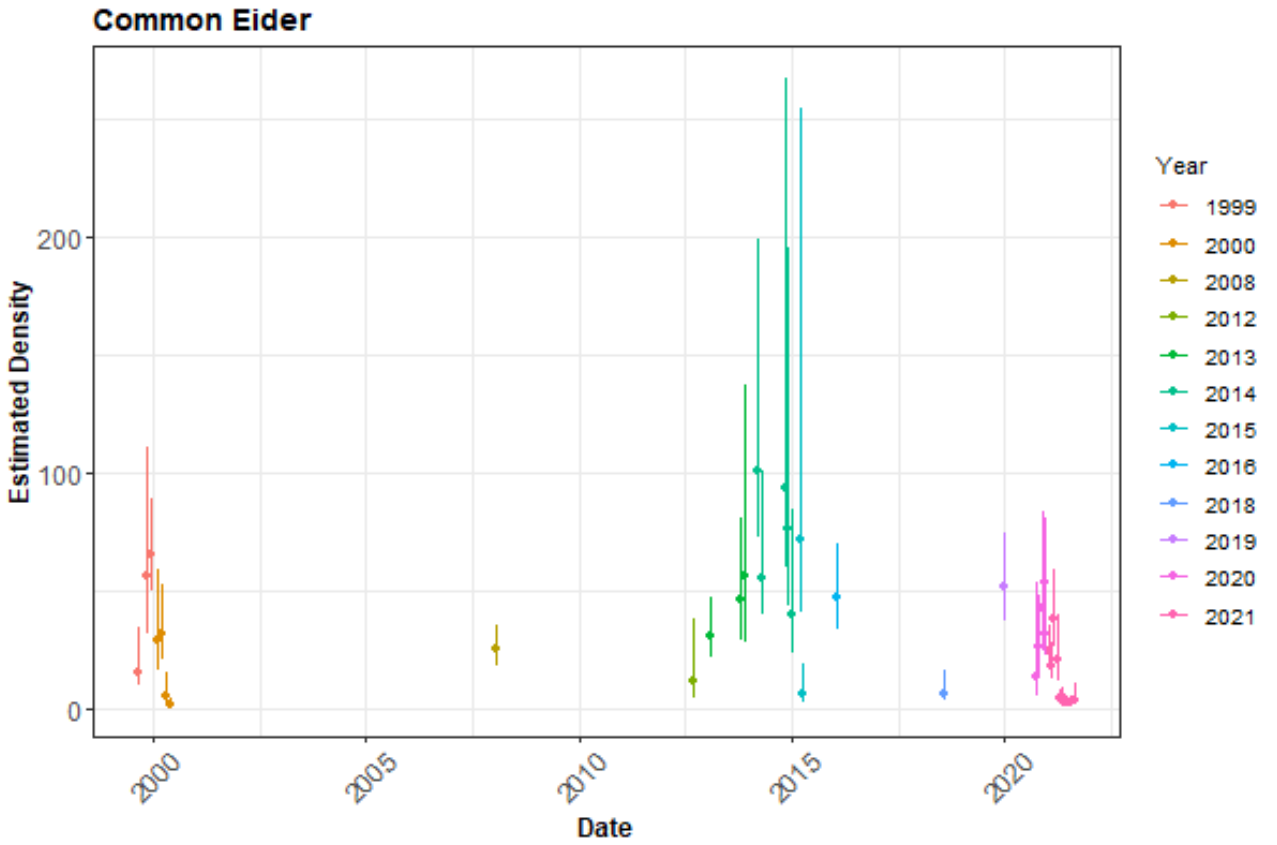

Figure 5.5. The estimated density of Common Eiders for each survey. The 95% CI are percentile-based confidence intervals are from a parametric bootstrap with 500 replicates. Densities are presented rather than counts as the study area for each survey is different.

5.1.5 Spatial Results

Figure 5.6 shows the estimated counts of Common Eiders species in each 500x500 m grid cell for each survey. Generally, the estimated abundances fit well to the raw data and there are no notable misalignments. The common scale applied to all surveys makes it difficult to see the underlying structure of the fitted surfaces in detail however, output CSV files are provided for all predictions and individual survey-based estimated surface plots are available in the file "extraplots-eider.docx".

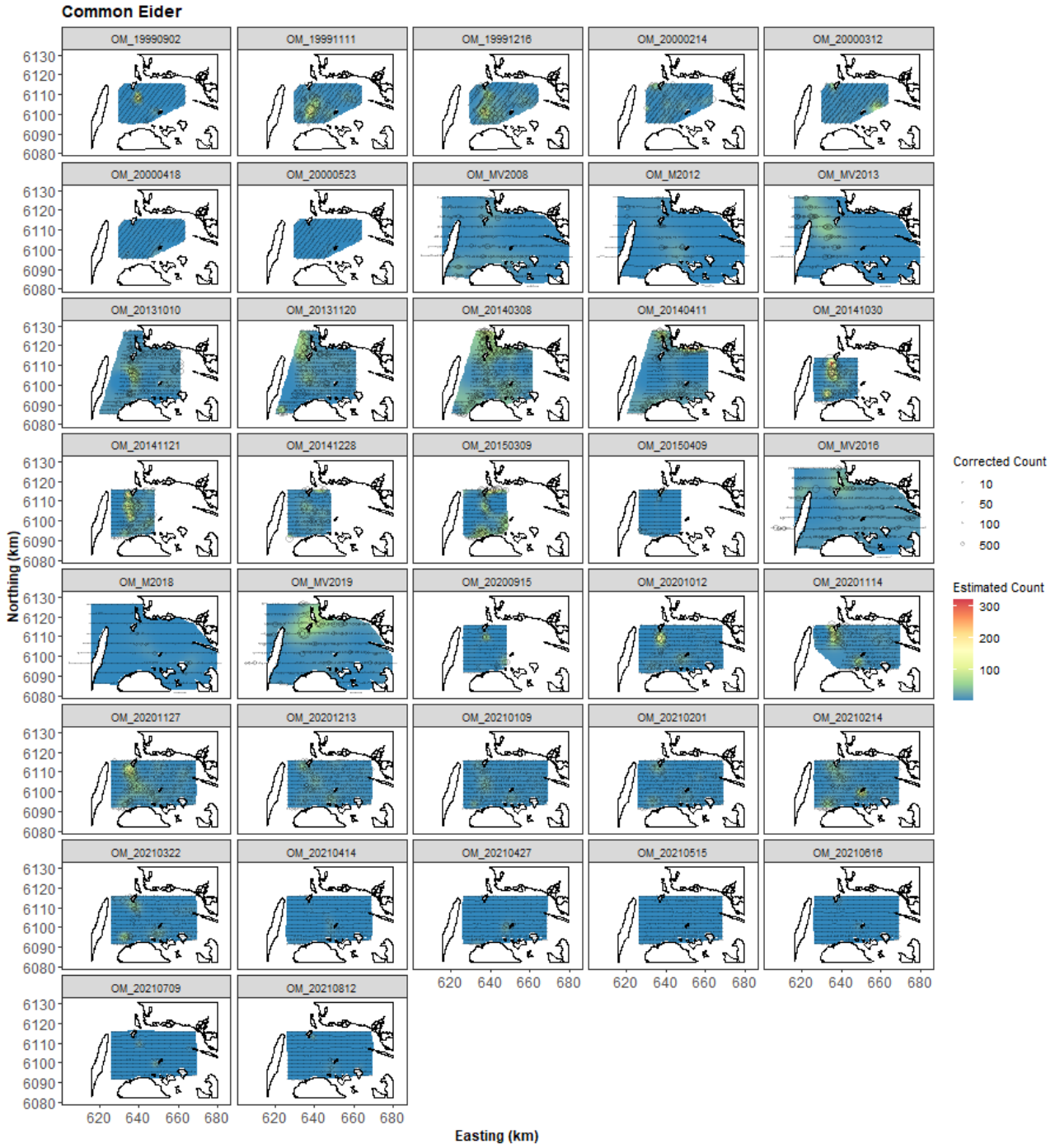

Figure 5.6. Figure showing the estimated Common Eider abundance across the study site for each of the surveys. The title of the each subfigure after the underscore ("OM_") details the survey year (4 digits) and in years with multiple surveys, survey month (2 digits) and day (2 digits) follows the year. The estimated counts are per 500x500m grid cell. The open circles show the observed corrected count. The coloured graphics represent the predicted values in each location.

5.1.6 Uncertainty in the spatial predictions

The highest coefficient of variation (CoV) scores was associated with the very smallest predictions, however it is known that the CoV metric is highly sensitive to any uncertainty for very small predictions. There was no material overlap between high values of the CoV metric and the transect lines/locations with non-zero counts and therefore results in no concerns in this case (Figure 5.7 and Figure 5.8).

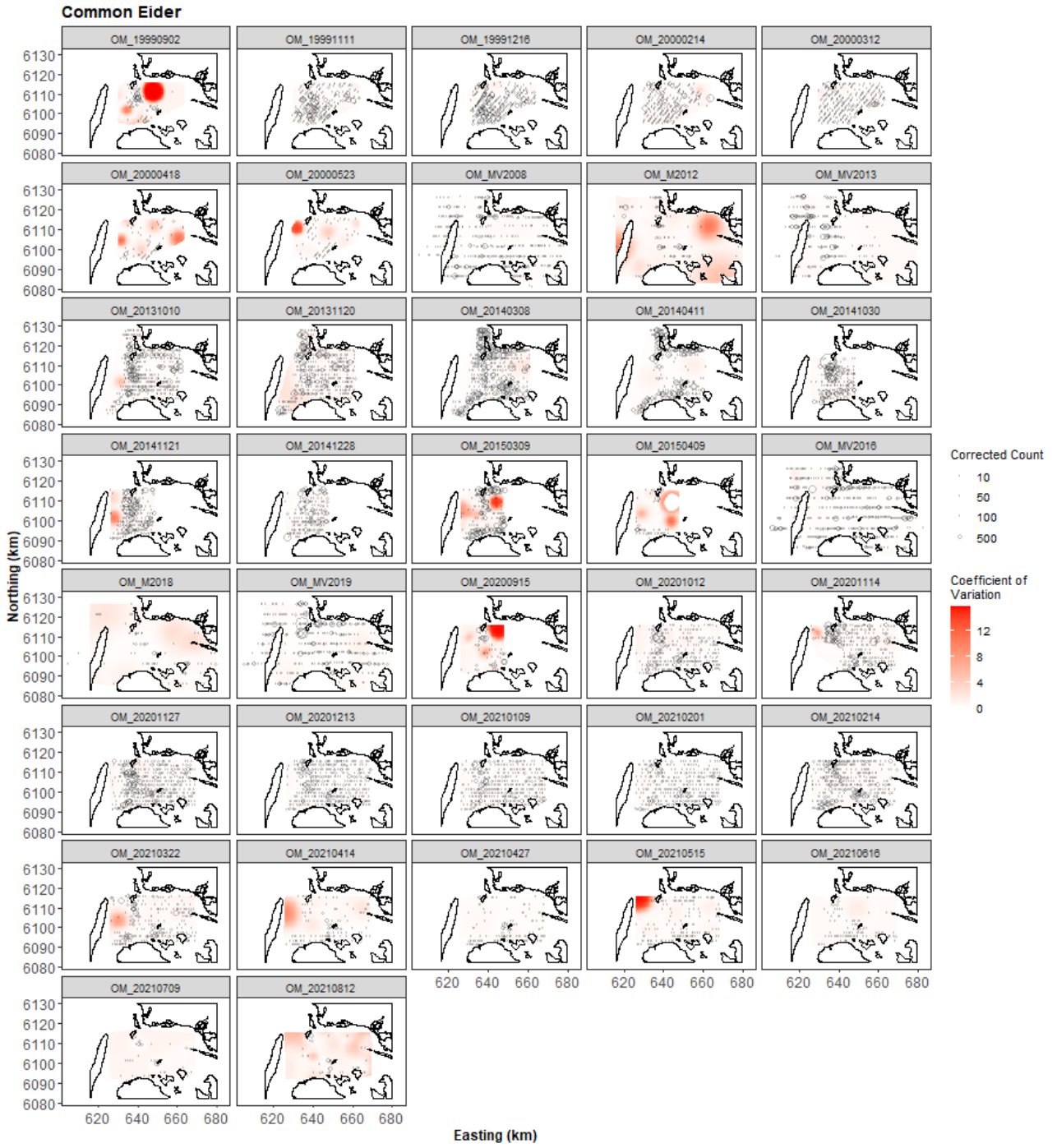

Figure 5.7. Figure showing the coefficient of variation across the study region for each of the surveys. The open circles show the distance corrected counts, where applicable. The presence of dark red CV scores in areas with virtually zero predictions are an artifact of the very small prediction rather than of any notable concern.

Figure 5.8. Figure showing the coefficient of variation across the study region for each of the surveys with a threshold applied to account for the very small predicted values. The open circles show the distance corrected counts, where applicable. The presence of dark red CV scores in areas with virtually zero predictions are an artifact of the very small prediction rather than of any notable concern.

5.1.7 Model Diagnostics

A blocking structure was used to account for potential residual non-independence for each model and a robust standard error approach was based on unique transects. In each case, we saw a reassuring decay to zero (indicated by the red and grey lines for an example plot in Figure 5.9) implying that an appropriate blocking structure was used.

The assumed mean-variance relationship was examined and generally showed agreement between the assumed (red) lines and the observed values (Figure 5.9). However, in some cases the residuals for the largest fitted values were in practice more variable than that assumed (above the line) suggesting that the variance is underestimated for these. There were no systematic

clusters of negative or positive residuals for the 37 surveys (the individual plots are available on request) and thus represent good agreement between the data and the model.

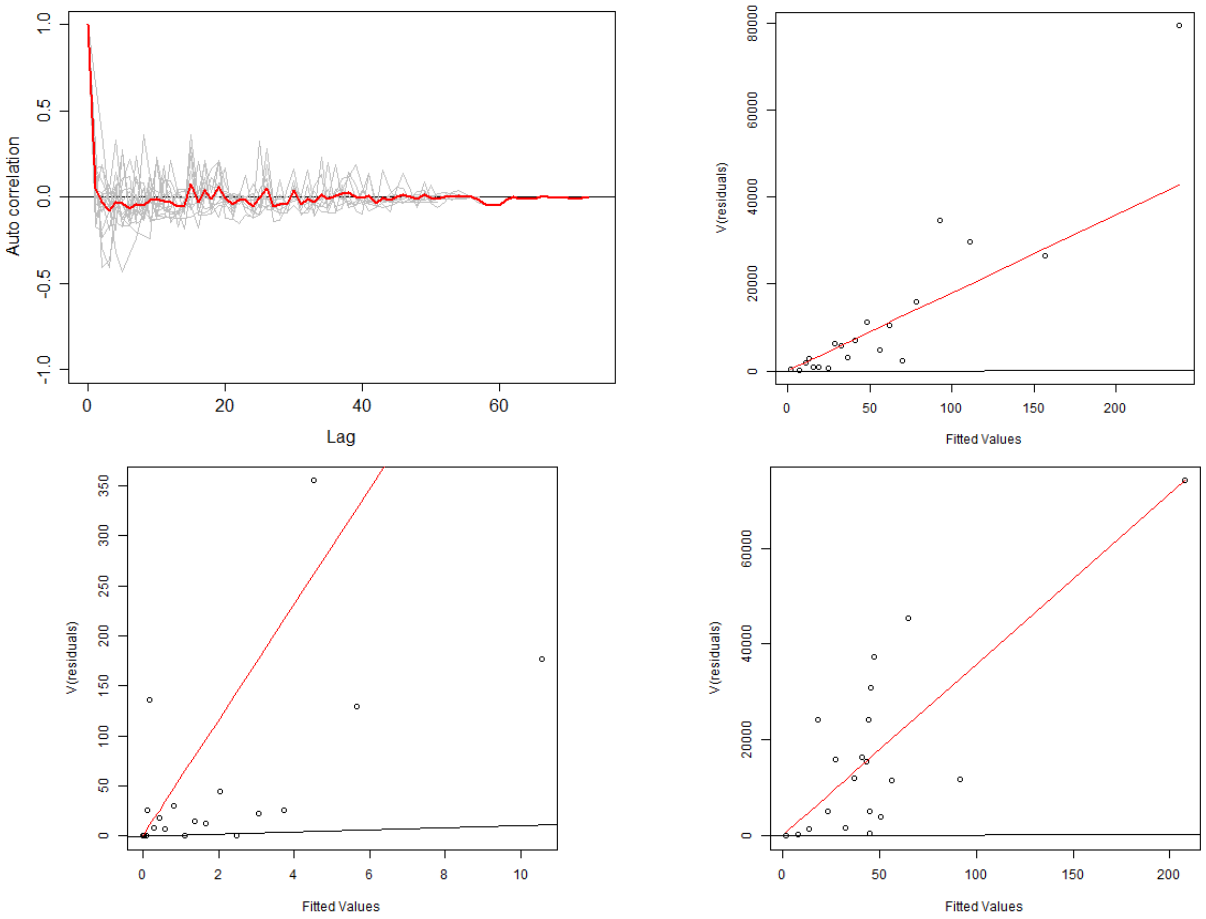

Figure 5.9. Autocorrelation function plot (top left) demonstrating the typical decline in residual autocorrelation within blocks. The grey lines represent the residual correlation observed in each transect and the red line the average of these values across transects. On the top right and bottom row are figures showing the assumed (red line) and actual (open circles) mean-variance relationship for three models. The open circles are based on 20 quantiles of the model residuals and for reference, the black line shows the 1:1 relationship. The top right illustrates when the variance for the largest predictions is more than expected under the model, while the bottom left illustrates less than expected while the bottom right is line with expectations.

5.1.8 Areas of Persistence

From 1999 to 2021 there is evidence of approximately 60% persistence in the central northern part of the reduced survey area, and very low persistence towards the west and north-eastern edge of the survey area (Figure 5.10). This moderate persistence also predominantly characterises some of the proposed wind farm footprint, with an elevation of persistence (~0.5) in the northern area of the proposed footprint.

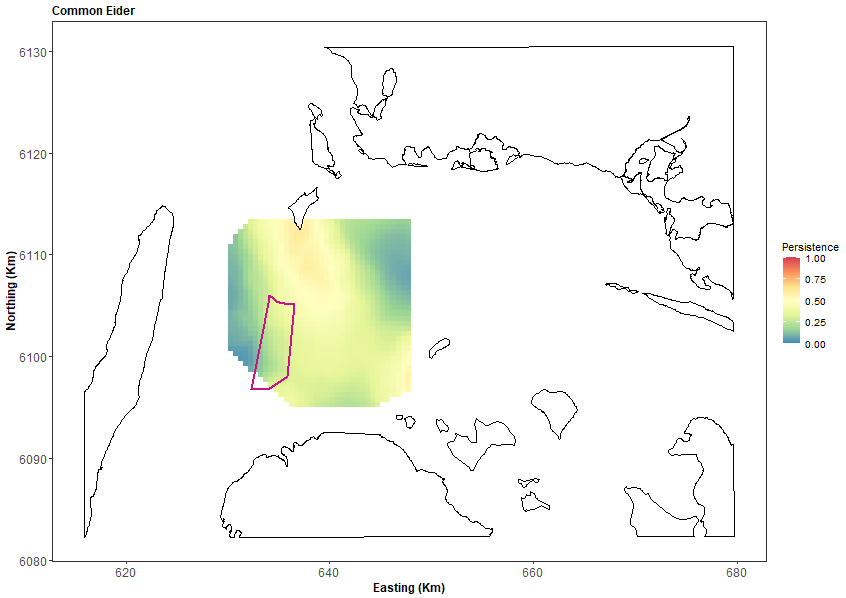

Figure 5.10. Persistence scores for Common Eider across the persistence for survey data for all surveys. The area of the proposed offshore wind farm is indicated (polygon with red outline).

There was relatively high persistence (~0.7) identified in the central 'belt' of the large-scale survey area (Figure 5.11). These areas of high persistence were however, not found inside the proposed windfarm footprint. The proposed footprint contained moderate to low persistence (~< 0.4) while there were notably lower values immediately to the west of the proposed windfarm footprint and in the north-eastern and south-eastern areas.

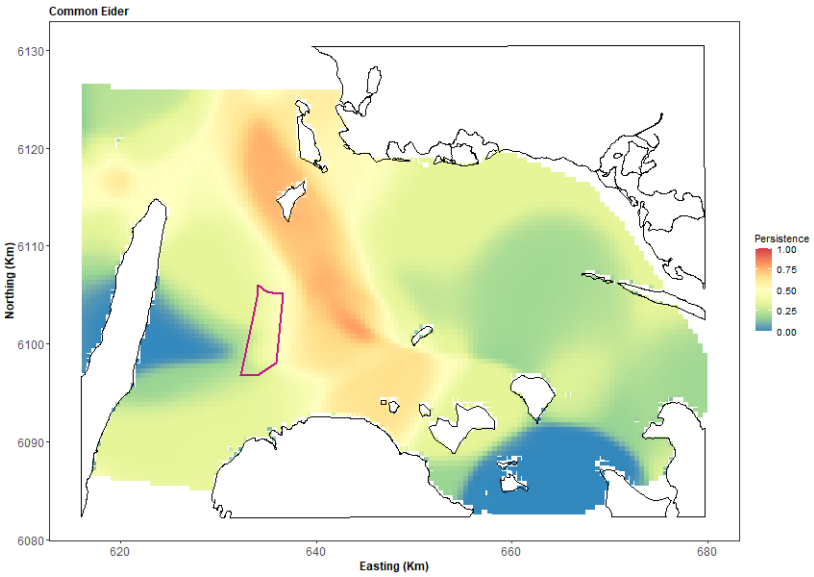

Figure 5.11. Persistence scores for Common Eider across the large scale MV surveys (2008, 2012, 2013, 2016, 2018, 2019).

There were two high persistence areas for October 2020 to August 2021 (Figure 5.12) in the north-western and south-central areas and only moderate persistence inside the windfarm footprint.

Notably, this relatively moderate, but non-trivial, persistence inside the windfarm footprint was a common feature of all summaries across surveys.

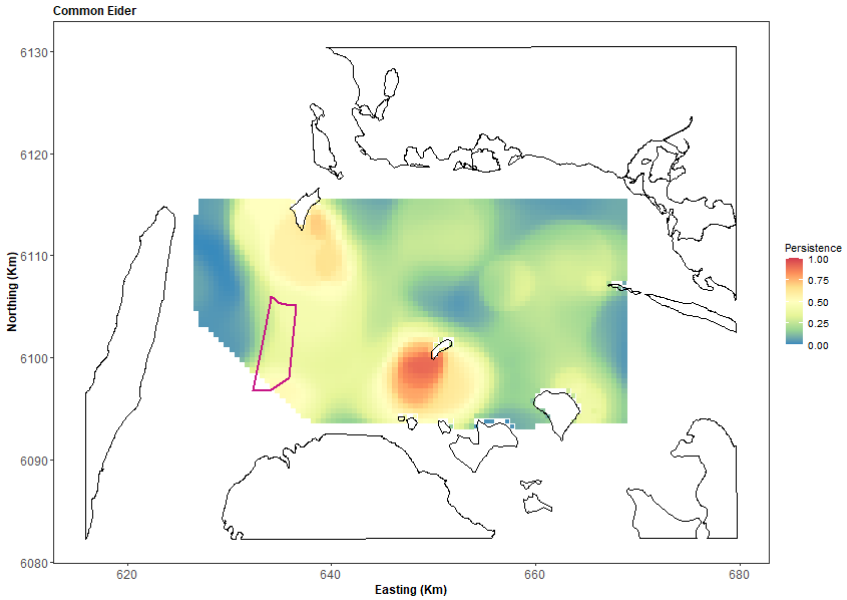

Figure 5.12. Persistence scores for Common Eider across the persistence for survey data with the same coverage surveys (Oct 2020 to Aug 2021).

5.2 Impact Scenarios

The first scenario for Common Eiders was a 25% decline in the footprint of the proposed wind farm with a linear return to no change in a 2km buffer. This led to a reduction in densities ranging from <1 birds per km² to ~34 birds per km² across surveys, in line with the densities predicted under each survey-specific model (Table 5.3). Regardless of the decline in each case, the confidence intervals for the densities both before and after the impact shared values in each case. This indicates no compelling evidence for a difference before and after the impact scenarios imposed. Figure 5.13 shows an example scenario based on one of the bootstrap replicates and the latest large-scale survey (OM_MV2019).

Table 5.3. Table showing the effect of scenario 1 implementation on Common Eider numbers in the proposed wind farm footprint and buffer regions. "Area" is the area in km² of the available prediction cells in the footprint + buffer area for each survey (2012 onwards). "Density Change" is the after density minus the before density. "95% CI" figures represent the 95 percentile-based confidence intervals for each estimate.

Survey	Area (km²)	Density Before	95% CI Before	Density After	95% CI After	95% CI Expected Impacted Birds
OM_MV2012	82.2	16.7	(6.02, 41.4)	14.15	(5.13, 34.98)	(-528, -73)
OM_MV2013	82.2	68.3	(54.08, 84.6)	57.76	(45.76, 71.43)	(-1084, -686)
OM_20131010	82.2	80.75	(53.69, 145.99)	70.57	(47.11, 126.76)	(-1682, -529)
OM_20131120	82.2	69.98	(49.32, 151.37)	58.38	(41.13, 125.59)	(-2121, -673)
OM_20140308	82.2	65.32	(46.68, 117.82)	55.18	(39.59, 99.57)	(-1501, -585)
OM_20140411	82.2	8.53	(4.04, 21.77)	7.42	(3.57, 18.63)	(-251, -38)
OM_20141030	82.2	206.82	(157.93, 853.29)	173.15	(132.05, 707.63)	(-11981, -2113)
OM_20141121	82.2	149.31	(115.81, 479.77)	123.44	(95.25, 388.53)	(-7507, -1701)
OM_20141228	82.2	58.2	(44.67, 99.93)	48.83	(37.67, 83.91)	(-1201, -576)
OM_20150309	82.2	45.71	(23.66, 153.33)	40.37	(21.05, 129.25)	(-1998, -193)

OM_20150409	82.2	5.09	(2.71, 10.49)	4.25	(2.26, 8.65)	(-155, -35)
OM_MV2016	82.2	22.37	(17.36, 29.31)	18.92	(14.72, 24.73)	(-379, -215)
OM_M2018	82.2	4.85	(3.54, 6.41)	4.13	(3.01, 5.45)	(-78, -43)
OM_MV2019	82.2	36.31	(28.73, 48.65)	30.87	(24.47, 41.29)	(-608, -351)
OM_20200915	82.2	7.24	(3.55, 19.83)	6.27	(3.09, 16.77)	(-241, -35)
OM_20201012	82.2	38.02	(24.98, 61.15)	32.91	(21.46, 52.72)	(-675, -282)
OM_20201114	68	56.82	(34.67, 90.27)	48.34	(29.46, 77.5)	(-918, -362)
OM_20201127	82.2	91.75	(70.41, 120.55)	78.06	(60.1, 102.15)	(-1499, -845)
OM_20201213	82.2	33.14	(23.11, 52.8)	28.07	(19.62, 44.59)	(-680, -288)
OM_20210109	82.2	46.35	(39.27, 54.97)	39.1	(33.3, 46.16)	(-721, -501)
OM_20210201	82.2	21.06	(13.55, 34.46)	17.98	(11.57, 29.33)	(-425, -162)
OM_20210214	82.2	45.75	(36.9, 57.9)	39.03	(31.59, 49.3)	(-714, -436)
OM_20210322	82.2	23.29	(13.26, 42.24)	20.35	(11.69, 36.22)	(-502, -131)
OM_20210414	82.2	0.49	(0.28, 0.99)	0.44	(0.25, 0.87)	(-10, -2)
OM_20210427	82.2	0.45	(0.22, 0.99)	0.39	(0.2, 0.86)	(-11, -2)
OM_20210515	82.2	0.54	(0.28, 1.22)	0.47	(0.24, 1.05)	(-14, -3)
OM_20210616	82.2	1.47	(0.65, 3.03)	1.24	(0.55, 2.56)	(-39, -8)
OM_20210709	82.2	0.7	(0.21, 2.49)	0.6	(0.18, 2.11)	(-32, -3)
OM_20210812	82.2	0.56	(0.2, 1.65)	0.48	(0.17, 1.39)	(-21, -2)

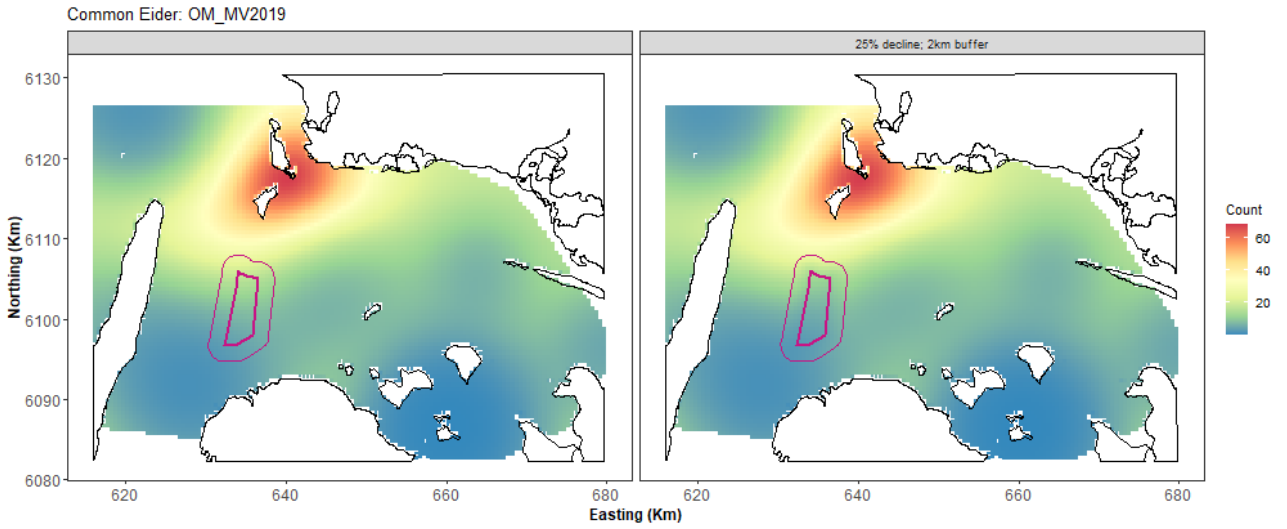

Figure 5.13. Example of displacement scenario 1 for Common Eider. On the left is one of the estimated bootstrap predictions from the OM_MV2019 model. On the right is the same set of predictions but with the scenario imposed. The footprint is shown by the thick purple line and the buffer the thinner purple line.

The second scenario for Common Eiders was a 25% decline in the footprint of the proposed wind farm with a linear return to no change in a 1km buffer. This led to a decline in density of between less than 1 bird per km^2 and up to 40 birds per km^2 (Table 5.4). Regardless of the decline in each case, the confidence intervals for the densities both before and after the impact shared values in each case. This indicates no compelling evidence for a difference before

and after the impact scenarios imposed. Figure 5.14 shows an example scenario based on one of the bootstrap replicates and the latest large-scale survey (OM_MV2019).

Table 5.4. Table showing the effect of scenario 2 implementation on bird numbers in the proposed wind farm footprint and buffer regions. "Area" is the area in km^2 of the available prediction cells in the footprint + buffer area for each survey (2012 onwards). "Density Change" is the after density minus the before density. "95% CI" figures represent the 95 percentile-based confidence intervals for each estimate.

Survey	Area (km^2)	Density Before	95% CI Before	Density After	95% CI After	Density Change	95% CI Change
OM_M2012	-	16.13	(5.52, 40.99)	13.18	(4.54, 33.49)	-2.95	(-7.5, -0.98)
OM_MV2013	50	66.89	(52.87, 84)	54.75	(43.23, 68.63)	-12.14	(-15.27, -9.59)
OM_20131010	50	62.38	(37.68, 127.57)	53.05	(32.25, 107.7)	-9.33	(-21.58, -5.24)
OM_20131120	50	75.62	(53.03, 169.81)	61.43	(43.09, 137.73)	-14.19	(-32.08, -9.95)
OM_20140308	50	62.77	(43.93, 113.59)	51.18	(35.9, 92.61)	-11.59	(-20.98, -8.02)
OM_20140411	50	6.06	(2.39, 18.17)	5.02	(2.01, 14.95)	-1.04	(-3.22, -0.39)
OM_20141030	50	214.83	(162.13, 940.37)	175.11	(132.4, 765.53)	-39.72	(-174.84, -29.78)
OM_20141121	50	167.61	(134.3, 607.4)	135.04	(108.51, 484.29)	-32.57	(-123.11, -26.36)
OM_20141228	50	60.17	(43.95, 90.24)	49.02	(35.76, 73.02)	-11.15	(-17.22, -8.01)
OM_20150309	50	31.21	(11.55, 157.91)	26.27	(9.98, 128.5)	-4.94	(-29.43, -1.65)
OM_20150409	50	5.33	(2.65, 12.21)	4.31	(2.15, 9.78)	-1.02	(-2.41, -0.5)
OM_MV2016	50	21.57	(16.31, 28.88)	17.59	(13.33, 23.51)	-3.98	(-5.37, -2.98)
OM_M2018	50	4.52	(3.24, 6.05)	3.73	(2.67, 4.96)	-0.8	(-1.08, -0.57)
OM_MV2019	50	34.43	(26.79, 46.65)	28.21	(21.98, 38.17)	-6.23	(-8.48, -4.82)
OM_20200915	50	5.66	(2.42, 18.87)	4.74	(2.03, 15.6)	-0.92	(-3.46, -0.38)
OM_20201012	50	30.77	(20.53, 48.45)	25.6	(17.02, 40.42)	-5.18	(-8.16, -3.51)
OM_20201114	43.5	51.14	(32.02, 80.87)	42.06	(26.32, 66.48)	-9.07	(-14.29, -5.7)
OM_20201127	50	84.89	(63.67, 113.96)	69.72	(52.31, 93.61)	-15.17	(-20.35, -11.25)
OM_20201213	50	32.03	(21.95, 51.81)	26.19	(17.95, 42.29)	-5.84	(-9.52, -3.99)
OM_20210109	50	46.15	(38.43, 56.13)	37.7	(31.45, 45.76)	-8.45	(-10.38, -6.98)
OM_20210201	50	18.49	(11.61, 31.21)	15.17	(9.53, 25.57)	-3.32	(-5.65, -2.08)
OM_20210214	50	40.35	(31.68, 53.32)	33.13	(26.03, 43.7)	-7.22	(-9.64, -5.64)
OM_20210322	50	15.29	(7.69, 34.95)	12.78	(6.49, 28.75)	-2.51	(-6.12, -1.2)
OM_20210414	50	0.25	(0.12, 0.67)	0.21	(0.1, 0.56)	-0.04	(-0.11, -0.02)
OM_20210427	50	0.3	(0.13, 0.77)	0.25	(0.11, 0.63)	-0.05	(-0.14, -0.02)
OM_20210515	50	0.44	(0.21, 1.09)	0.36	(0.17, 0.9)	-0.08	(-0.2, -0.03)
OM_20210616	50	1.44	(0.63, 3.01)	1.17	(0.52, 2.45)	-0.27	(-0.56, -0.12)
OM_20210709	50	0.66	(0.19, 2.37)	0.54	(0.16, 1.93)	-0.12	(-0.44, -0.04)
OM_20210812	50	0.51	(0.18, 1.58)	0.41	(0.14, 1.29)	-0.09	(-0.29, -0.03)

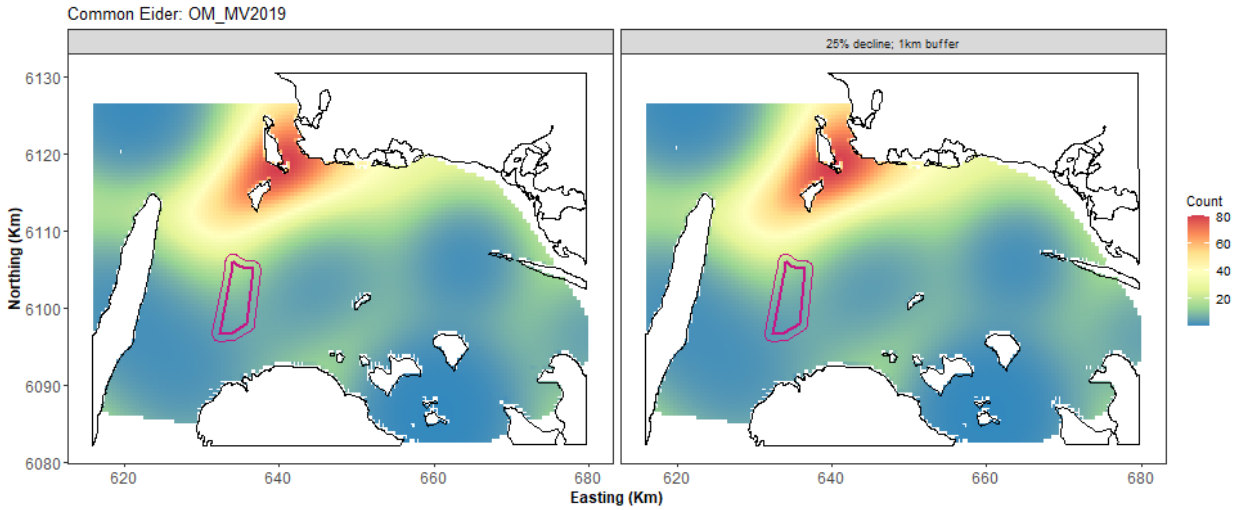

Figure 5.14. Example of displacement scenario 2 for Common Eider. On the left is one of the estimated bootstrap predictions from the MV2019 model. On the right is the same set of predictions but with the scenario imposed. The footprint is shown by the thick purple line and the buffer the thinner purple line.

6 Common Scoter *Melanitta nigra*

6.1.1 Distance Analysis

Detection function from data with four transect bands

The average probability of sighting Common Scoters was estimated to be 0.23 (CV=0.05). This probability was estimated using a hazard rate detection function that varied with cluster size (Figure 6.1). No other covariates were selected. For larger group sizes there appears to be an issue with detecting them under the plane and an over estimation in the next bin. Additionally, as expected, the detectability of large groups is much higher than for small groups furthest from the transect line.

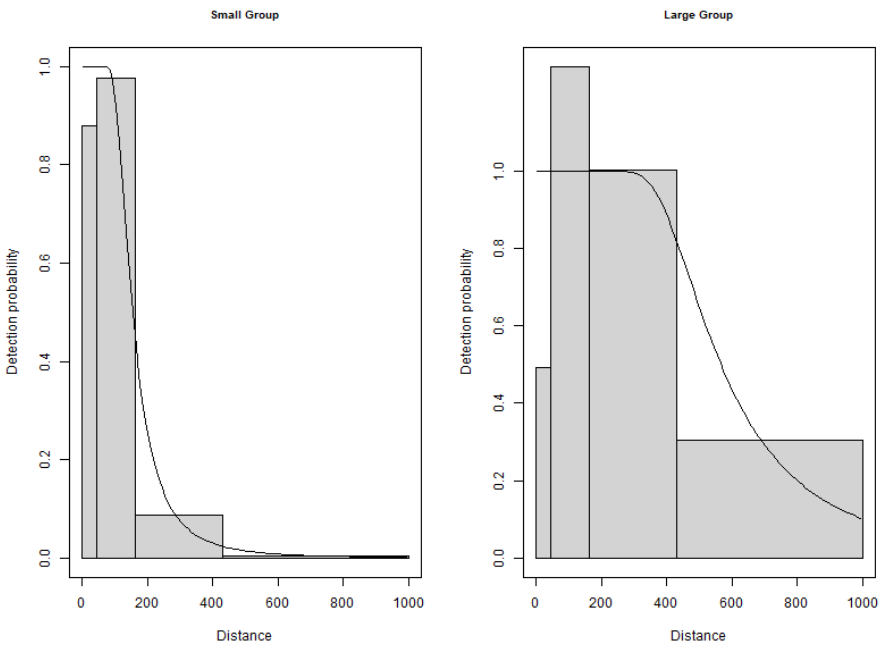

Figure 6.1. Figure showing the estimated detection function for examples of a large group and a small group of Common Scoters. The histograms are the distances of the observed sightings.

6.1.2 Detection function from data with three transect bands

The average probability of sighting common scoters was estimated to be 0.27 (CV=0.02). This probability was estimated using a hazard rate detection function that varied with cluster size, sea state, and glare (Figure 6.2, Figure 6.3 and Figure 6.4). No other covariates were selected. As for the surveys conducted with four transect bands, there is an issue with detecting large groups in the first distance band. This may occur if the aggregation of birds is larger than the width of the first band.

Figure 6.2. Figure showing the estimated detection function for examples of a large group and a small group of Common Scoters. The histograms are the distances of the observed sightings.

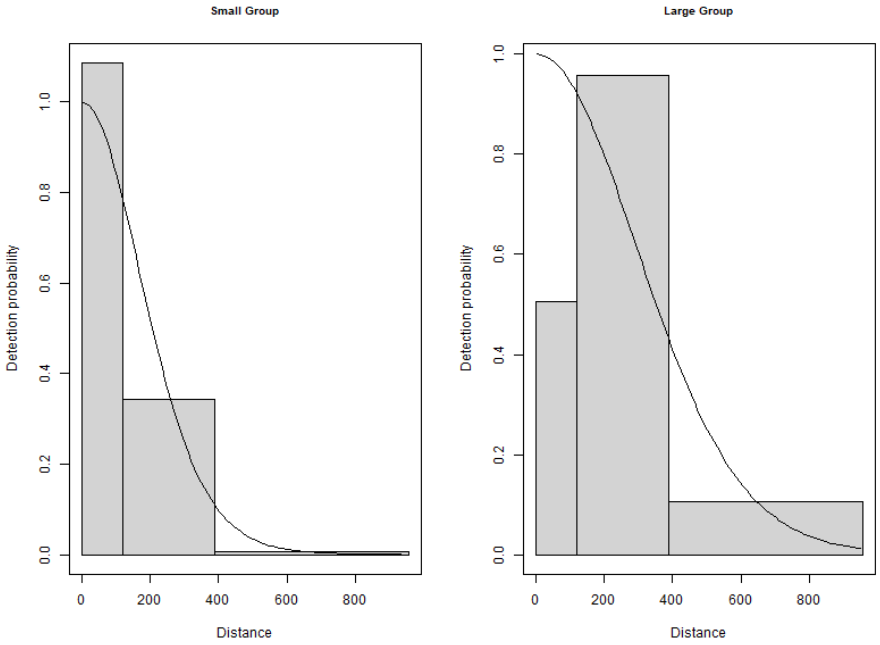

Figure 6.3. Figure showing the estimated detection function for Common Scoter for different amounts of glare. The histograms are the distances of the observed sightings.

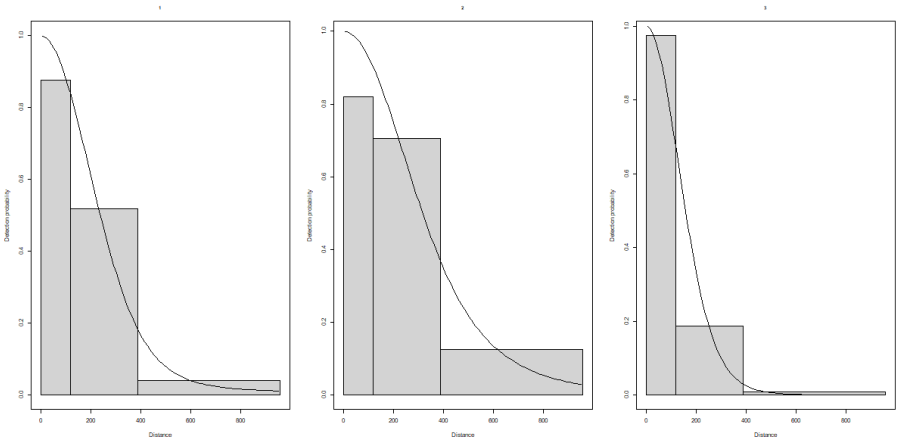

Figure 6.4. Figure showing the estimated detection function for Common Scoter for different sea states. The histograms are the distances of the observed sightings.

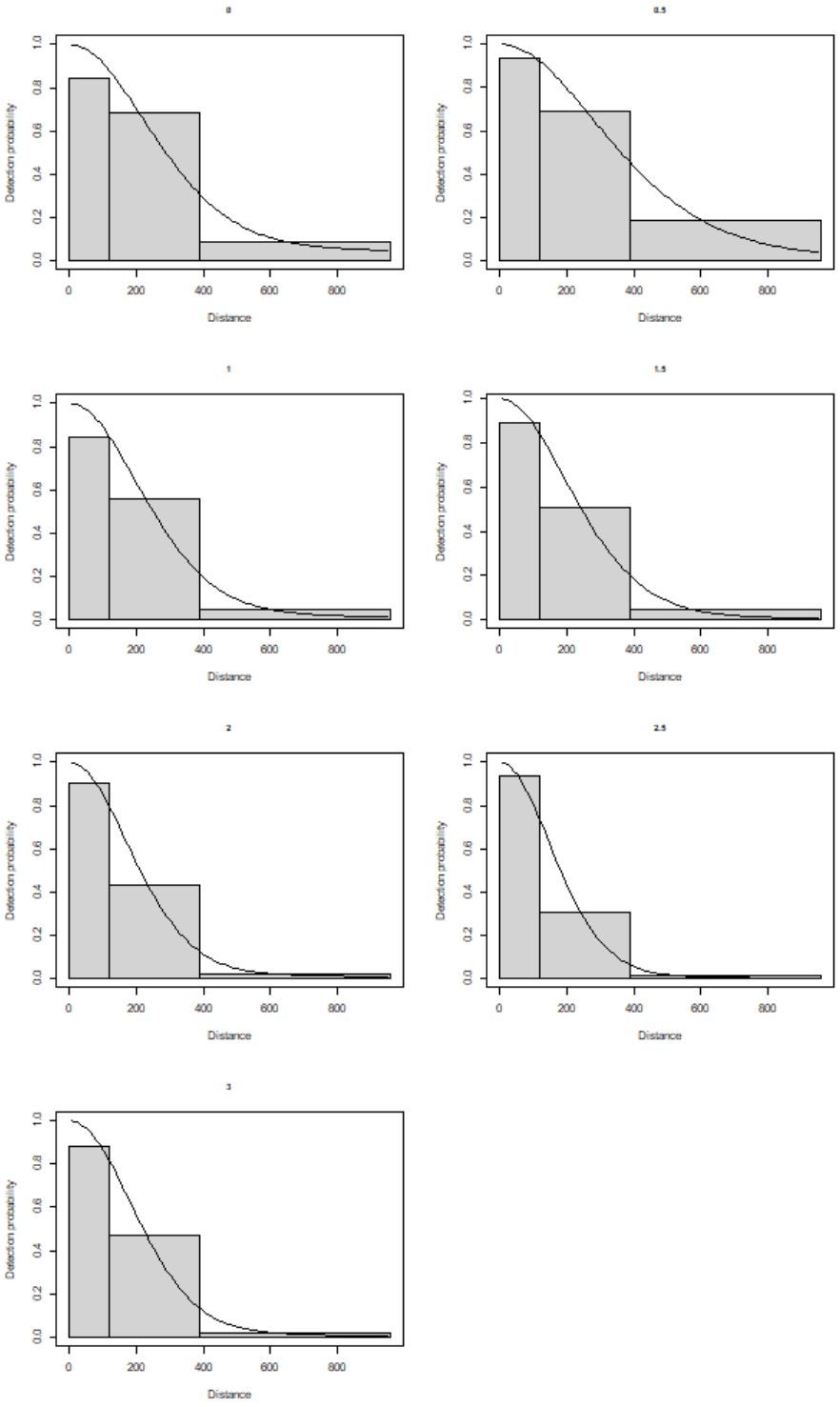

6.1.3 Spatial analysis

The two datasets were combined for the spatial analysis and contained 31,512 segments, 5.8% of which were segments containing Common Scoter sightings. Figure 6.5 shows the distribution of the distance corrected counts for all 37 surveys. Two of the 37 surveys had zero observations and a further 4 had too few observations for a spatial analysis to be conducted (less than 12 observations).

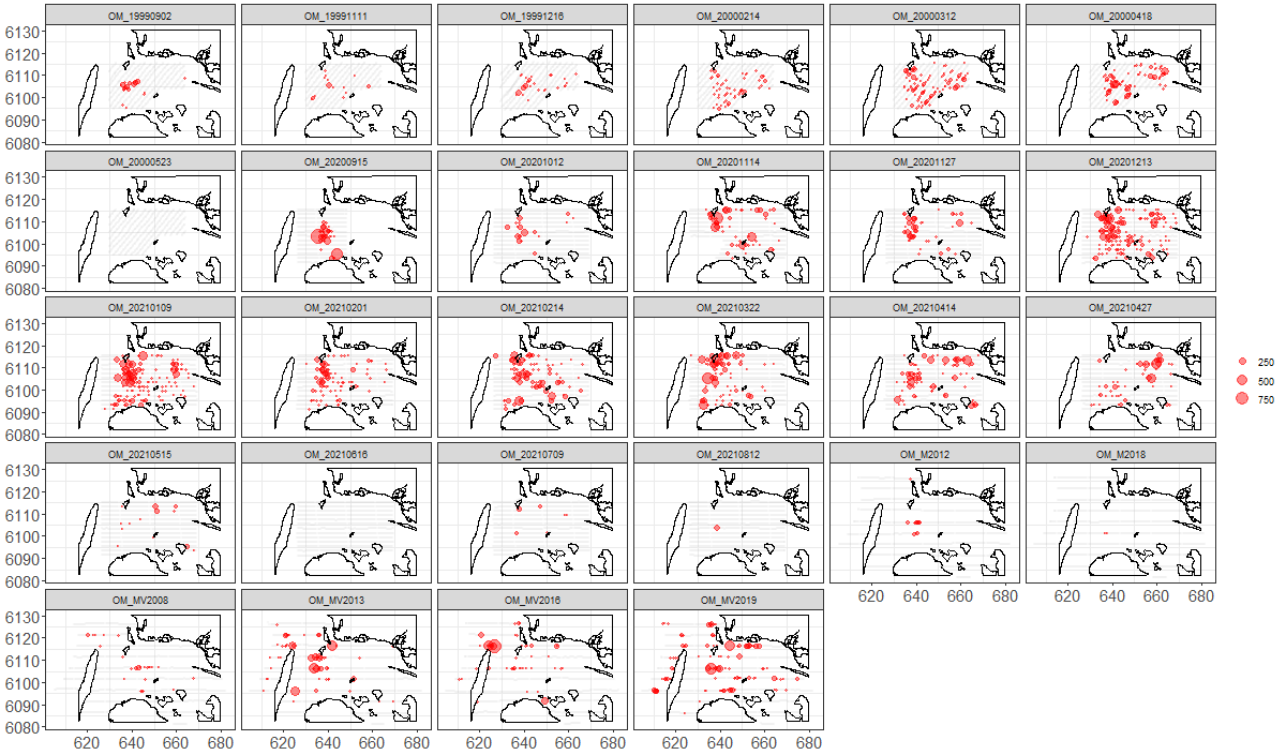

Figure 6.5. Counts for the Common Scoters across the 28 surveys. The red circles indicate the distance-corrected counts along the transect lines while the polygons represent land. Grey dots are segments with a count of zero.

6.1.4 Model Selection results

Only 31 surveys had sufficient observations to enable a fitted model (e.g., n>10) and each model selected included a spatial term of typically low to medium complexity (2-10 parameters). In addition to the spatial term a linear depth term was selected for two of the 31 surveys analysed. Both surveys had similar patterns with the highest estimated counts at shallow depths and declining abundance with increasing depth. Distance to coast (either as a linear or smooth term) was not selected for any of the survey-based models. This shows that while there was compelling evidence for non-uniform spatial patterns in each survey, there was little evidence for a depth relationship and no evidence for a distance to coast based relationship over and above the spatial terms (Table 6.1).

The estimated abundances and associated 95 percentile confidence intervals for each survey are given in Table 6.2, while the equivalent values for density and a visual representation of these estimates (with associated uncertainties) are shown in Figure 6.6.

Table 6.1. Model selection results for Common Scoters for each survey. The Variables column represents the terms in the model while the 'degrees of freedom' column indicates the number of parameters allocated to each smooth term. The extra-Poisson dispersion parameter estimates are listed in the far-right column. Empty cells indicate too few observations for the spatial analysis, e.g. n=12.

Year	Month	Survey	Variables	Degrees of freedom	Dispersion parameter estimate
1999	09	OM_19990902	s(x.pos, y.pos)	2	62.2
	11	OM_19991111	s(x.pos, y.pos)	5	65.5
	12	OM_19991216	-		
2000	02	OM_20000214	s(x.pos, y.pos)	6	20.9
	03	OM_20000312	s(x.pos, y.pos)	10	30.9
	04	OM_20000418	s(x.pos, y.pos)	5	63.1
	05	OM_20000523	-		
2008	01/02	OM_MV2008	s(x.pos, y.pos)	6	18.3
2012	08/09	OM_MV2012	s(x.pos, y.pos)	4	15.8
2013	01	OM_MV2013	s(x.pos, y.pos)	3	188.2
2013	10	OM_20131010	Depth + s(x.pos, y.pos)	6	146.7
	11	OM_20131120	s(x.pos, y.pos)	8	103.2
2014	03	OM_20140308	s(x.pos, y.pos)	4	177.9
	04	OM_20140411	s(x.pos, y.pos)	6	343.8
	10	OM_20141030	s(x.pos, y.pos)	5	57.3
	11	OM_20141121	s(x.pos, y.pos)	8	94.5
	12	OM_20141228	s(x.pos, y.pos)	5	25.5
2015	03	OM_20150309	s(x.pos, y.pos)	6	55.8
	04	OM_20150409	s(x.pos, y.pos)	5	116.7
2016	01	OM_MV2016	s(x.pos, y.pos)	4	78.1
2018	07	OM_MV2018	-		
2019	12	OM_MV2019	s(x.pos, y.pos)	4	103.3
2020	09	OM_20200915	Depth + s(x.pos, y.pos)	3	89.6
	10	OM_20201012	s(x.pos, y.pos)	3	80.0
	11	OM_20201114	s(x.pos, y.pos)	7	97.2
	11	OM_20201127	s(x.pos, y.pos)	5	74.0
	12	OM_20201213	s(x.pos, y.pos)	8	65.8
2021	01	OM_20210109	s(x.pos, y.pos)	7	103.3
	02	OM_20210201	s(x.pos, y.pos)	8	45.6
	02	OM_20210214	s(x.pos, y.pos)	4	115.5
	03	OM_20210322	s(x.pos, y.pos)	4	124.8
	04	OM_20210414	s(x.pos, y.pos)	5	121.0
	04	OM_20210427	s(x.pos, y.pos)	3	107.0
	05	OM_20210515	s(x.pos, y.pos)	6	53.0
	06	OM_20210616	-		
	07	OM_20210709	-		
	08	OM_20210812	-		

Table 6.2. Estimated density of Common Scoters for each survey. The 95% CI are percentile-based confidence intervals. The area is the area of the prediction region (convex hull around the data).

Year	Month	Survey	Area (km^2)	Estimated Count	95% CI Count	Estimated Density	95% CI Density
1999	09	OM_19990902	591	1103	(516, 2298)	1.9	(0.9, 3.9)
	11	OM_19991111	585	450	(116, 2583)	0.8	(0.2, 4.4)
2000	02	OM_20000214	591	1549	(906, 3002)	2.6	(1.5, 5.1)
	03	OM_20000312	590	3093	(1712, 8476)	5.2	(2.9, 14.4)
	04	OM_20000418	588	3213	(1580, 7675)	5.5	(2.7, 13)
2008	10	OM_MV2008	1938	1430	(755, 3629)	0.7	(0.4, 1.9)
2012	11	OM_MV2012	1926	1221	(692, 2722)	0.6	(0.4, 1.4)
2013		OM_MV2013	1940	10452	(5834, 20126)	5.4	(3, 10.4)
	10	OM_20131010	1085	1626	(823, 3710)	1.5	(0.8, 3.4)
	11	OM_20131120	1070	4257	(1959, 12753)	4	(1.8, 11.9)
2014	03	OM_20140308	1071	12136	(7095, 22039)	11.3	(6.6, 20.6)
	04	OM_20140411	1071	39732	(23013, 73493)	37.1	(21.5, 68.6)
	10	OM_20141030	474	2116	(842, 6901)	4.5	(1.8, 14.6)
	11	OM_20141121	507	3546	(2055, 7390)	7	(4.1, 14.6)
	12	OM_20141228	507	495	(244, 1379)	1	(0.5, 2.7)
2015	03	OM_20150309	515	2755	(1773, 4735)	5.4	(3.4, 9.2)
	04	OM_20150409	491	3137	(1939, 5774)	6.4	(3.9, 11.8)
2016		OM_MV2016	1937	6441	(4300, 11681)	3.3	(2.2, 6)
2019		OM_MV2019	1918	11675	(6560, 24520)	6.1	(3.4, 12.8)
2020	09	OM_20200915	508	3068	(1571, 7125)	6	(3.1, 14)
	10	OM_20201012	964	1173	(560, 3270)	1.2	(0.6, 3.4)
	11	OM_20201114	879	4117	(1757, 12825)	4.7	(2, 14.6)
	11	OM_20201127	968	2585	(1427, 5560)	2.7	(1.5, 5.7)
	12	OM_20201213	966	7435	(4601, 12710)	7.7	(4.8, 13.2)
2021	01	OM_20210109	974	7913	(4665, 14614)	8.1	(4.8, 15)
	02	OM_20210201	982	3892	(2332, 7487)	4	(2.4, 7.6)
	02	OM_20210214	969	5359	(3229, 9894)	5.5	(3.3, 10.2)
	03	OM_20210322	980	5388	(3498, 9411)	5.5	(3.6, 9.6)
	04	OM_20210414	978	4355	(2226, 9975)	4.5	(2.3, 10.2)
	04	OM_20210427	970	3012	(1286, 8281)	3.1	(1.3, 8.5)
	05	OM_20210515	957	488	(319, 935)	0.5	(0.3, 1)

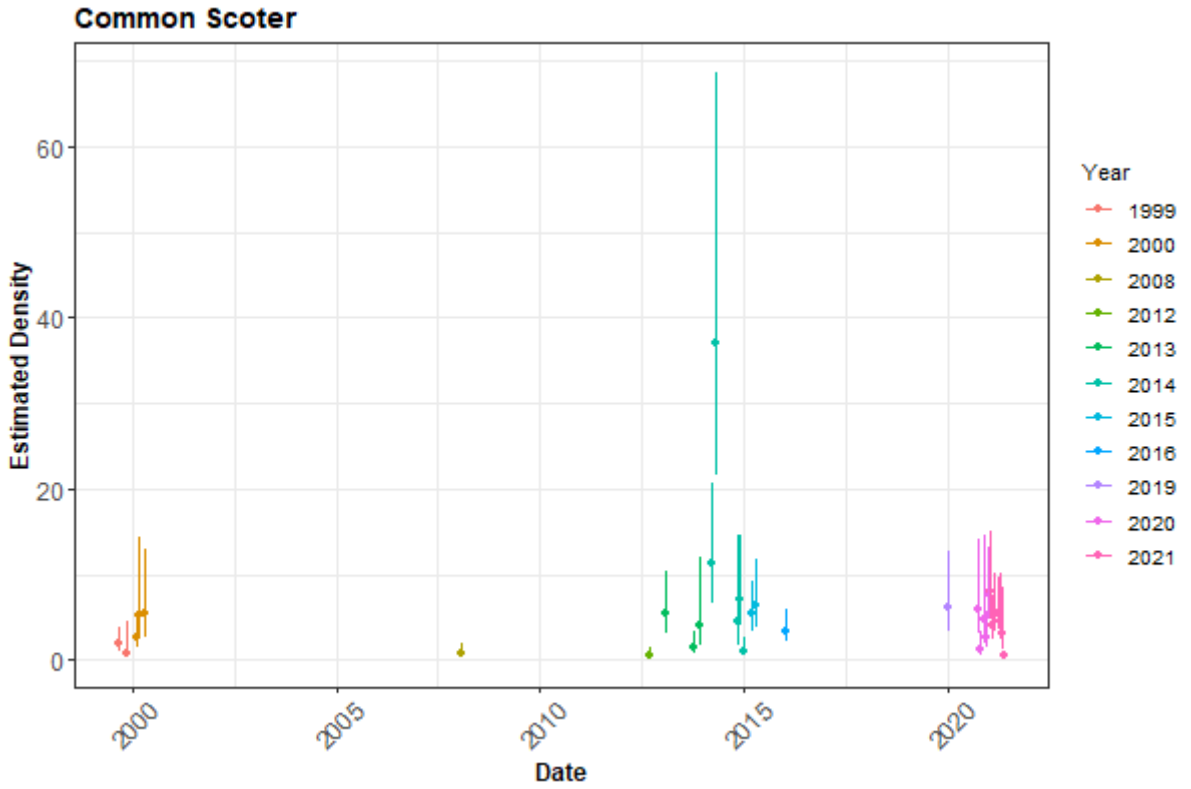

Figure 6.6. The estimated density of Common Scoters for each survey. The 95% CI are percentile-based confidence intervals are from a parametric bootstrap with 500 replicates. Densities are presented rather than counts as the study area for each survey is different.

6.1.5 Spatial Results

Figure 6.7 shows the estimated counts of Common Scoter in each 500x500 m grid cell for each survey. Generally, the estimated abundances fit well to the raw data and there are no concerning departures. The common scale applied to all surveys makes it difficult to see the underlying structure of the fitted surfaces in detail however, output CSV files are provided for all predictions and individual survey-based estimated surface plots are available in the file "extraplots-scoters.docx".

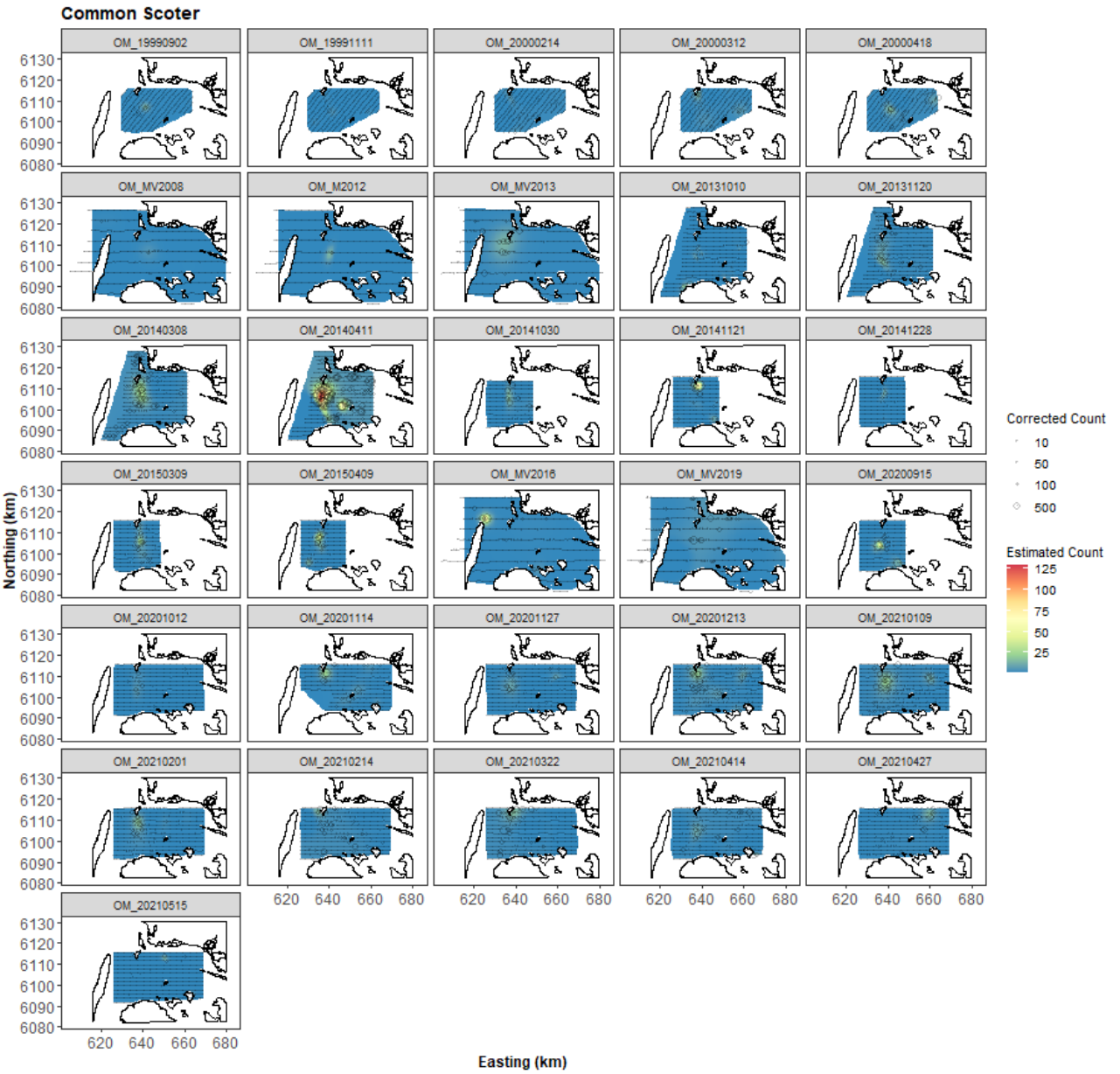

Figure 6.7. Figure showing the estimated Common Scoter abundance across the study site for each of the surveys. The title of each subfigure after the underscore ("OM_") details the survey year (4 digits) and in years with multiple surveys, survey month (2 digits) and day (2 digits) follows the year. The estimated counts are per 500x500m grid cell. The open circles show the observed corrected count. The coloured graphics represent the predicted values in each location.

6.1.6 Uncertainty in the spatial predictions

The highest coefficient of variation (CoV) scores was associated with the very smallest predictions, however it is known that the CoV metric is highly sensitive to any uncertainty for very small predictions. There was no material overlap between high values of the CoV metric and the transect lines/locations with non-zero counts and therefore results in no concerns in this case (Figure 6.8 and Figure 6.9).

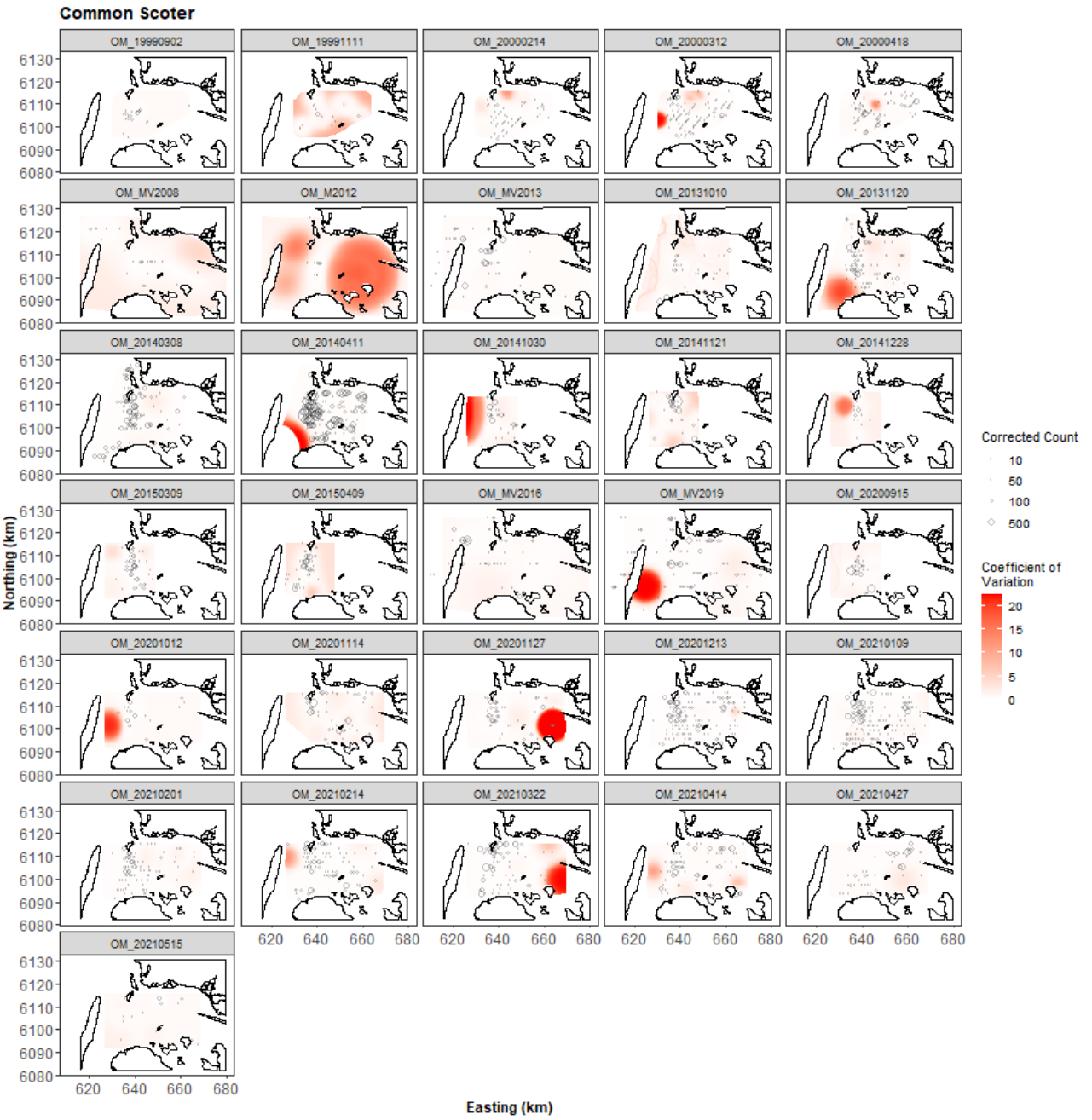

Figure 6.8. Figure showing the coefficient of variation across the study region for each of the surveys. The open circles show the distance corrected counts, where applicable. The presence of dark red CV scores in areas with virtually zero predictions are an artifact of the very small prediction rather than of any notable concern.

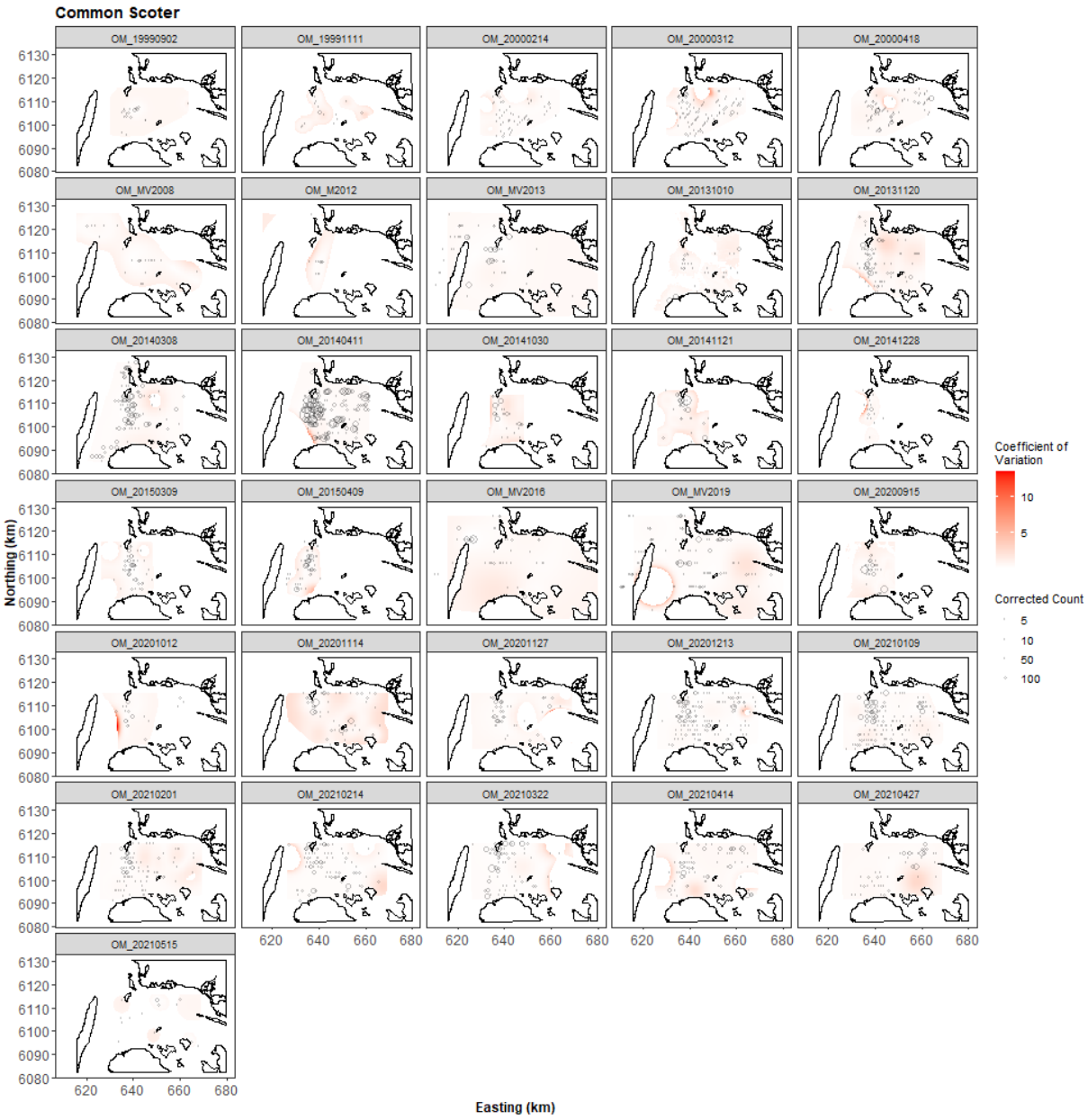

Figure 6.9. Figure showing the coefficient of variation across the study region for each of the surveys with a threshold applied to account for the very small predicted values. The open circles show the distance corrected counts, where applicable. The presence of dark red CV scores in areas with virtually zero predictions are an artifact of the very small prediction rather than of any notable concern.

6.1.7 Model Diagnostics

A blocking structure was used to account for potential residual non-independence for each model and a robust standard error approach was based on unique transects. In each case, we saw a reassuring decay to zero implying that an appropriate blocking structure was used.

The assumed mean-variance relationship was examined and generally showed agreement between the assumed (red) lines and the observed values. However, in some cases the residuals for the largest fitted values were in practice more variable than that assumed (above the line) suggesting that the variance is underestimated for these. There were no systematic clusters of negative or positive residuals for the 10 surveys and thus represent good agreement between the data and the model. The individual diagnostic plots are available on request.

6.2 Areas of Persistence

Across all surveys, there is evidence of moderate persistence in the central region of the reduced survey area, and very low persistence towards the south edge of the survey area (Figure 6.10). This low-to-moderate persistence (~0.5) also appears in the northern part of the proposed wind farm footprint, with much reduced persistence (~0.2) in the southern area of the proposed footprint.

For the wide scale surveys carried out across years (2008, 2012, 2013, 2016, 2019; Figure 6.11) the alignment of a relatively high persistence (~0.6) near the north-eastern edge, and to the north-east of the proposed wind farm footprint was clear. For the majority of the proposed windfarm footprint persistence was moderate (~0.5) while the southwestern area the persistence was much reduced (~0.25).

Notably, in the most recent surveys however (2020-2021; Figure 6.12), this area of high persistence appears to have shifted to be located north of the footprint and in particular, for some of this relatively high persistence (~0.7) to be shared with the centre-east of the proposed wind farm footprint.

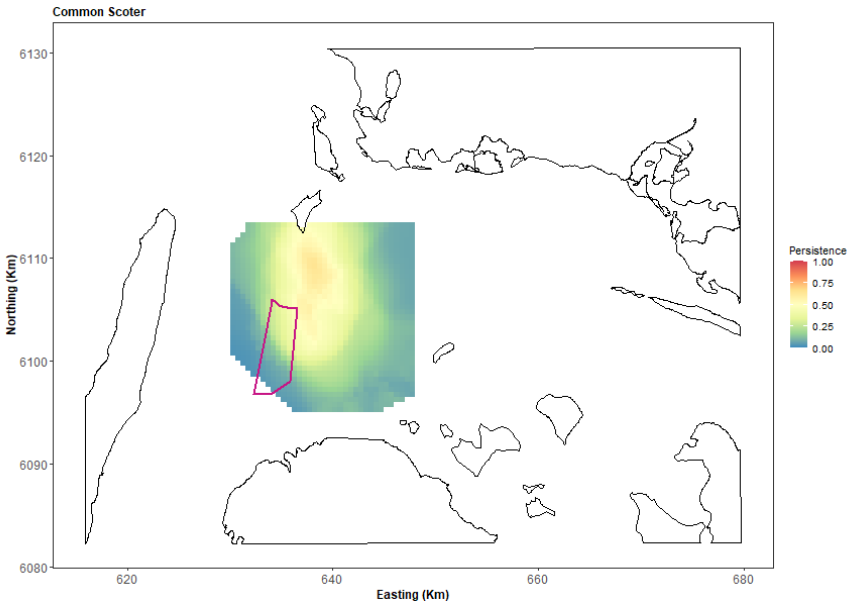

Figure 6.10. Persistence scores for Common Scoter across the persistence for survey data for all surveys. The area of the proposed offshore wind farm is indicated (polygon with red outline).

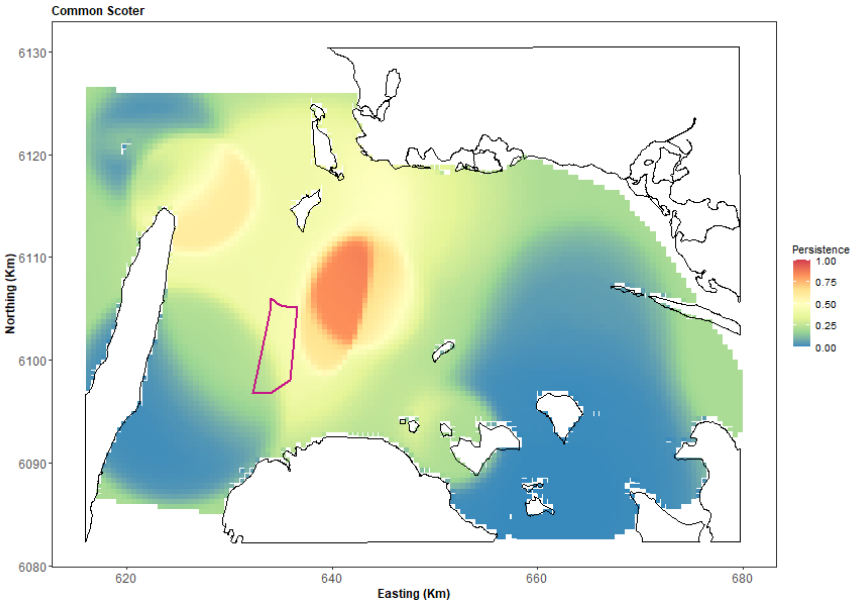

Figure 6.11. Persistence scores for Common Scoter across the large scale MV surveys (2008, 2012, 2013, 2016, 2019). The area of the proposed offshore wind farm is indicated (polygon with red outline).

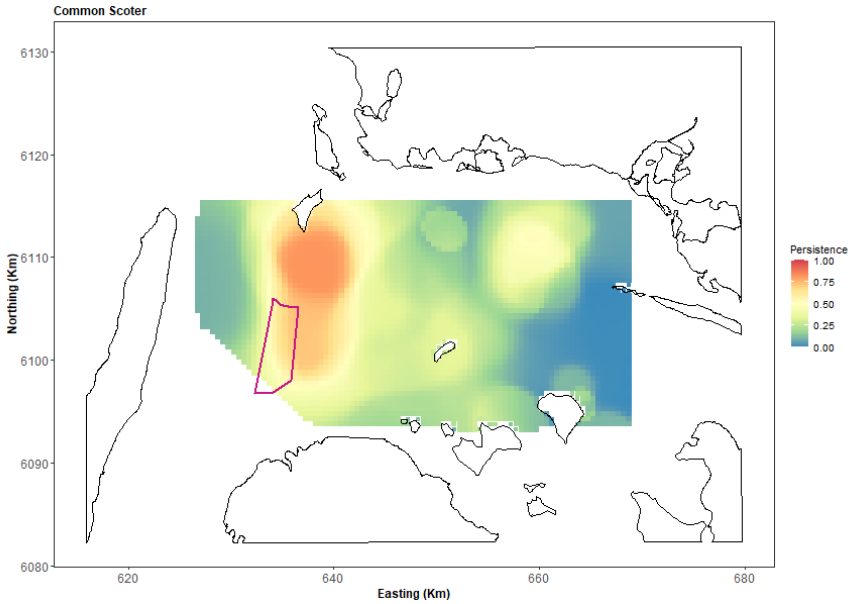

Figure 6.12. Persistence scores for Common Scoter across the persistence for survey data across 2020-2021. The area of the proposed offshore wind farm is indicated (polygon with red outline).

6.2.1 Impact Scenarios

The impact scenario undertaken for Common Scoters was an 50% decline in the footprint of the proposed wind farm with a linear return to no change in a 5km buffer. Across surveys, this returned a range of scenario outcomes ranging from 1-5 (Survey OM_20210515) to 7,427 birds (Table 6.3, OM_20140411). Eight scenarios estimated a decline as high as (at least) 1000 birds, while only one survey estimated this loss to be less than 100 birds. Figure 6.13 shows an example scenario based on one of the bootstrap replicates and the survey OM_20140308.

Table 6.3. Table showing the effect of scenario 1 implementation on Common Scoter numbers in the proposed wind farm footprint and buffer regions. "Area" is the area in km^2 of the available prediction cells in the footprint + buffer area for each survey (2012 onwards). "95% CI Expected Impacted Birds" is the after abundance minus the before abundance. "95% CI" figures represent the 95 percentile-based confidence intervals for each estimate.

Survey	Area (km^2)	Density Before	95% CI Before	Density After	95% CI After	95% CI Expected Impacted Birds
OM_MV2012	218.5	3.92	(2.66, 5.95)	3.29	(2.25, 4.99)	(-258, -88)
OM_MV2013	218.5	15.85	(8.49, 33.96)	11.85	(6.7, 24)	(-2173, -408)
OM_20131010	218.5	2.22	(1.48, 3.33)	1.65	(1.12, 2.51)	(-193, -81)
OM_20131120	218.5	10.77	(7.31, 18.03)	7.61	(5.18, 12.35)	(-1231, -471)
OM_20140308	218.5	21.31	(15.83, 28.03)	16.68	(12.49, 21.58)	(-1377, -728)
OM_20140411	218.5	89.41	(70.86, 118.12)	63.3	(49.7, 84.81)	(-7427, -4408)
OM_20141030	218.5	7.71	(4.6, 15.52)	5.41	(3.23, 10.95)	(-1022, -318)
OM_20141121	218.5	3.8	(2.08, 7.56)	3.05	(1.74, 5.77)	(-387, -73)
OM_20141228	218.5	2	(1.65, 3.36)	1.51	(1.24, 2.5)	(-197, -87)
OM_20150309	218.5	8.32	(6.9, 10.26)	6.53	(5.42, 8.09)	(-500, -317)
OM_20150409	218.2	14.5	(12.45, 17.79)	9.94	(8.57, 12.31)	(-1279, -816)
OM_MV2016	218.5	1.01	(0.24, 4.85)	0.76	(0.19, 3.59)	(-276, -12)
OM_MV2019	218.5	8.44	(5.51, 13.94)	6.42	(4.19, 10.65)	(-758, -284)
OM_20200915	218.5	9.77	(7.19, 13.68)	5.62	(4.03, 8.08)	(-1274, -668)
OM_20201012	218.5	3.83	(2.68, 7.24)	2.74	(1.92, 4.75)	(-577, -160)
OM_20201114	159.8	3.59	(1.77, 8.6)	3.07	(1.55, 6.98)	(-256, -34)
OM_20201127	218.5	7.65	(4.84, 12.76)	5.49	(3.54, 9.02)	(-824, -283)
OM_20201213	218.5	10.01	(6.61, 15.66)	7.71	(5.15, 11.89)	(-833, -309)
OM_20210109	218.5	16.85	(12.46, 24.84)	12.78	(9.53, 18.58)	(-1381, -618)
OM_20210201	218.5	10.2	(7.97, 14.33)	7.76	(6.17, 10.83)	(-774, -393)
OM_20210214	218.5	6.78	(4.18, 11.86)	5.08	(3.14, 8.88)	(-656, -228)
OM_20210322	218.5	7.95	(5.01, 11.84)	6.05	(3.86, 8.96)	(-632, -250)
OM_20210414	218.5	7.61	(5.89, 10.5)	5.4	(4.18, 7.32)	(-711, -351)
OM_20210427	218.5	1.25	(0.53, 2.63)	0.93	(0.4, 1.94)	(-150, -29)
OM_20210515	218.5	0.04	(0.01, 0.14)	0.03	(0.01, 0.12)	(-5, -1)

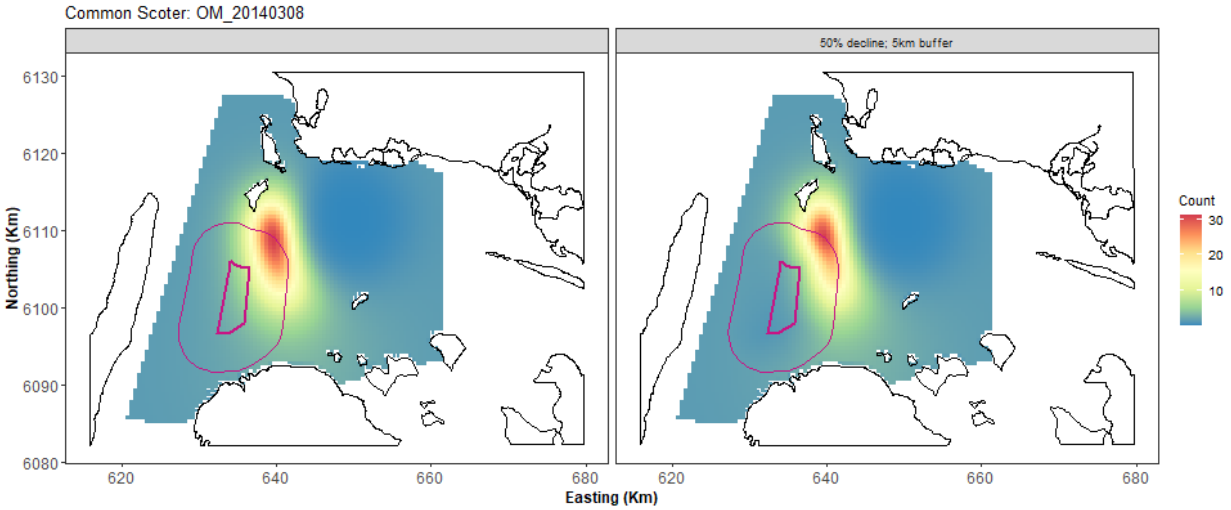

Figure 6.13. Example of displacement scenario 1 for Common Scoter. On the left is one of the estimated bootstrap predictions from the OM_20140308 model. On the right is the same set of predictions but with the scenario imposed. The footprint is shown by the thick purple line and the buffer the thinner purple line.

7 Long-tailed Duck *Clangula hyemalis*

7.1.1 Distance Analysis

Detection function from data with four transect bands

The average probability of sighting Long-tailed Ducks was estimated to be 0.12 (CV=0.1). This probability was estimated using a half normal detection function that did not vary with any covariates (Figure 7.1). Owing to an issue with low detectability in the first bin, the first two bins were merged for this analysis. The assumption was that this issue stemmed from the birds flushing from under the plane into the second bin.

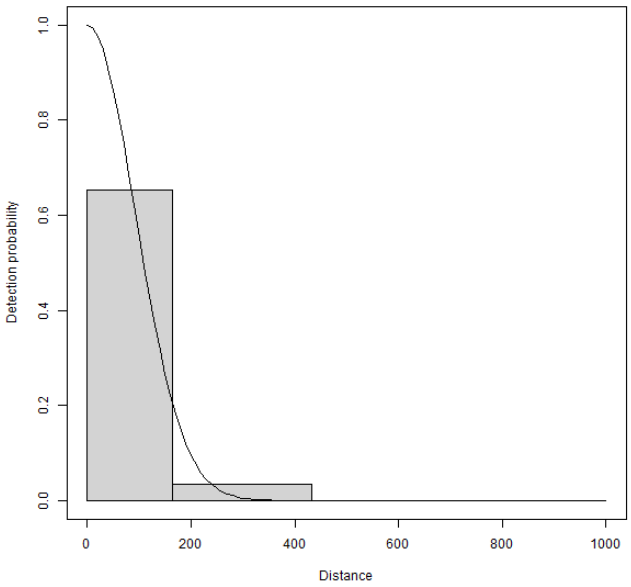

Figure 7.1. Figure showing the estimated detection function. The histogram is the distances of the observed sightings.

7.1.2 Detection function from data with three transect bands

The average probability of sighting Long-tailed Ducks was estimated to be 0.19 (CV=0.04). This probability was estimated using a half normal detection function that did not vary with any covariates (Figure 7.2).

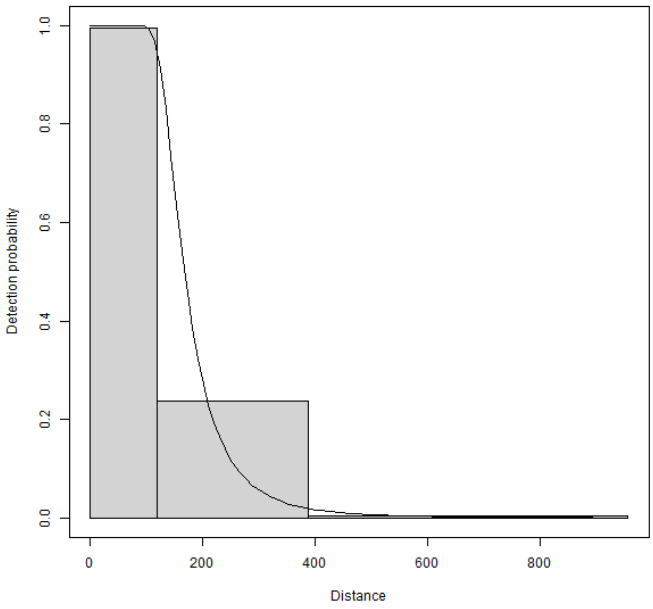

Figure 7.2. Figure showing the estimated detection function for Long-tailed Duck. The histogram is the distances of the observed sightings.

7.1.3 Spatial analysis

The two datasets were combined for the spatial analysis and contained 31512 segments, 1.8% of which were segments containing Long-tailed Duck sightings. Figure 7.3 shows the distribution of the distance corrected counts for all 37 surveys. Ten of the 37 surveys had zero observations and a further 9 had too few observations for a spatial analysis to be conducted (less than 12 observations).

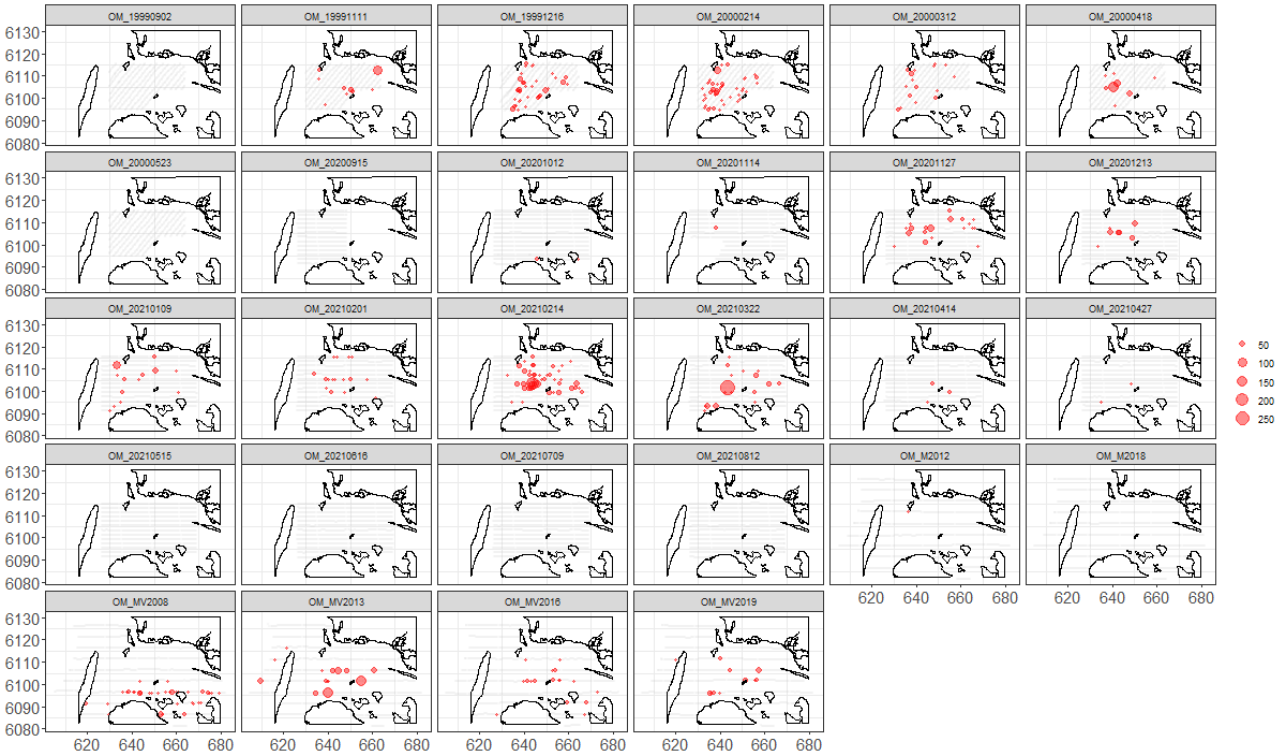

Figure 7.3. Counts for the Long-tailed Duck across the 28 surveys. The red circles indicate the distance-corrected counts along the transect lines while the polygons represent land. Grey dots are segments with a count of zero.

7.1.4 Model Selection results

Only 18 surveys had sufficient observations to enable a fitted model and each model selected included a spatial term of typically low to medium complexity (2-8 parameters). In addition to the spatial term a depth term was selected for two of the 18 'successful' surveys analysed (one as a linear term and one as a smooth term). Both surveys had similar patterns with the highest estimated counts at shallow depths and declining abundance with increasing depth, either linearly or as a smooth decay function. Distance to coast (either as a linear or smooth term) was not selected for any of the survey-based models. This shows that while there was compelling evidence for non-uniform spatial patterns in each survey, there was little evidence for a depth relationship and no evidence for a distance to coast-based relationship over and above the spatial terms (Table 7.1).

The estimated abundances and associated 95 percentile confidence intervals for each survey are given in Table 7.2, while the equivalent values for density and a visual representation of these estimates (with associated uncertainties) are shown in Figure 7.4.

Table 7.1. Model selection results for Long-tailed Duck for each survey. The Variables column represents the terms in the model while the 'degrees of freedom' column indicates the number of parameters allocated to each smooth term. The extra-Poisson dispersion parameter estimates are listed in the far-right column. Empty cells indicate too few observations for the spatial analysis, e.g. n=12.

Year	Month	Survey	Variables	Degrees of freedom	Dispersion parameter estimate
1999	09	OM_19990902	-		
	11	OM_19991111	s(x.pos, y.pos)	5	41.64
	12	OM_19991216	s(x.pos, y.pos)	8	14.27
2000	02	OM_20000214	s(x.pos, y.pos)+ s(depth,df=3)	2	12.48
	03	OM_20000312	Depth + s(x.pos, y.pos)	8	7.21
	04	OM_20000418	-		
	05	OM_20000523	-		
2008	01/02	OM_MV2008	s(x.pos, y.pos)	2	9.41
2012	08/09	OM_MV2012	-		
2013	01	OM_MV2013	s(x.pos, y.pos)	3	46.15
2013	10	OM_20131010	-		
	11	OM_20131120	s(x.pos, y.pos)	4	45.36
2014	03	OM_20140308	s(x.pos, y.pos)	5	95.34
	04	OM_20140411	-		
	10	OM_20141030	-		
	11	OM_20141121	s(x.pos, y.pos)	5	54.45
	12	OM_20141228	s(x.pos, y.pos)	5	42.63
2015	03	OM_20150309	s(x.pos, y.pos)	5	86.31
	04	OM_20150409	-		
2016	01	OM_MV2016	s(x.pos, y.pos)	3	9.93

2018	07	OM_MV2018	-		
2019	12	OM_MV2019	s(x.pos, y.pos)	4	20.06
2020	09	OM_20200915	-		
	10	OM_20201012	-		
	11	OM_20201114	-		
	11	OM_20201127	s(x.pos, y.pos)	7	29.52
	12	OM_20201213	-		
2021	01	OM_20210109	s(x.pos, y.pos)	4	16.27
	02	OM_20210201	s(x.pos, y.pos)	7	10.47
	02	OM_20210214	s(x.pos, y.pos)	5	23.16
	03	OM_20210322	s(x.pos, y.pos)	7	21.39
	04	OM_20210414	-		
	04	OM_20210427	-		
	05	OM_20210515	-		
	06	OM_20210616	-		
	07	OM_20210709	-		
	08	OM_20210812	-		

Table 7.2. Estimated density of Long-tailed Duck for each survey. The 95% CI are percentile-based confidence intervals. The area is the area of the prediction region (convex hull around the data).

Year	Month	Survey	Area (km^2)	Estimated Count	95% CI Count	Estimated Density	95% CI Density
1999		OM_19991111	585	219	(106, 525)	0.4	(0.2, 0.9)
		OM_19991216	617	572	(269, 1462)	0.9	(0.4, 2.4)
2000		OM_20000214	591	605	(315, 1174)	1	(0.5, 2)
		OM_20000312	590	251	(87, 934)	0.4	(0.1, 1.6)
2008		OM_MV2008	1938	982	(582, 1674)	0.5	(0.3, 0.9)
2013		OM_MV2013	1940	1449	(789, 2967)	0.7	(0.4, 1.5)
		OM_20131120	1070	585	(231, 1806)	0.5	(0.2, 1.7)
2014		OM_20140308	1071	757	(320, 4174)	0.7	(0.3, 3.9)
		OM_20141121	507	354	(211, 812)	0.7	(0.4, 1.6)
		OM_20141228	507	518	(300, 1289)	1	(0.6, 2.5)
2015		OM_20150309	515	1024	(509, 3016)	2	(1, 5.9)
2016		OM_MV2016	1937	493	(202, 1193)	0.3	(0.1, 0.6)
2019		OM_MV2019	1918	473	(236, 921)	0.2	(0.1, 0.5)
2020		OM_20201127	968	403	(197, 1011)	0.4	(0.2, 1)
2021		OM_20210109	974	254	(105, 741)	0.3	(0.1, 0.8)
		OM_20210201	982	175	(64, 757)	0.2	(0.1, 0.8)
		OM_20210214	969	1117	(485, 2580)	1.2	(0.5, 2.7)
		OM_20210322	980	567	(228, 1794)	0.6	(0.2, 1.8)

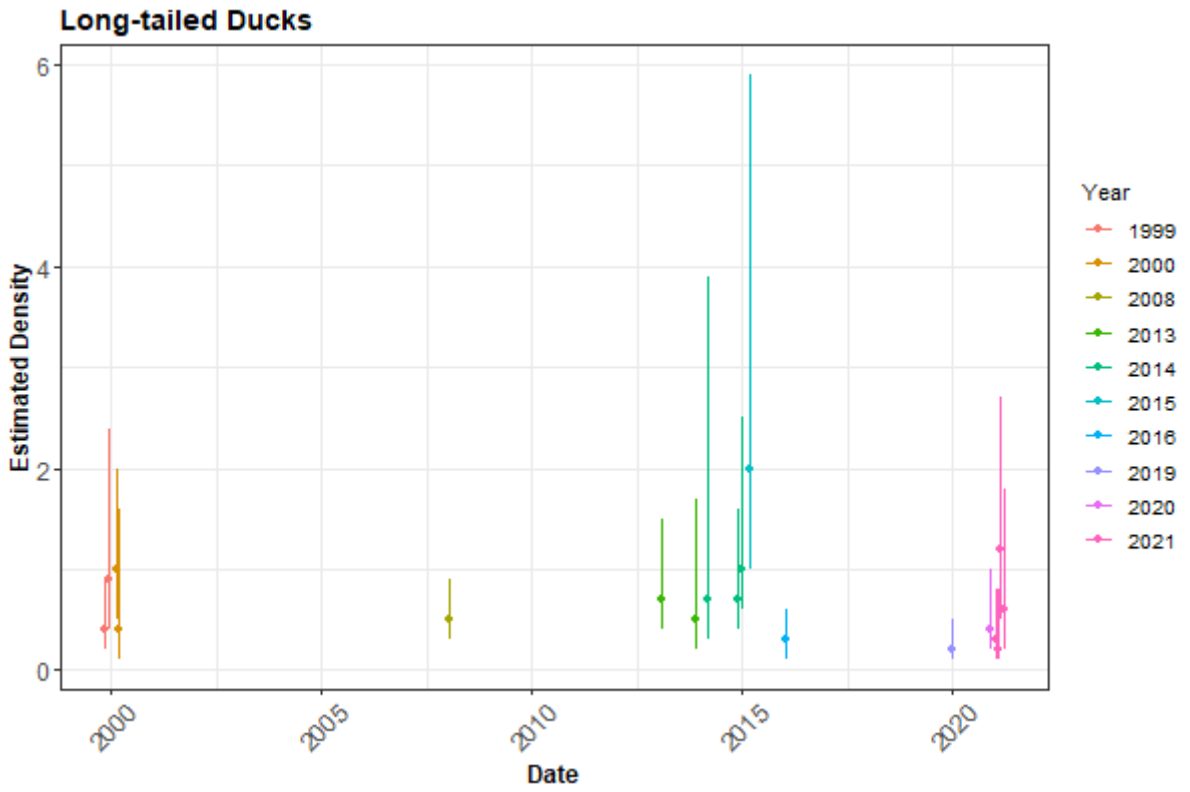

Figure 7.4. The estimated density of Long-tailed Duck for each survey. The 95% CI are percentile-based confidence intervals are from a parametric bootstrap with 500 replicates. Densities are presented rather than counts as the study area for each survey is different.

7.1.5 Spatial Results

Figure 7.5 shows the estimated counts of Long-tailed Duck in each 500x500 m grid cell for each survey. Generally, the estimated abundances fit well to the raw data and there are no concerning departures. The common scale applied to all surveys makes it difficult to see the underlying structure of the fitted surfaces in detail however, output CSV files are provided for all predictions and individual survey-based estimated surface plots are available in the file "extraplots-longtails.docx".

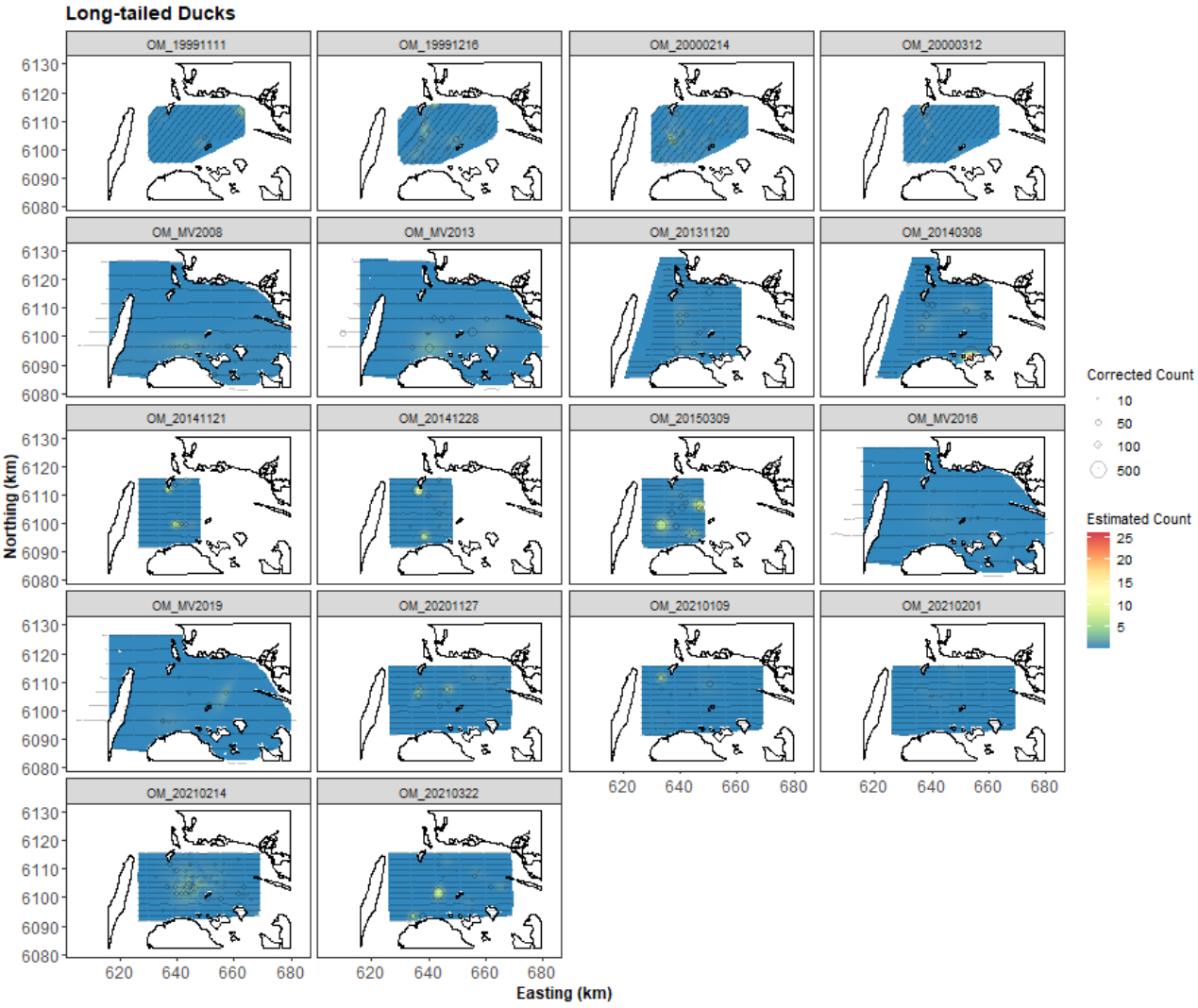

Figure 7.5. Figure showing the estimated Long-tailed Duck abundance across the study site for each of the surveys. The title of each subfigure after the underscore ("OM_") details the survey year (4 digits) and in years with multiple surveys, survey month (2 digits) and day (2 digits) follows the year. The estimated counts are per 500x500m grid cell. The open circles show the observed corrected count. The coloured graphics represent the predicted values in each location.

7.1.6 Uncertainty in the spatial predictions

The highest coefficient of variation (CoV) scores was associated with the very smallest predictions, however it is known that the CoV metric is highly sensitive to any uncertainty for very small predictions. There was no material overlap between high values of the CoV metric and the transect lines/locations with non-zero counts and therefore results in no concerns in this case (Figure 7.6 and Figure 7.7).

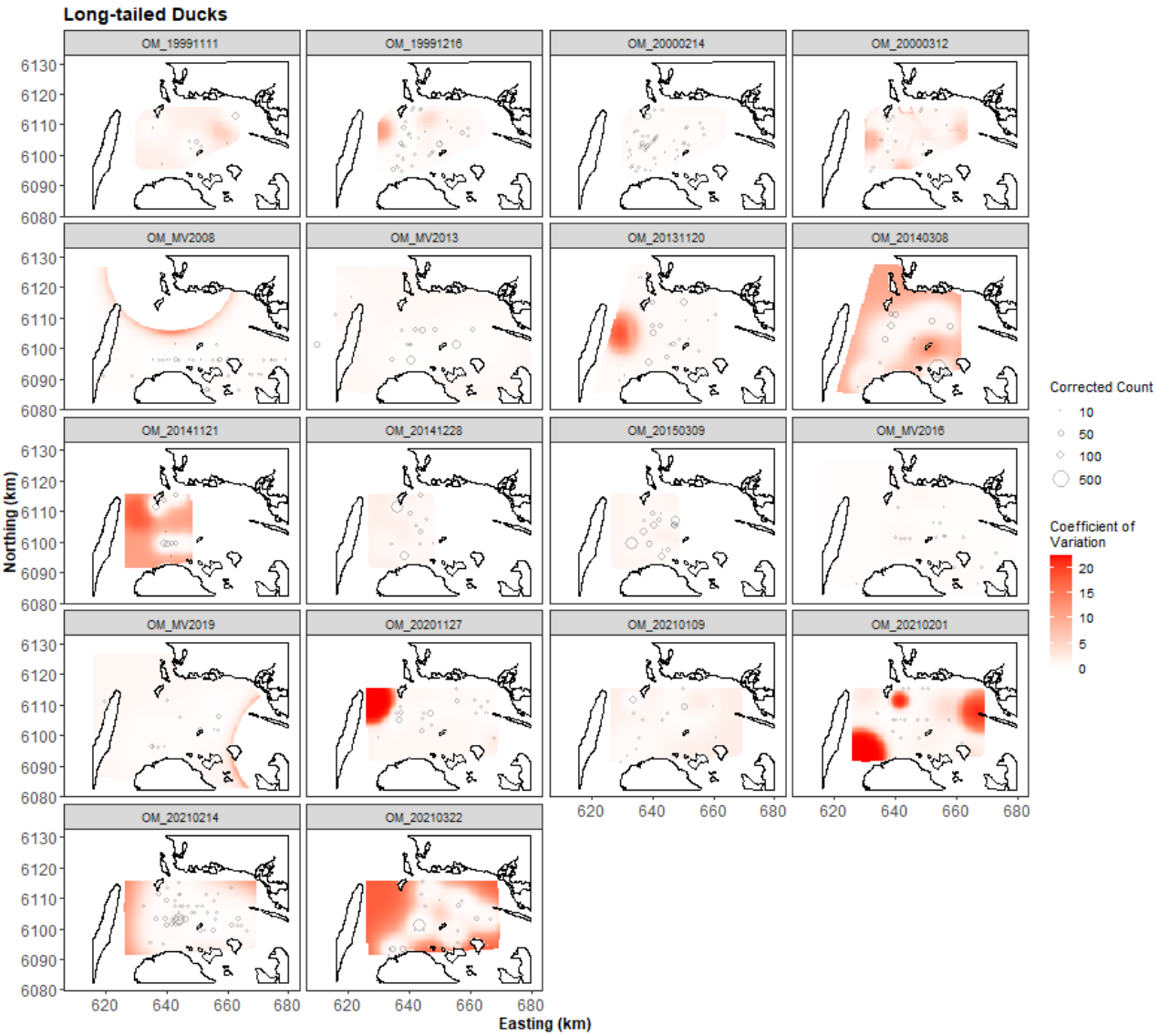

Figure 7.6. Figure showing the coefficient of variation across the study region for each of the surveys. The open circles show the distance corrected counts, where applicable. The presence of dark red CV scores in areas with virtually zero predictions are an artifact of the very small prediction rather than of any notable concern.

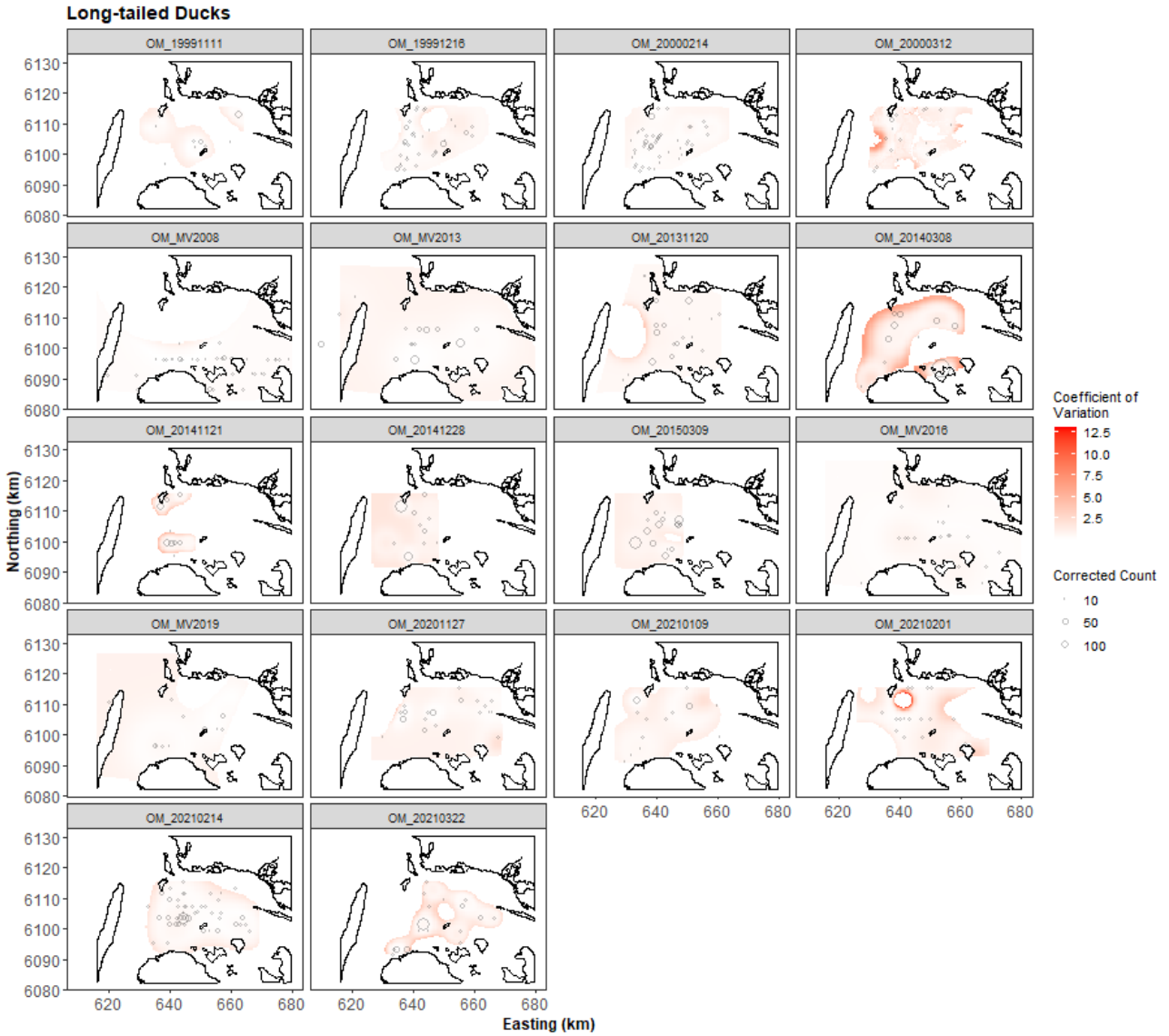

Figure 7.7. Figure showing the coefficient of variation across the study region for each of the surveys with a threshold applied to account for the very small predicted values. The open circles show the distance corrected counts, where applicable. The presence of dark red CV scores in areas with virtually zero predictions are an artifact of the very small prediction rather than of any notable concern.

7.1.7 Model Diagnostics

A blocking structure was used to account for potential residual non-independence for each model and a robust standard error approach was based on unique transects. In every case, we saw a reassuring decay to zero implying that an appropriate blocking structure was used.

The assumed mean-variance relationship was examined and generally showed agreement between the assumed (red) lines and the observed values. However, in some cases the residuals for the largest fitted values were in practice more variable than that assumed (above the line) suggesting that the variance is underestimated for these. There were no systematic clusters of negative or positive residuals for any of the surveys and thus represent good agreement between the data and the model. The individual diagnostic plots are available on request.

7.1.8 Areas of Persistence

Across all surveys, there is evidence of moderate persistence across the survey area, except in the western edge of the survey area, where the persistence falls to 0.25 or below (Figure 7.8). This moderate persistence (~0.5) dominates the proposed wind farm footprint, with some lower persistence (~0.2) on the western edge.

For the wide scale surveys carried out across years (2008, 2013, 2016, 2019; Figure 7.9) there was a striking and relatively high persistence section in the central-southern part of the survey area. At first glance, this appears to be in contrast to the scale indicated for the much smaller area in the centre of the survey area, calculated across all surveys (Figure 7.8). However, this is largely due to the relative nature of the persistence metric which in this much larger area has a much lower mean. This means that the threshold is (in some sense) easier to exceed in certain parts but nevertheless, indicates the variation in persistence across the larger area. For the southern area of the proposed wind-farm footprint persistence was relatively high (~0.8).

Notably, in the most recent surveys however (2020-2021; Figure 7.10), this area of higher persistence appears to have shifted to be located north of the footprint.

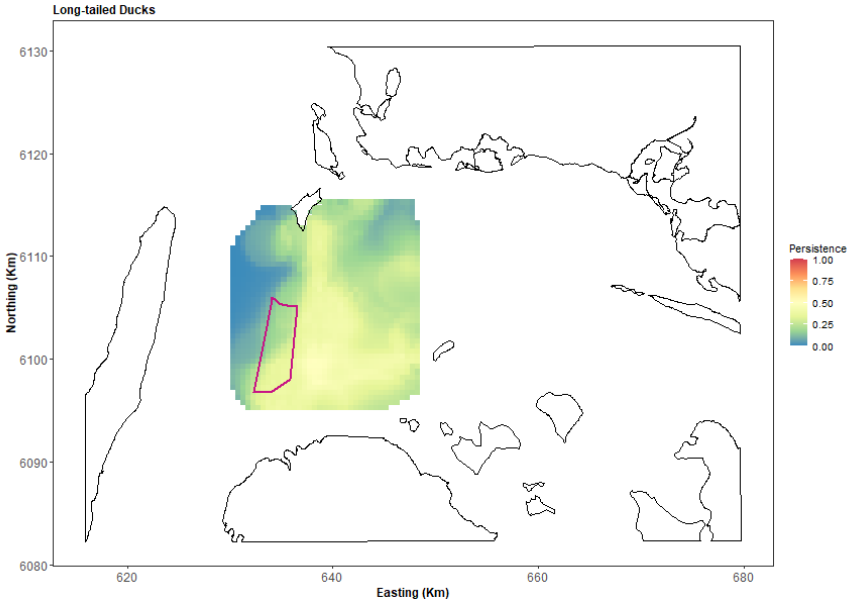

Figure 7.8. Persistence scores of Long-tailed Duck across the persistence for survey data for all surveys. The area of the proposed offshore wind farm is indicated (polygon with red outline).

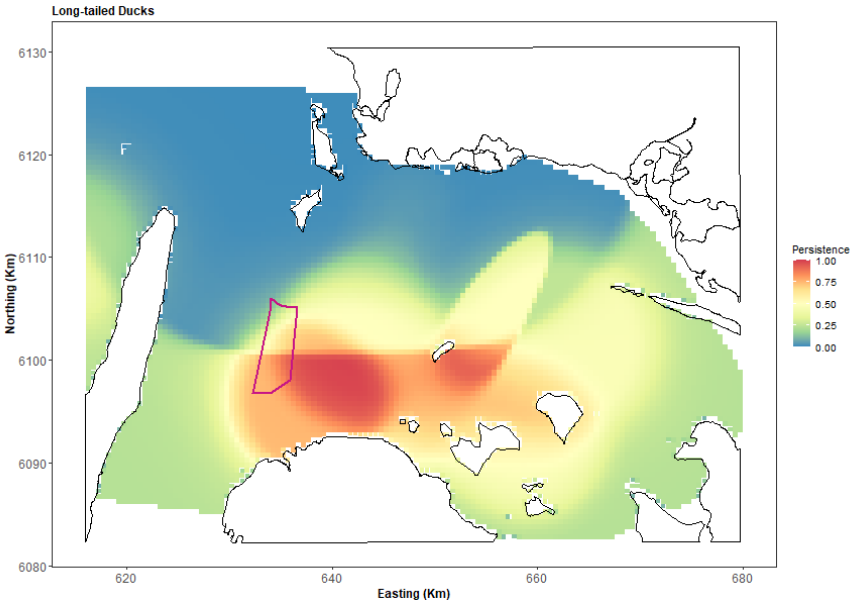

Figure 7.9. Persistence scores of Long-tailed Duck across the large scale MV surveys (2008, 2013, 2016, 2019). The area of the proposed offshore wind farm is indicated (polygon with red outline).

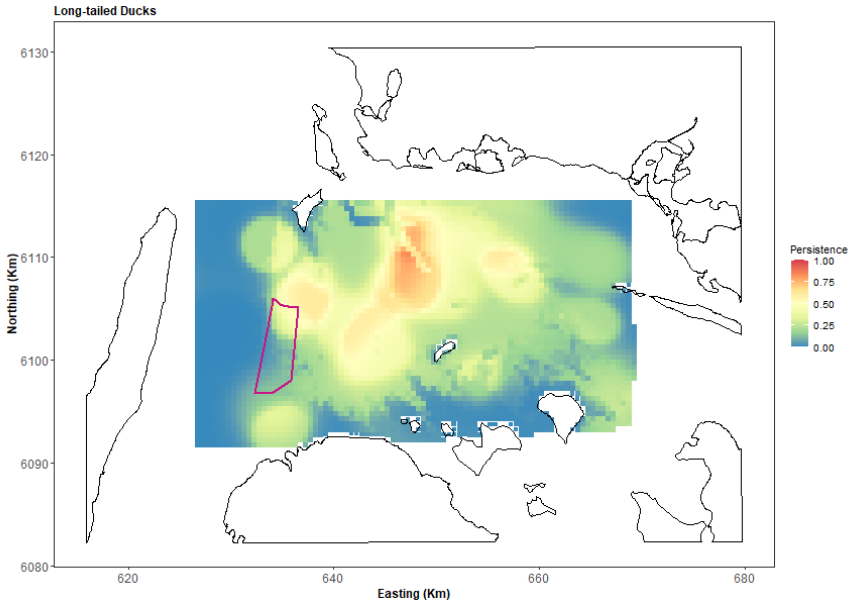

Figure 7.10. Persistence scores of Long-tailed Duck across the persistence for survey data across 2020-2021. The area of the proposed offshore wind farm is indicated (polygon with red outline

7.1.9 Impact Scenarios

The impact scenario undertaken for Long-tailed Duck was an 50% decline in the footprint of the proposed wind farm with a linear return to no change in a 2km buffer. Across surveys, this returned a range of scenario outcomes ranging from no reduction in birds for 3 surveys (Table 7.3) to up to 595 birds. Figure 7.11 shows an example scenario based on one of the bootstrap replicates and the survey MV2019.

Table 7.3. Table showing the effect of scenario 1 implementation on Long-tailed Duck numbers in the proposed wind farm footprint and buffer regions. "Area" is the area in km^2 of the available prediction cells in the footprint + buffer area for each survey (2012 onwards). "95% CI Expected Impacted Birds" is the after abundance minus the before abundance. "95% CI" figures represent the 95 percentile-based confidence intervals for each estimate

Survey	Area (km^2)	Density Before	95% CI Before	Density After	95% CI After	95% CI Expected Impacted Birds
OM_MV2013	82.2	1.35	(0.77, 2.57)	0.94	(0.54, 1.77)	(-66, -18)
OM_20131120	82.2	0.1	(0.02, 0.86)	0.08	(0.02, 0.64)	(-18, 0)
OM_20140308	82.2	1.2	(0.4, 4.35)	0.81	(0.27, 2.99)	(-118, -10)
OM_20141121	82.2	0.08	(0.02, 0.47)	0.07	(0.02, 0.38)	(-8, 0)
OM_20141228	82.2	0.23	(0.08, 0.91)	0.17	(0.06, 0.64)	(-22, -2)
OM_20150309	82.2	5	(2.24, 16.8)	2.89	(1.33, 9.5)	(-595, -72)
OM_MV2016	82.2	0.39	(0.18, 0.88)	0.27	(0.12, 0.61)	(-22, -5)
OM_MV2019	82.2	0.86	(0.42, 1.5)	0.58	(0.28, 1.02)	(-40, -11)
OM_20201127	82.2	1.04	(0.8, 1.35)	0.71	(0.56, 0.93)	(-34, -21)
OM_20210109	82.2	0.24	(0.08, 0.59)	0.16	(0.06, 0.4)	(-15, -2)
OM_20210201	82.2	0.19	(0.09, 0.42)	0.14	(0.07, 0.3)	(-10, -2)
OM_20210214	82.2	0.42	(0.19, 0.85)	0.31	(0.14, 0.62)	(-19, -3)
OM_20210322	82.2	0.02	(0, 0.29)	0.02	(0, 0.23)	(-5, 0)

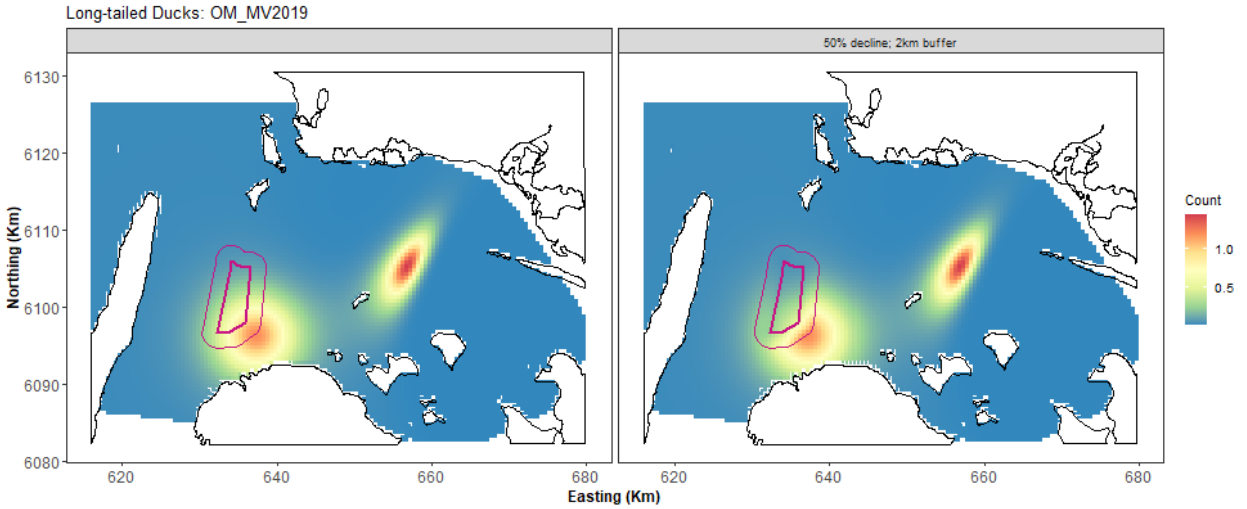

Figure 7.11. Example of displacement scenario for Long-tailed Duck. On the left is one of the estimated bootstrap predictions from the MV_2019 model. On the right is the same set of predictions but with the scenario imposed. The footprint is shown by the thick purple line and the buffer the thinner purple line.

8 Red-breasted Merganser *Mergus serrator*

8.1.1 Distance Analysis

Detection function from data with four transect bands

The average probability of sighting Red-breasted Merganser was estimated to be 0.13 (CV=0.08). This probability was estimated using a half normal detection function that did not vary with any covariates (Figure 8.1). Owing to an issue with low detectability in the first bin, the first two bins were merged for this analysis. The assumption was that this issue stemmed from the birds flushing from under the plane into the second bin.

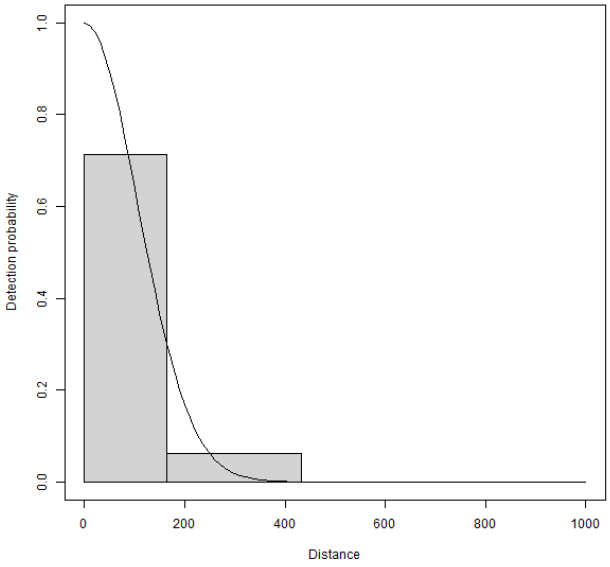

Figure 8.1. Figure showing the estimated detection function for Red-breasted Merganser. The histogram is the distances of the observed sightings.

8.1.2 Detection function from data with three transect bands

The average probability of sighting Red-breasted Merganser was estimated to be 0.23 (CV=0.03). This probability was estimated using a hazard rate detection function that varied with cluster size (Figure 8.2). No other covariates were selected. As for the surveys conducted using four transect bands, there is an issue with detecting large groups in the first distance band. This may occur if the aggregation of birds is larger than the width of the first band.

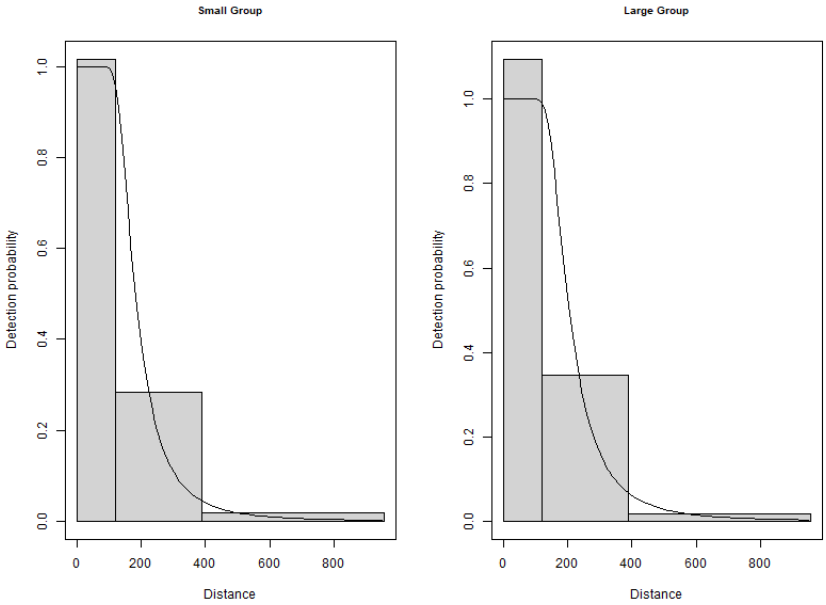

Figure 8.2. Figure showing the estimated detection function for examples of a large group and a small group of Red-breasted Mergansers. The histograms are the distances of the observed sightings.

8.1.3 Spatial analysis

The two datasets were combined for the spatial analysis and contained 31,512 segments, 3% of which were segments containing Red-breasted Merganser sightings. Figure 8.3 shows the distribution of the distance corrected counts for all 37 surveys. Two of the 37 surveys had zero observations and a further 15 had too few observations for a spatial analysis to be conducted (less than 12 observations).

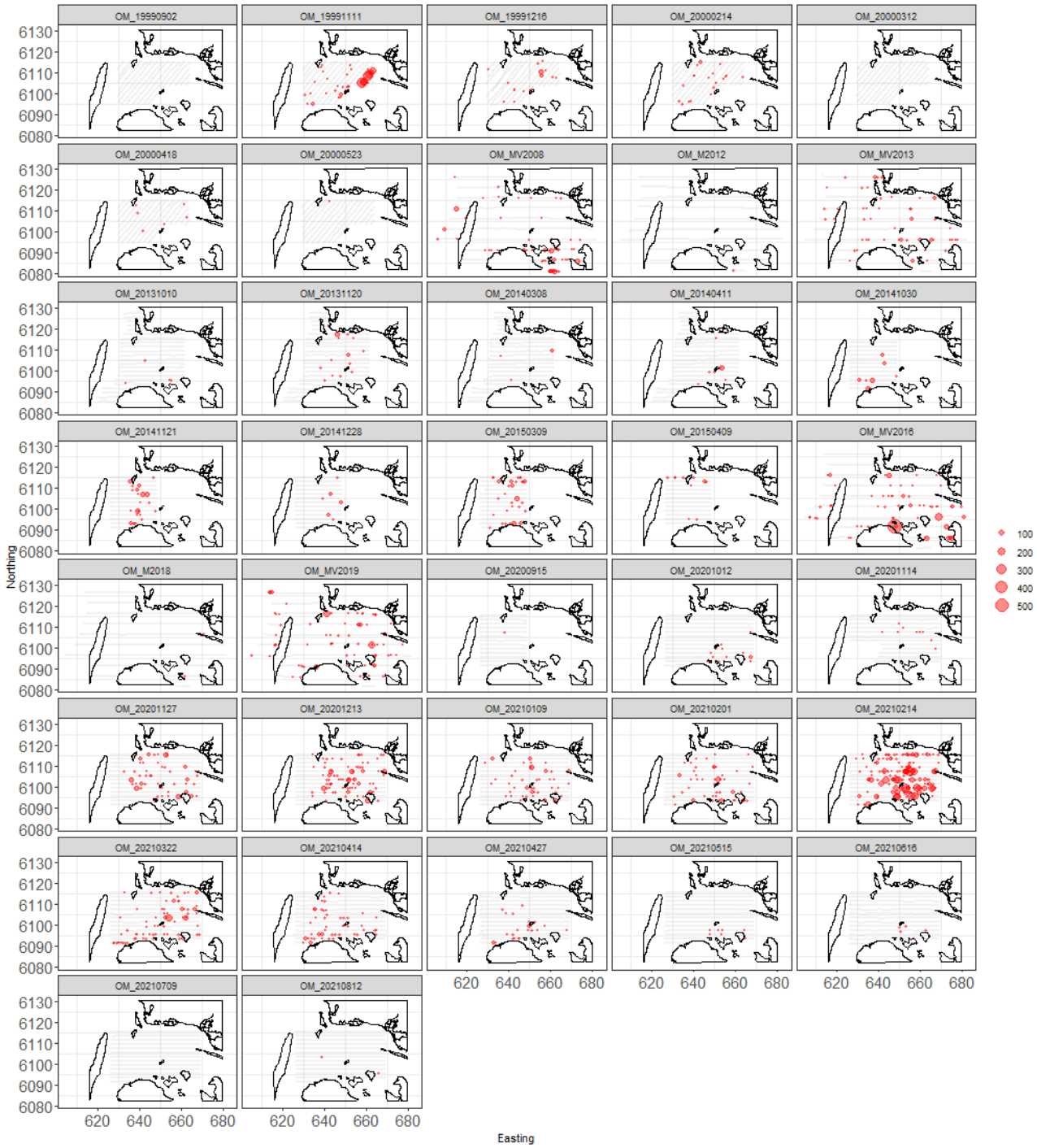

Figure 8.3. Counts for Red-breasted Merganser across the 37 surveys. The red circles indicate the distance-corrected counts along the transect lines while the polygons represent land. Grey dots are segments with a count of zero.

8.1.4 Model Selection results

Only 20 surveys had sufficient observations to enable a fitted model and each model selected included a spatial term of typically low to medium complexity (2-8 parameters). In addition to the spatial term a depth term was selected for two of the 20 'successful' surveys analysed (as linear terms). Both surveys had similar patterns with the highest estimated counts at shallow depths and declining abundance with increasing depth. Distance to coast (either as a linear or smooth term) was not selected for any of the survey-based models. This shows that while there was compelling evidence for non-uniform spatial patterns in each survey, there was little evidence for a depth relationship and no

evidence for a distance to coast-based relationship over and above the spatial terms (Table 8.1).

The estimated abundances and associated 95 percentile confidence intervals for each survey are given in Table 8.2, while the equivalent values for density and a visual representation of these estimates (with associated uncertainties) are shown in Figure 8.4.

Table 8.1. Model selection results for Red-breasted Merganser for each survey. The Variables column represents the terms in the model while the 'degrees of freedom' column indicates the number of parameters allocated to each smooth term. The extra-Poisson dispersion parameter estimates are listed in the far-right column. Empty cells indicate too few observations for the spatial analysis, e.g. n=12.

Year	Month	Survey	Variables	Degrees of freedom	Dispersion parameter estimate
1999	09	OM_19990902	-		
	11	OM_19991111	s(x.pos, y.pos)	6	90.74
	12	OM_19991216	s(x.pos, y.pos)	8	7.95
2000	02	OM_20000214	s(x.pos, y.pos)	8	10.01
	03	OM_20000312	-		
	04	OM_20000418	-		
	05	OM_20000523	-		
2008	01/02	OM_MV2008	s(x.pos, y.pos)	5	25.51
2012	08/09	OM_MV2012	-		
2013	01	OM_MV2013	s(x.pos, y.pos)	3	18.67
2013	10	OM_20131010	-		
	11	OM_20131120	s(x.pos, y.pos)	2	22.89
2014	03	OM_20140308	-		
	04	OM_20140411	-		
	10	OM_20141030	-		
	11	OM_20141121	s(x.pos, y.pos)	3	29.98
	12	OM_20141228	-		
2015	03	OM_20150309	s(x.pos, y.pos)	3	28.63
	04	OM_20150409	-		
2016	01	OM_MV2016	s(x.pos, y.pos)	2	112.09
2018	07	OM_MV2018	-		
2019	12	OM_MV2019	s(x.pos, y.pos)	4	37.62
2020	09	OM_20200915	-		
	10	OM_20201012	s(x.pos, y.pos)	2	6.84
	11	OM_20201114	s(x.pos, y.pos)	2	5.4
	11	OM_20201127	Depth + s(x.pos, y.pos)	3	25.57
	12	OM_20201213	s(x.pos, y.pos)	6	28.26
2021	01	OM_20210109	Depth + s(x.pos, y.pos)	3	25.67
	02	OM_20210201	s(x.pos, y.pos)	5	20.38
	02	OM_20210214	s(x.pos, y.pos)	3	62.45
	03	OM_20210322	s(x.pos, y.pos)	3	33.94

	04	OM_20210414	s(x.pos, y.pos)	4	15.49
	04	OM_20210427	s(x.pos, y.pos)	3	15.16
	05	OM_20210515	-		
	06	OM_20210616	-		
	07	OM_20210709	-		
	08	OM_20210812	-		

Table 8.2. Estimated density of Red-breasted Merganser for each survey. The 95% CI are percentile-based confidence intervals. The area is the area of the prediction region (convex hull around the data).

Year	Month	Survey	Area (km^2)	Estimated Count	95% CI Count	Estimated Density	95% CI Density
1999		OM_19991111	585	1543	(923, 17487)	2.6	(1.6, 29.9)
		OM_19991216	617	245	(125, 594)	0.4	(0.2, 1)
2000		OM_20000214	591	269	(98, 905)	0.5	(0.2, 1.5)
2008		OM_MV2008	1938	1709	(817, 4215)	0.9	(0.4, 2.2)
2013		OM_MV2013	1940	1661	(958, 2962)	0.9	(0.5, 1.5)
		OM_20131120	1070	271	(132, 2591)	0.3	(0.1, 2.4)
2014		OM_20141121	507	462	(207, 1321)	0.9	(0.4, 2.6)
2015		OM_20150309	515	560	(273, 1302)	1.1	(0.5, 2.5)
2016		OM_MV2016	1937	3956	(2039, 9749)	2	(1.1, 5)
2019		OM_MV2019	1918	2797	(1670, 5905)	1.5	(0.9, 3.1)
2020		OM_20201012	964	142	(88, 211)	0.1	(0.1, 0.2)
		OM_20201114	879	66	(26, 152)	0.1	(0, 0.2)
		OM_20201127	968	977	(596, 1808)	1	(0.6, 1.9)
		OM_20201213	966	1360	(795, 2529)	1.4	(0.8, 2.6)
2021		OM_20210109	974	697	(394, 1419)	0.7	(0.4, 1.5)
		OM_20210201	982	620	(317, 1966)	0.6	(0.3, 2)
		OM_20210214	969	5287	(3020, 11865)	5.5	(3.1, 12.2)
		OM_20210322	980	1027	(557, 2074)	1	(0.6, 2.1)
		OM_20210414	978	662	(343, 1533)	0.7	(0.4, 1.6)
		OM_20210427	970	294	(157, 575)	0.3	(0.2, 0.6)

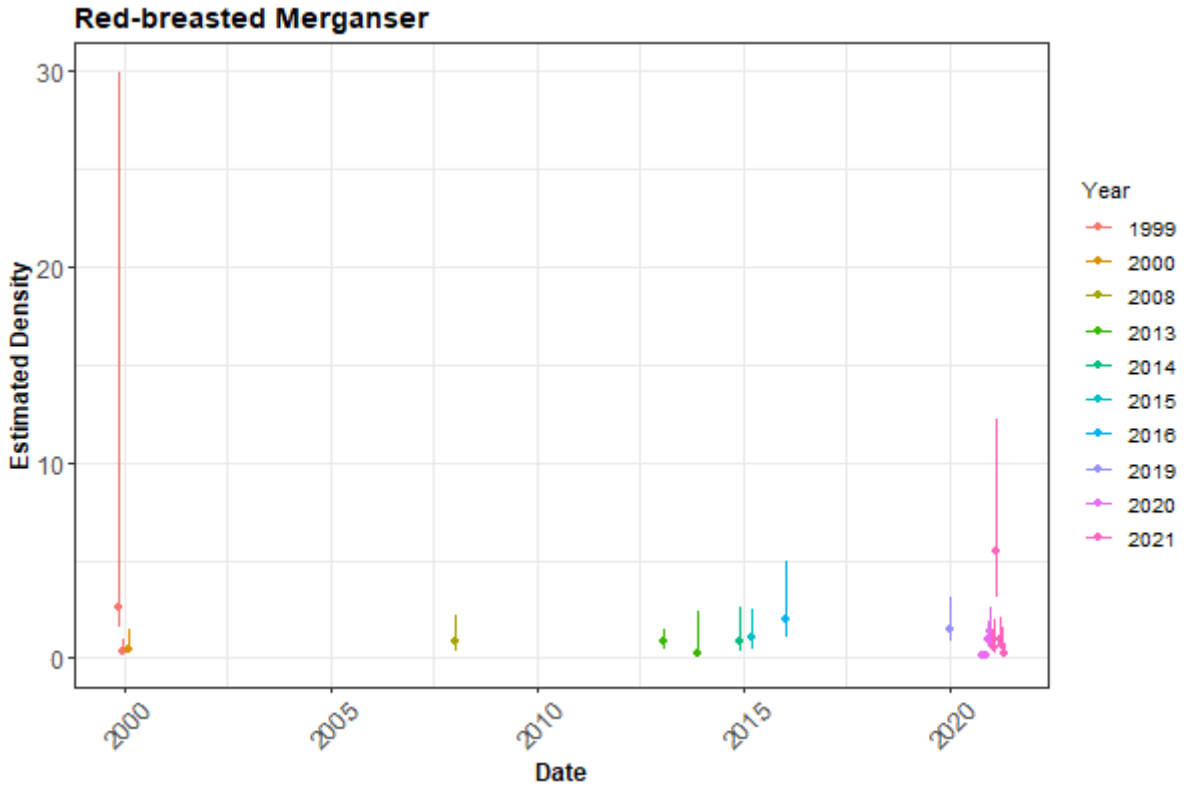

Figure 8.4. The estimated density of Red-breasted Merganser for each survey. The 95% CI are percentile-based confidence intervals are from a parametric bootstrap with 500 replicates. Densities are presented rather than counts as the study area for each survey is different.

8.1.5 Spatial Results

Figure 8.5 shows the estimated counts of Red-breasted Mergansers in each 500x500 m grid cell for each survey. Generally, the estimated abundances fit well to the raw data and there are no concerning departures. The common scale applied to all surveys makes it difficult to see the underlying structure of the fitted surfaces in detail however, output CSV files are provided for all predictions and individual survey-based estimated surface plots are available in the file "extraplots-mergansers.docx".

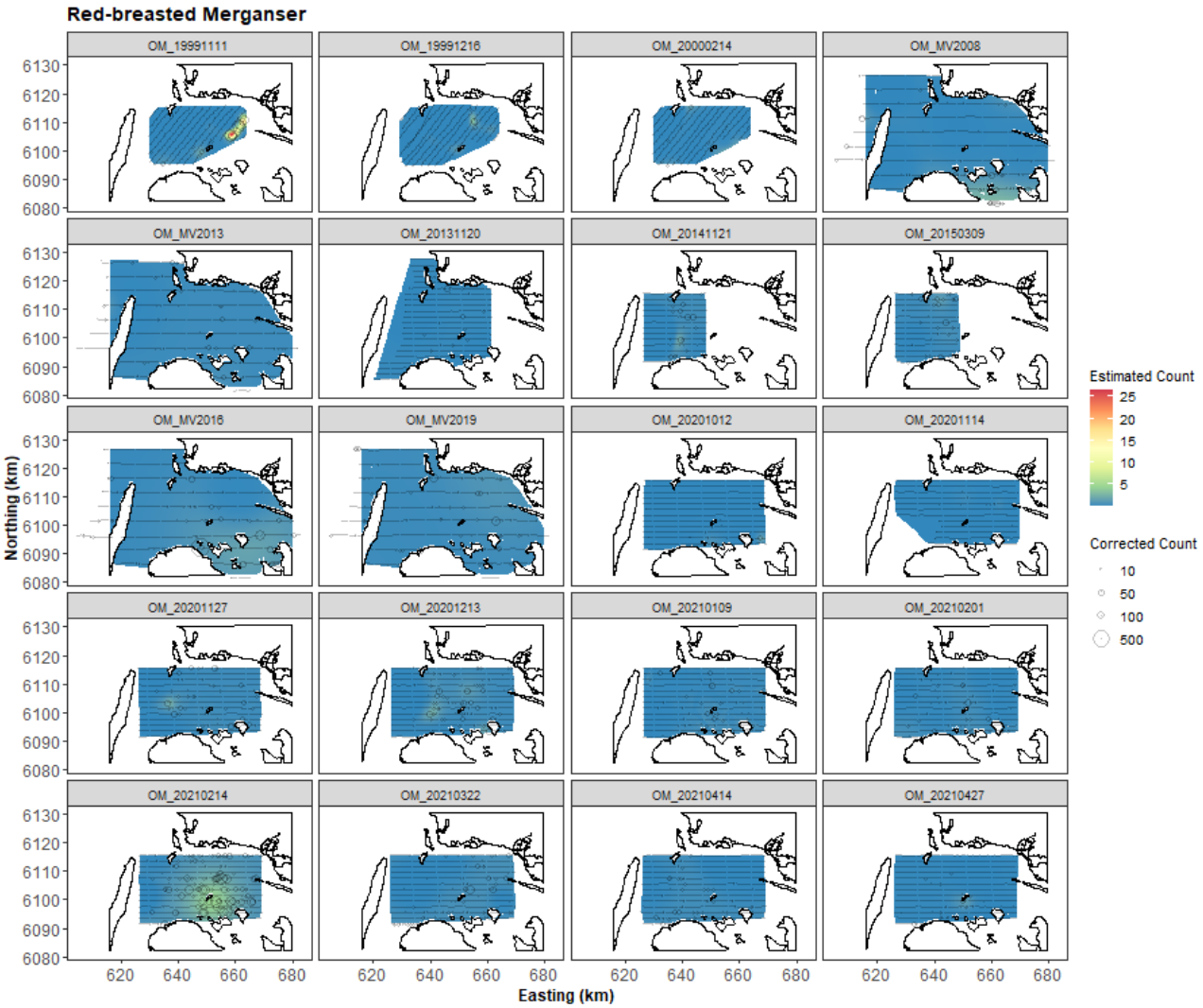

Figure 8.5. Figure showing the estimated Red-breasted Merganser abundance across the study site for each of the surveys. The title of each subfigure after the underscore ("OM_") details the survey year (4 digits) and in years with multiple surveys, survey month (2 digits) and day (2 digits) follows the year. The estimated counts are per 500x500m grid cell. The open circles show the observed corrected count. The coloured graphics represent the predicted values in each location.

8.1.6 Uncertainty in the spatial predictions

The highest coefficient of variation (CoV) scores were associated with the very smallest predictions, however it is known that the CoV metric is highly sensitive to any uncertainty for very small predictions. There was no material overlap between high values of the CoV metric and the transect lines/locations with non-zero counts and therefore results in no concerns in this case (Figure 8.6 and Figure 8.7).

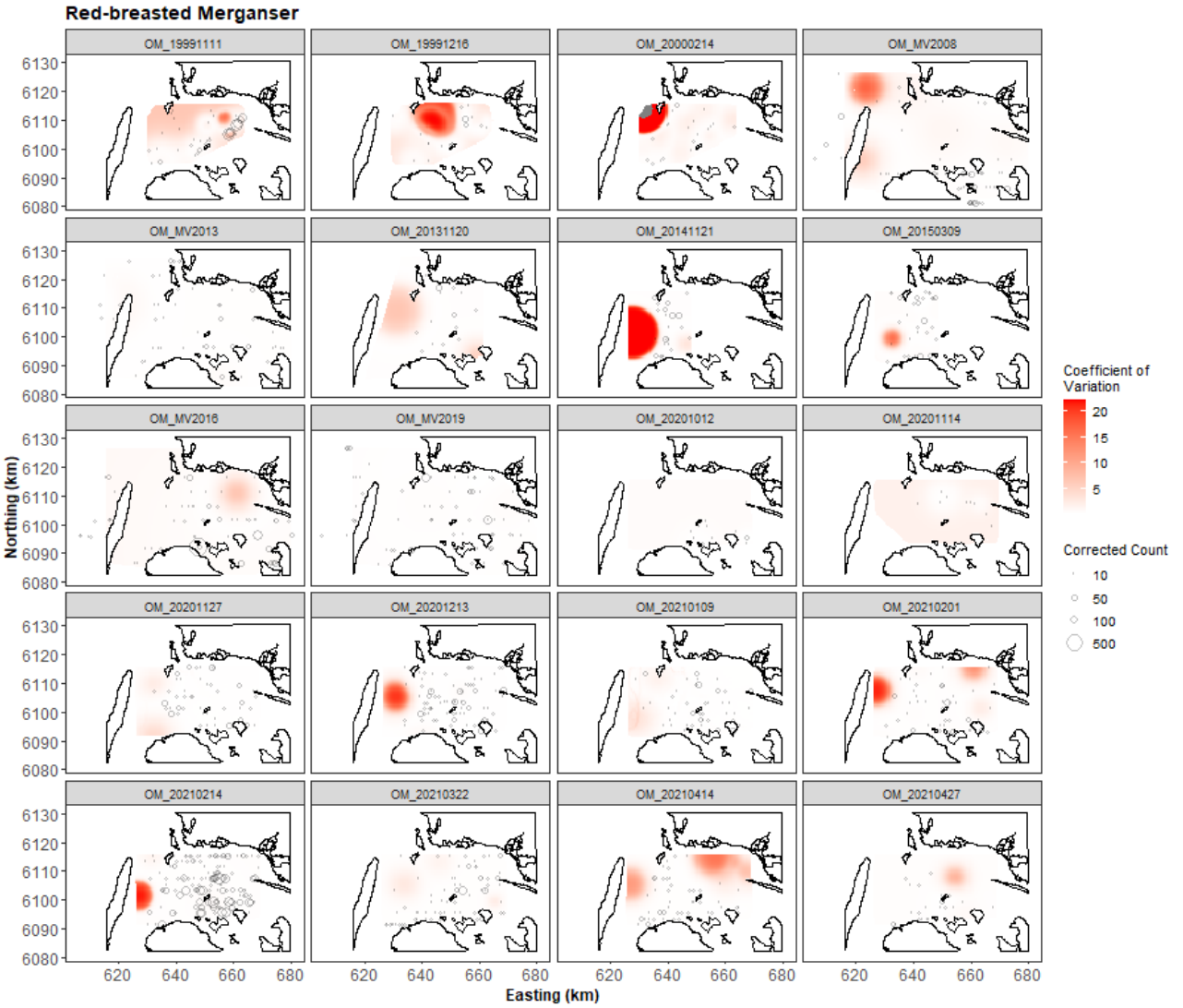

Figure 8.6. Figure showing the coefficient of variation across the study region for each of the surveys. The open circles show the distance corrected counts, where applicable. The presence of dark red CV scores in areas with virtually zero predictions are an artifact of the very small prediction rather than of any notable concern.

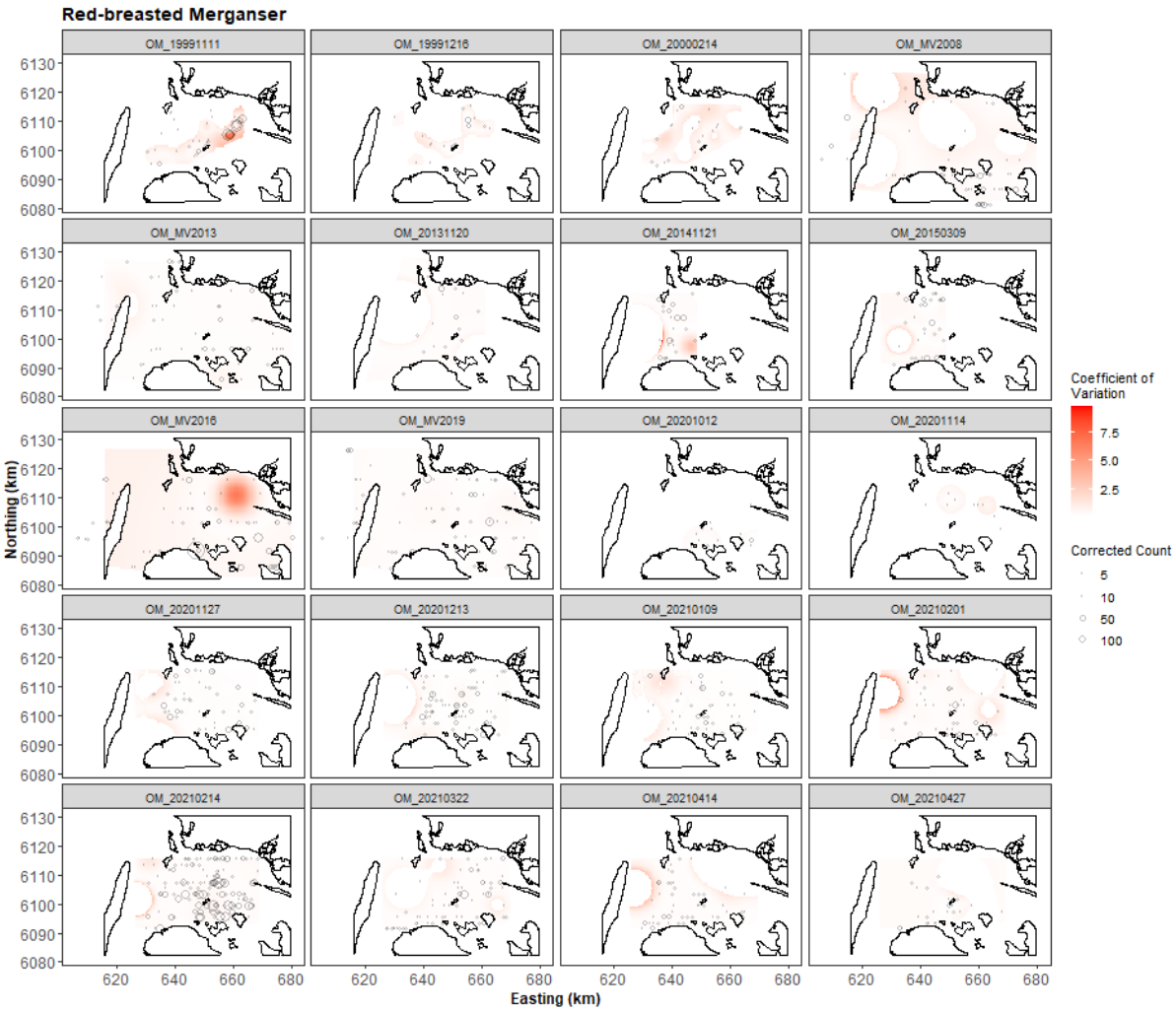

Figure 8.7. Figure showing the coefficient of variation across the study region for each of the surveys with a threshold applied to account for the very small predicted values. The open circles show the distance corrected counts, where applicable. The presence of dark red CV scores in areas with virtually zero predictions are an artifact of the very small prediction rather than of any notable concern.

8.1.7 Model Diagnostics

A blocking structure was used to account for potential residual non-independence for each model and a robust standard error approach was based on unique transects. In every case, we saw a reassuring decay to zero implying that an appropriate blocking structure was used.

The assumed mean-variance relationship was examined and generally showed agreement between the assumed (red) lines and the observed values. However, in some cases the residuals for the largest fitted values were in practice more variable than that assumed (above the line) suggesting that the variance is underestimated for these. There were no systematic clusters of negative or positive residuals for the 20 surveys and thus represent good agreement between the data and the model. The individual diagnostic plots are available on request.

8.1.8 Areas of Persistence

Across all surveys, there is evidence of low-to-moderate persistence across the survey area, except in the western edge of the survey area, where the

persistence falls to 0.25 or below (Figure 8.8). Relatively low persistence (~0.25) dominates the proposed wind farm footprint.

For the wide scale surveys carried out across years (2008, 2013, 2016, 2019; Figure 8.9) there was a very similar picture and in the most recent surveys (2020-2021; Figure 8.10), persistence appears to have decreased somewhat in the south-western edge of the footprint.

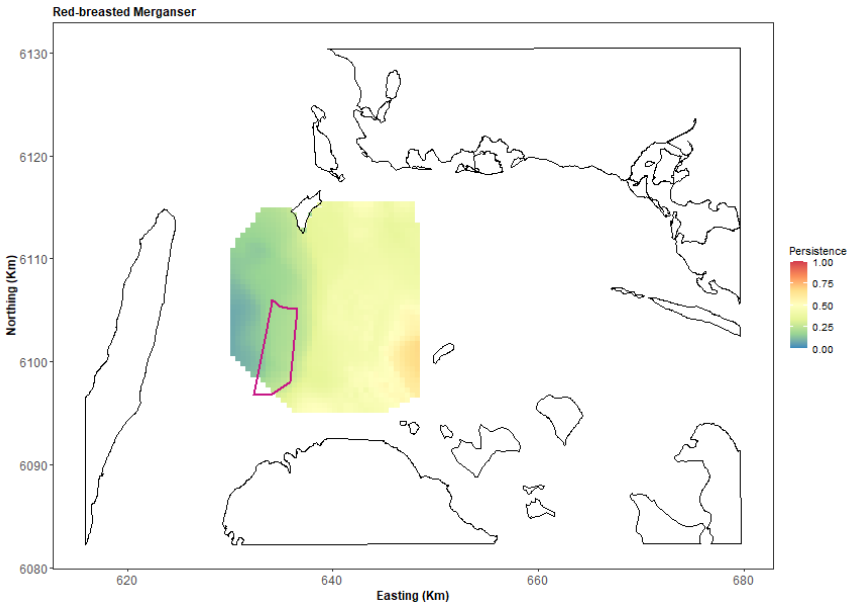

Figure 8.8. Persistence scores for Red-breasted Merganser across the persistence for survey data for all surveys. The area of the proposed offshore wind farm is indicated (polygon with red outline).

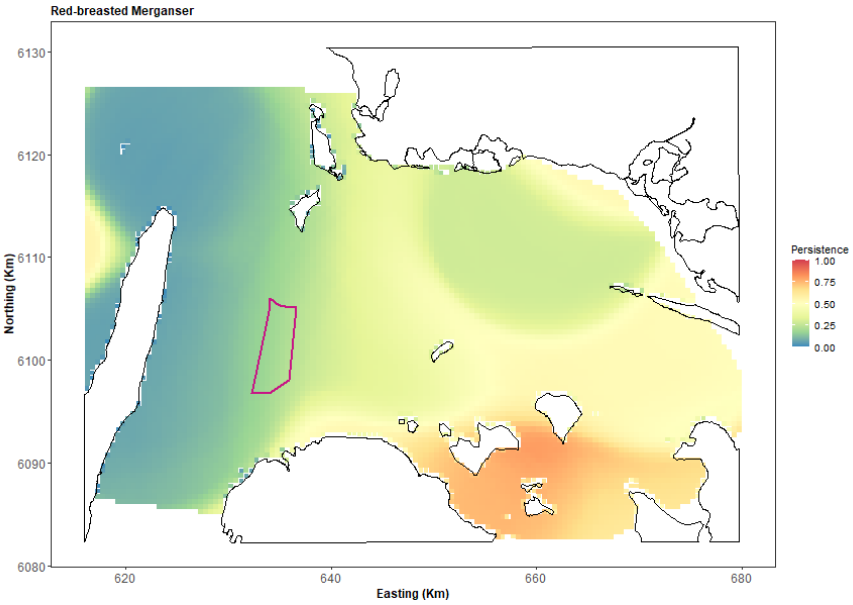

Figure 8.9. Persistence scores Red-breasted Merganser across the large scale MV surveys (2008, 2013, 2016, 2019). The area of the proposed offshore wind farm is indicated (polygon with red outline).

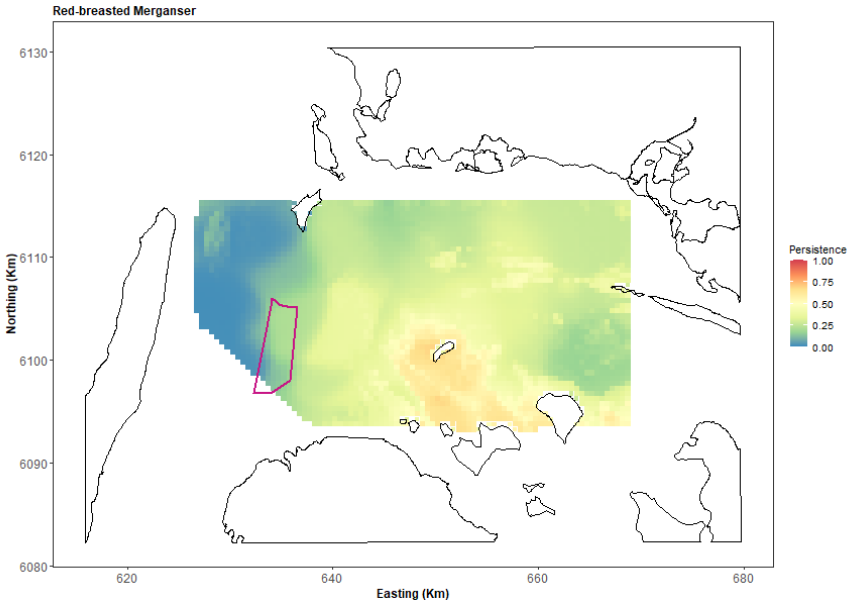

Figure 8.10. Persistence scores Red-breasted Merganser across the persistence for survey data across 2020-2021. The area of the proposed offshore wind farm is indicated (polygon with red outline).

8.1.9 Impact Scenarios

The impact scenario undertaken for the Red-breasted Mergansers was an 30% decline in the footprint of the proposed wind farm with a linear return to no change in a 2km buffer. Across surveys, this returned a range of scenario outcomes ranging from a negligible, or no, reduction in birds (Table 8.3) to a moderate reduction of up to 65 birds. Figure 8.11 shows an example scenario based on one of the bootstrap replicates and the OM_20201127 survey.

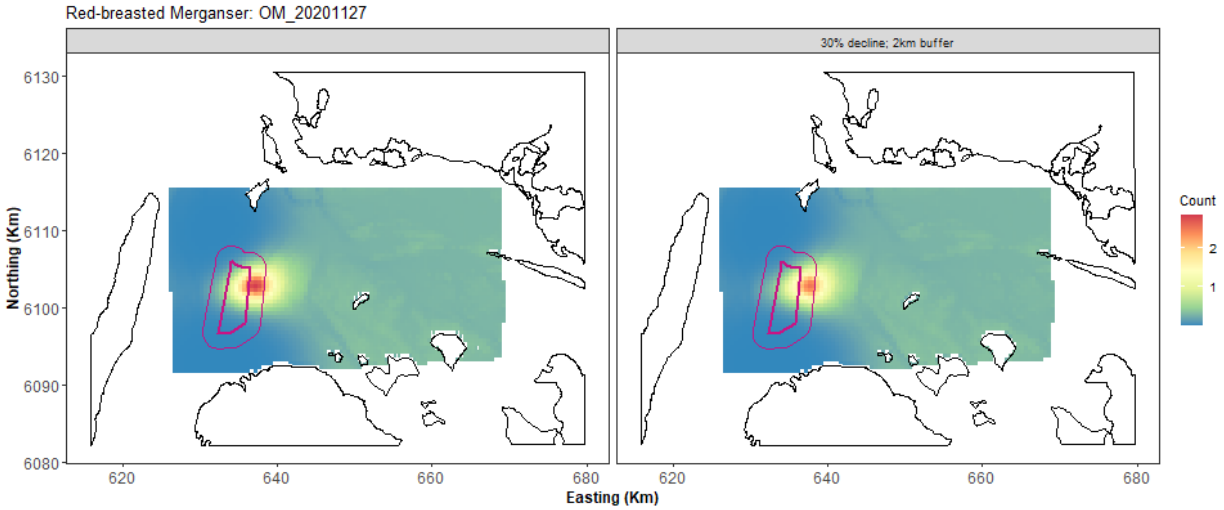

Figure 8.11. Example of displacement scenario for Red-breasted Merganser. On the left is one of the estimated bootstrap predictions from the OM_20201127 model. On the right is the same set of predictions but with the scenario imposed. The footprint is shown by the thick purple line and the buffer the thinner purple line.

Table 8.3. Table showing the effect of scenario 1 implementation on Red-breasted Merganser numbers in the proposed wind farm footprint and buffer regions. "Area" is the area in km^2 of the available prediction cells in the footprint + buffer area for each survey (2012 onwards). "95% CI Expected Impacted Birds" is the after abundance minus the before abundance. "95% CI" figures represent the 95 percentile-based confidence intervals for each estimate.

Survey	Area (km^2)	Density Before	95% CI Before	Density After	95% CI After	95% CI Expected Impacted Birds
OM_MV2013	82.2	0.75	(0.48, 1.16)	0.6	(0.39, 0.94)	(-18, -8)
OM_20131120	82.2	0.09	(0.03, 3.52)	0.07	(0.03, 2.98)	(-45, 0)
OM_20141121	82.2	0.2	(0.04, 2.36)	0.19	(0.04, 2.06)	(-22, 0)
OM_20150309	82.2	0.28	(0.12, 1.45)	0.24	(0.11, 1.15)	(-25, -1)
OM_MV2016	82.2	1.54	(0.61, 4.15)	1.25	(0.5, 3.36)	(-65, -10)
OM_MV2019	82.2	0.87	(0.46, 1.85)	0.71	(0.37, 1.5)	(-29, -7)
OM_20201012	82.2	0.03	(0.01, 0.06)	0.02	(0.01, 0.05)	(-1, 0)
OM_20201114	68	0.01	(0, 0.05)	0.01	(0, 0.04)	(-1, 0)
OM_20201127	82.2	1.88	(1.08, 3.36)	1.49	(0.86, 2.65)	(-59, -18)
OM_20201213	82.2	0.34	(0.15, 1.28)	0.3	(0.13, 1.06)	(-18, -1)
OM_20210109	82.2	0.16	(0.06, 0.69)	0.13	(0.05, 0.56)	(-11, -1)
OM_20210201	82.2	0.49	(0.25, 1.31)	0.4	(0.2, 1.08)	(-19, -4)
OM_20210214	82.2	2.17	(1.15, 4.14)	1.77	(0.93, 3.36)	(-64, -17)
OM_20210322	82.2	0.14	(0.07, 0.32)	0.12	(0.06, 0.27)	(-4, -1)
OM_20210414	82.2	0.65	(0.27, 1.91)	0.53	(0.23, 1.56)	(-29, -4)
OM_20210427	82.2	0.26	(0.12, 0.55)	0.21	(0.1, 0.45)	(-9, -2)

9 Conclusion

Red-throated Divers/Black-throated Divers were recorded in the study area in varying numbers across the 37 aerial surveys, estimating up to more than 1,300 individuals within the area in October 2014. From this survey an estimated 297 to 1,246 individuals was estimated to be displaced by an Omø Syd Offshore Wind Farm.

Red-necked Grebes were recorded in significant numbers in the study area. Since these birds are small and inconspicuous, they are difficult to detect from aerial surveys. The estimated numbers are therefore based on a strip transect estimation, assuming 100 % probability of detection in transect band A. This assumption is unlikely to be met, and estimated numbers are therefore likely to be underestimated. The described distribution of the birds across the survey area is on the other hand considered to be valid.

Altogether, 14 of the 37 aerial surveys had enough data to estimate total abundances and distributions of Red-necked Grebes. The maximum numbers was 2,209 individuals, estimated on the basis of a November survey of 1999. For ten surveys the potential number of displaced Red-necked Grebes could be estimated. Within these ten surveys the highest number of displaced birds, using the displacement scenario of 80 % reduction in the wind farm area and a linearly reduced effect out to a distance of 10 km from the wind farm periphery, was between 254 and 833 individuals, based on data from a survey conducted in November 2014. Using the alternative displacement scenario of 50 % reduction within the wind farm site and a gradually decreased effect up to 5 km from the periphery, the number of displaced Red-necked Grebes was estimated to be between 47 and 156 individuals.

Common Eiders are present in the study area all year. Total numbers could be estimated for all 37 surveys. The estimated number ranged from 1,216 in May 2000 to 107,986 in March 2014. The Omø Syd Offshore Wind Farm showed low to medium persistency values across the surveys. Based on two displacement scenarios, one with a 25 % reduction within the wind far area and a reduced effect out to 2 km from the periphery of the wind farm, the other with a reduction rate of 25 % and a graduate reduced effect out to 1 km from the periphery of the wind farm, the following reduction effects was estimated. Maximum number of between 2,113 and 11,981 displaced Common Eiders was estimated for a survey performed in October 2014 under the first displacement scenario, while minimum numbers of between 2 and 10 individuals was estimated for a survey in April 2021. For the alternative displacement scenario, the corresponding numbers were between 1,489 and 8,742 individuals in the maximum displacement survey and between 0 and 6 individuals for the minimum displacement survey.

Long-tailed Duck is primarily a wintering and passage species in the study area. Of the 37 aerial surveys, 18 provided data that allowed for estimation of density and abundance. 13 provided displacement estimates. Maximum numbers were found for the winter 2013 survey, when 1,449 individuals were estimated.

The Long-tailed Duck persistency scores for the Omø Syd wind farm area was relatively high. When using the displacement scenario of 50 % reduction

within the Omø Syd Offshore Wind Farm and a graduate reduction of effect out to 2 km from the wind farm periphery, a total of between 72 and 595 displaced individuals was estimated, based on a survey from March 2015.

Estimation of Common Scoter could be achieved from 32 and the 37 aerial surveys in the study area. The highest estimated number was 39,732 individuals, based on a survey from April 2014. Common Scoter persistency was moderate to low in the area of the Omø Syd Offshore Wind Farm.

Estimation of the number of displaced Common Scoters was performed for 25 of those surveys. A displacement scenario of 50 % reduction within the Omø Syd Offshore Wind Farm was used, and a gradually decreased effect up to 5 km distance from the periphery of the wind farm. This led to a maximum number of displaced Common Scoters between 4,408 and 7,427 individuals, based on data from a survey from April 2014.

Estimation of Red-breasted Merganser was achieved from 20 of the 37 aerial surveys. The highest estimated numbers were 5,287 individuals, based on survey data from February 2021. Red-breasted Merganser persistency was low to low in the area of the Omø Syd Offshore Wind Farm.

Estimation of number of displaced Red-breasted Merganser was achieved from 16 of the 37 aerial surveys. From those a maximum of between 10 and 65 individuals were estimated to be displaced from the proposed Offshore Wind Farm, estimated on the background of data from the midwinter survey of 2016.

Displacement from a preferred staging area does not cause direct mortality, but is likely to influence birds with altered conditions, potentially leading to changes in reproduction and survival rates. It is not possible to translate such changes to the impact on the population level of the selected species at present.

Litterature

Buckland, S. T., Anderson, D. R., Burnham, K. P., Laake, J. L., Borchers, D. L., and Thomas, L. 2001. Introduction to Distance Sampling. Oxford University Press.

DHI 2015. Smålandsfarvandet Offshore Wind Farm Birds and bats. Baseline and impact assessment in relation to birds and bats. Report commissioned by Ramboll. 207 pp.

Heinänen, S., Zydelis, R., Kleinschmidt, B., Dorsch, M., Burger, C., Morkunas, J., Quillfeldt, P. & Nehls, G. 2020. Satellite telemetry and digital aerial surveys show strong displacement of red-throated divers (Gavia stellata) from offshore wind farms. - Marine Environmental Research 160 (2020) 104989.

Hedley, S. L. and Buckland, S. T. (2004). Spatial models for line transect sampling. Journal of Agricultural, Biological and Environmental Statistics 9, 181–199.

Holm, T.E., Nielsen, R.D., Clausen, P., Bregnballe, T., Clausen, K.K., Petersen, I.K, Sterup, J., Bals-by, T.J.S., Pedersen, C.L., Mikkelsen, P & Bladt, J. 2021. Fugle 2018-2019. NOVANA. Aarhus Universitet, DCE – Nationalt Center for Miljø og Energi. Videnskabelig rapport fra DCE - Natio-nalt Center for Miljø og Energi nr. 420. novana.au.dk

Mendel, B., P. Schwemmer, V. Peschko, S. Müller, H. Schwemmer, M. Mercker & S. Garthe 2019: Operational offshore wind farms and associated ship traffic cause profound changes in distribution patterns of Loons (Gavia spp.). – J. Environ. Manage. 231: 429-438.

ORBICON 2016. Omø Syd kystnær Havmøllepark. VVM – vurdering af virkning på miljøet og Miljørapport.

Petersen, I.K. & Clausager, I. 2000. VVM-redegørelse for havvindmøllepark på Omø Stålgrun-de. Teksnisk rapport vedrørende fugle. Report commissioned by SEAS A/S from Danmarks Miljøundersøgelser. – 75 pp

Petersen, I.K., Nielsen, R.D., Pihl, S., Clausen, P., Therkildsen, O., Christensen, T.K., Kahlert, J. & Hounisen, J.P. 2010. Landsdækkende optælling af vandfugle i Danmark, vinteren 2007/2008. Danmarks Miljøundersøgelser, Aarhus Universitet. 78 s. – Arbejdsrapport fra DMU nr. 261.

Petersen, I.K., M.L. MacKenzie, E. Rexstad, M.S. Wisz & A.D. Fox 2011: Comparing pre- and post-construction distributions of long-tailed ducks Clangula hyemalis in and around the Nysted offshore wind farm, Denmark: a quasi-designed experiment accounting for imperfect detection, local surface features and autocorrelation. – CREEM Technical Report, no. 2011-1, University of St Andrews.

Petersen, I.K., R.D. Nielsen & M.L. Mackenzie 2014: Post-construction evaluation of bird abundances and distributions in the Horns Rev 2 offshore wind farm area, 2011 and 2012. – Report Commissioned by Dong Energy. Danish Centre for Environment and Energy, Aarhus University.

Scott-Hayward, L, Mackenzie, M, Donovan, C and G Walker 2014. CReSS – Complex Region Spatial Smoother. Journal of Computational and Graphical Statistics. 23 (2) 340-360

Scott-Hayward, L (2013). Novel Methods for species distribution mapping including spatial models in complex regions: Chapter 5 for SALSA2D methods. PhD Thesis, University of St Andrews.

Scott-Hayward LAS, Oedekoven CS, Mackenzie ML, Walker CG (2019a). MRSea package v1.01: Statistical Modelling of bird and cetacean distributions in offshore renewables development areas. University of St. Andrews: Contract with Marine Scotland: SB9 (CR/2012/05)

Scott-Hayward LAS, Oedekoven CS, Mackenzie ML, Walker CG (2019b). "Vignette for the MRSea Package v1.01: Statistical Modelling of bird and cetacean distributions in offshore renewables development areas." University of St. Andrews.

Scott-Hayward, L, Mackenzie, M (2022). The background report to this report.

Walker, C, M. Mackenzie, C Donovan and M O'Sullivan (2010). SALSA - a Spatially Adaptive Local Smoothing Algorithm. Journal of Statistical Computation and Simulation, 81(2):179-191

APPENDICES

Executive summary of the modelling methods

The data collected are animal counts in some specified area and as both survey types were collected using visual aerial surveys, correction for declining detectability with increasing distance from the plane was accounted for. The resulting distance corrected counts tend to show that the variation in the number of birds increases as the average number of birds increases (i.e., there is a mean-variance relationship) so an overdispersed Poisson-based count model was used for spatial analysis.

As each survey was analysed separately, only spatial explanatory variables were considered. Since bird numbers are often thought to be related to environmental characteristics, such as the depth of the water or distance to coastline, these variables were considered as part of each analysis. To ensure these relationships were suitably informed by the data a flexible approach to these relationships was taken, and the shape of these relationships was evidence-based. For example, a species could show a preference for a particular depth range (i.e., the shape of the relationship between bird numbers and depth could rise and fall) or it could be simpler (e.g., numbers could systematically increase/decrease with depth).

The model selection approach used in the following analyses selects the details of these relationships informed by the data, while ensuring that the resulting relationships are not "overfitted" (i.e., more complex than necessary) to the data available. The underlying relationships in each case were sought, rather than a "fine-tuned" version of these relationships which would fit perfectly to the data set collected for each species in each survey, but not represent any other set of observations from this survey or area (even if they were collected at a similar time from the same area).

While including environmental relationships in models can be relatively simple to understand, it is important to note that if these terms are included in a model (in this way) they are assumed to be true everywhere across the survey region. That is, if bird numbers are assumed to be highest at some depth, this is assumed to be true for *all* areas of the study region with that depth.

This is often unrealistic in practice since there are many (other) influences in addition to the variable(s) under consideration which act together to make locations attractive/unattractive to birds (some of which might be changing daily). Additionally, all of the variables giving rise to bird numbers in particular locations are unlikely to be known or available for consideration/selection in the model and thus localised spatial patterns often remain. For this reason, and to account for localised surface patterns, a spatial surface was also considered for inclusion in each model. These terms were also permitted to be flexible (and informed by the data) but were chosen in order not to be "overfitted" to any particular survey – instead they represent the underlying spatial patterns likely to be observed at a similar time in the same survey area.

To achieve this balance between fit to the survey data and to avoid "fine-tuning" each model to represent the exact observations sampled for each survey, a "10-fold cross validation" procedure was used. This simply divides the data

up into buckets (folds) with (relatively) equal numbers of observations (whilst maintaining transects) and uses 9 of these folds to choose a model and the remaining fold (which is left out of model fitting and selection) to "test" the model. This prevents overfitting since a finely tuned model would fit almost perfectly to the 9 folds but would look very different from the 'left-out' fold since it was not included in the model fitting and choice, even though it was collected as part of each survey.

The additional feature of these analyses is that the way in which the data were collected was acknowledged and respected when reporting the level of uncertainty in model results. In particular, these data were collected along transects over time and data collected this way tends to result in data points close together (in space or time) that are more similar than data points collected randomly from potentially very different parts of the survey area within some time window. This is akin to measuring the body weight of 10 human subjects, monthly for 10 consecutive months (N=100) compared with measuring the body weight of 100 different human subjects once throughout a 10-month period (also N=100). Traditional ways of reporting the uncertainty about model estimates (e.g., bird counts in any given location) often assumes the modelled data are either randomly sampled in some way, or the variables included in the model *fully* explain these patterns of similarity in these observations collected along transects (resulting in uncorrelated residuals (differences between observed and predicted values)). This is far from guaranteed, and the approach used here was to simply measure the extent of similarity observed in model residuals (within transects – the correlated panels/blocks) and use this value to increase the uncertainty about model estimates so that the results can be interpreted in the usual way. For example: "With 95% confidence we estimate the number of birds in this location to be between 5 and 8 birds, on average."

Output File Descriptions

*species*Preds_surveys.csv

AREA – area in meters of grid cell

ID – ID for grid cell (provided by Aarhus)

X_COORD – x-coordinate in UTMs. Unit is metres

Y_COORD – x-coordinate in UTMs. Unit is metres

depth – depth in meters.

DC – distance to nearest coast. Unit is kilometers

GAREA – area of grid cell with land removed. Derived from `AREA` column. Unit is meters.

CUTID – parameter provided by Aarhus

SLOPE – slope of the seabed (all values are 0)

area – area of grid cell in km² (derived from `GAREA`; used in analysis)

x.pos – x-coordinate in UTMs. Unit is kilometres

y.pos - y-coordinate in UTMs. Unit is kilometres

cellsize – unit length of square grid in km. Used for plotting.

index – index of the grid cell within the full prediction area. Predictions were only made to a convex hull around the transect data.

surveycells – column specifying whether or not the grid cell is within the convex hull of the survey data. In this data the values are all 1 as only survey data prediction cells were selected. The full data is available on request.

CruiseID – unique identifier for survey

preds – estimated counts for each grid cell based on the best model

Lower2.5 – lower 2.5-percentile of bootstrapped predictions. Forms a 95-percentile interval for each grid cell when in conjunction with "Upper97.5".

Upper97.5 – upper 97.5-percentile of bootstrapped predictions. Forms a 95-percentile interval for each grid cell when in conjunction with "Lower2.5".

bootsd – standard deviation of the estimated counts for each grid cell (from bootstraps)

bootmean – mean count for each grid cell, estimated from bootstraps

bootmedian – median count for each grid cell, estimated from bootstraps

cv – coefficient of variation for each grid cell. ("boot_sd"/"bootmean")

X1-Xn– bootstrap predictions for n bootstraps.

*species*persistencedata_*type*.csv

Type refers to one of

"all" (every available survey 1999-2021)

"MV" (every available wide scale survey, up to 6)

"2021" (every available survey from 2020 to 2021)

X_COORD – x-coordinate in UTMs. Unit is metres

Y_COORD – x-coordinate in UTMs. Unit is metres

area – area of grid cell in km^2 (derived from `GAREA`; used in analysis)

cellsize – unit length of square grid in km. Used for plotting.

x.pos – x-coordinate in UTMs. Unit is kilometres

y.pos - y-coordinate in UTMs. Unit is kilometres

Persist_*CruiseID*_ - number of bootstraps that are above mean density

Persistence – sum across survey persist scores and divide by (nboots * nsurveys)

All diagnostic plots for each survey and species are available on request

ABUNDANCES AND DISTRIBUTIONS OF SELECTED WATERBIRD SPECIES AROUND THE PROPOSED OMØ SYD OFFSHORE WIND FARM AREA

This report presents estimation of abundances and distributions of six waterbird species from the Smålandsfarvand study area in southern Denmark. The analyses also include estimation of the number of displaced individuals of each of the six waterbird species from the proposed Omø Syd Offshore Wind Farm, given a set of described displacement scenarios. The analyses will serve as background data for a NATURA2000 environmental assessment related to the wind farm. That assessment was beyond the scope of this report.

ISBN: 978-87-7156-772-4
ISSN: 2244-9981